Performance of iterative detection and decoding for MIMO-BICM systems

Author:
Yang, Tao

Publication Date:
2006

DOI:
https://doi.org/10.26190/unsworks/16075

PERFORMANCE OF ITERATIVE DETECTION AND DECODING FOR MIMO-BICM SYSTEMS

by

TAO YANG

A thesis
presented to the University of New South Wales
in fulfilment of the
thesis requirement for the degree of
Master by Research
in
Telecommunication Engineering

Kensington, Sydney, Australia

Originality Statement

I hereby declare that this submission is my own work and to the best of my knowledge it contains no material previously published or written by another person, or substantial proportions of material which have been accepted for the award of any other degree or diploma at UNSW or any other educational institution, except where due acknowledgement is made in the thesis. Any contribution made to the research by others, with whom I have worked at UNSW or elsewhere, is explicitly acknowledged in the thesis. I also declare that the intellectual content of this thesis is the product of my own work, except to the extent that assistance from others in the project's design and conception or in style, presentation and linguistic expression is acknowledged.

I further authorize the University of NSW to reproduce this thesis by photocopying or by other means, in total or in part, at the request of other institutions or individuals for the purpose of scholarly research.

Acknowledgments

As the author of this dissertation, I wish to thank Professor. Jinhong Yuan for his inspiration and direction throughout all the work of this research. Acknowledgements are also granted to other members in our research group at the University of New South Wales for their kind helps in various forms. Moreover, I want to deliver my gratitude to my family who render me consistent support and encouragement. Finally, I would like to appreciate the support and supervision from Dr. Zhenning Shi who is with the wireless signal processing program, National ICT Australia (NICTA).

Publications

(1) T. Yang, J. Yuan, Z. Shi and M. Reed, "Detection switching in the iterative receivers for MIMO-BICM, " *Proceedings. IEEE Information Theory Workshop (ITW) 2006,* Oct. 2006.

(2) T. Yang, J. Yuan and Z. Shi, "A new scheduling for the iterative receiver of MIMO-BICM, " *Proceedings. IEEE TENCON 2006,* Nov. 2006.

(3) T. Yang and J. Yuan, "Performance of MIMO-BICM with parallel interference canceller on slow fading channels, " *IEE Electronics Letters*, vol. 42, issue. 22, pp. 1292-1293, Oct. 2006.

Abstract

Multiple-input multiple-output (MIMO) wireless technology is an emerging cost-effective approach to offer multiple-fold capacity improvement relative to the conventional single-antenna systems. To achieve the capacities of MIMO channels, MIMO bit-interleaved-coded-modulation (BICM) systems with iterative detection and decoding (IDD) are studied in this thesis.

The research for this dissertation is conducted based on the iterative receivers with convolutional codes and turbo codes. A variety of MIMO detectors, such as a maximum a posteriori probability (MAP) detector, a list sphere detector (LSD) and a parallel interference canceller (PIC) together with a decision statistic combiner (DSC), are studied. The performance of these iterative receivers is investigated via bounding techniques or Monte-Carlos simulations. Moreover, the computational complexities of the components are quantified and compared.

The convergence behaviors of the iterative receivers are analyzed via variance transfer (VTR) functions and variance exchange graphs (VEGs). The analysis of convergence behavior facilitates the finding of components with good matching. For a fast fading channel, we show that the "waterfall region" of an iterative receiver can be predicted by VEG. For a slow fading channel, it is shown that the performance of an iterative receiver is essentially limited by the *early interception ratio* (ECR) which is obtained via simulations.

After the transfer properties of the detectors are unveiled, a detection switching (DSW) methodology is proposed and the switching criterion based on cross entropy (CE) is derived. By employing DSW, the performance of an iterative receiver with a list sphere detector (LSD) of a small list size is considerably improved. It is shown that the iterative receiver achieves a performance very close to that with a maximum a posteriori probability (MAP) detector but with a significantly reduced complexity.

For an iterative receiver with more than two components, various iteration schedules are explored. The schedules are applied in an iterative receiver with PIC-DSC. It is shown that the iterative receiver with a periodic scheduling outperforms that with the conventional scheduling at the same level of complexity.

Contents

List of Figures

List of Tables

Chapter 1

Introduction

1.1 Literature Review

Nowadays, wireless communication is playing a roll of ever increasing importance in our everyday lives. New wireless services such as mobile Internet with multimedia streaming are making their ways to the market. In this background, the availability of low-cost equipment providing high transmission quality and efficient spectrum utilization is crucial to the success of these services. Thanks to the overwhelming performance improvements as well as the cost-reduction in the electronic devices, a great deal of major theoretical developments can be put into practice.

The major constraints on the performance of the wireless communication systems are the channel effects such as noise, interferences and fading which distort the transmitted signals. The most straightforward approaches to level up the reliability as well as the speed of data transmission are to increase the transmit power and to use a larger bandwidth. However, these two resources are so expensive that high *power efficiency* and high *spectral efficiency* [1] are invariably desirable.

In 1948, Shannon established the fundamental limits on the transmission rates in digital communications [3, 4]. This inspired the research on error control coding (ECC) techniques to approach the capacity limits. The milestone of the ECC development

is the turbo coding technique which is proposed by Berrou and Glavieux in 1993. By employing a parallel concatenated convolutional code, named as a turbo code, the gap between the achievable channel utilization and the capacity limits of an additive white Gaussian noise (AWGN) channel is almost closed [6]. However, even the near-capacity performance of a single-transmit-single-receive antenna wireless system can not meet the required spectral efficiency for some applications such as the home Audio/Visual (A/V) networks. In this background, many advanced technologies are explored in order to achieve a higher spectral efficiency.

Multiple-input-multiple-output (MIMO) wireless is an emerging cost-effective technology that offers multiple-fold capacity than the conventional single-antenna wireless systems [7, 40]. By introducing antenna arrays at both transmitter and receiver, MIMO system enables increased achievable spectral efficiency and reliability for a given total transmit power. To approach the capacity of MIMO channels, space-time coding (STC) and related signal processing techniques have evolved into one of the most exciting research areas in wireless communications.

Initially, the designing of joint space-time dependencies in transmitted signals which endeavors to optimize the diversity [5] and coding gain [3] is of the greatest interests. The earlier research involves code design such as Alamouti space-time codes [31], space-time block codes (STBCs) and space-time trellis codes (STTCs) [25]. Recently, concentration has been shifted to independent multiple antenna transmissions which do not execute coding across antennas. The concept of bit-interleaved-coded-modulation (BICM) [26] are extended to MIMO cases and the MIMO-BICM systems attract significant attentions.

To achieve the optimal performance of a MIMO-BICM system, a maximum likelihood receiver [9] featuring joint detection and decoding is required. Unfortunately, the maximum likelihood receiver is of a complexity exponential to the number of transmit antennas as well as the block length of the channel code (due to the bit interleaver [38]). For a system with a large number of transmit antennas and a channel code with

a moderate block length, the complexity is prohibitive. Henceforth, iterative receivers which decouple the detection and decoding are currently under intensive investigations. Although there is no theoretical proof that the performance of an iterative receiver converges to that of the optimal maximum likelihood receiver, the turbo-principle is tested to be very effective in this scenario [8].

A typical iterative receiver for MIMO-BICM involves a maximum a posteriori probability (MAP) detector, a decoder, a bit interleaver and a bit de-interleaver. Soft information is exchanged between the detector and the decoder in an iterative fashion and the overall complexity of the receiver is no longer exponential to the block length of the channel code. However, the complexity of the MAP detector is still exponential to the number of transmit antennas so that its implementation is still infeasible, for a system with a large number of antennas. To replace the MAP detector, various sub-optimal [32] detection approaches are proposed and are well-exploited.

1.2 Motivation

The receiver for a wireless system can be studied via union bounding techniques [1, 3, 4]. For an iterative receiver with a decoder which is itself concatenated, however, deriving the bounds becomes very tough. Moreover, the union bounds may fail to predict the performance of an iterative receiver with a reduced-complexity detector in conjunction with a concatenated decoder, due to the high probability that the iterative processing does not converge to successful decoding. Therefore, empirical methods have been widely applied to tracking the iterative decoding in practice.

There have been many algorithms proposed for the MIMO detection. Among those, the one with the best performance and complexity trade-off has yet to be found for the iterative receivers. Moreover, the best iteration schedule [33] has yet to be discovered for an iterative receiver with more than two components.

1.3 Contribution

We conduct our research based on the iterative receivers with several kinds of detections and various channel codes. We apply the union bound technique to predict the bit error probability (BEP) of the iterative receiver with a parallel interference canceller (PIC) in conjunction with a decision statistics combining (DSC) (which is also referred to as an iterative PIC-DSC receiver) over a slow Rayleigh fading MIMO channel. A good match between the analytical bound and the simulated performance is presented.

We study the convergence behaviors of the iterative receivers via the evolution of the variances. For a fast fading channel, the "waterfall region" [10][30] of an iterative receiver is predicted. For a slow fading channel, we show that the performance of an iterative receiver is essentially limited by the *early interception ratio* defined in Chapter 4. After the transfer properties of the detectors are unveiled, a detection switching methodology (which performs switching between a list sphere detector and a PIC-DSC in the iterative receiver) is proposed and the switching criterion based on cross entropy is derived. We show a significant complexity-reduction by employing the detection switching.

For an iterative receiver with more than two components, iteration schedules are studied. In terms of performance and complexity trade-off, we show that an iterative PIC-DSC receiver with a periodic scheduling clearly outperforms that with the conventional scheduling.

1.4 Dissertation Overview

The dissertation is organized as the following. In Chapter 2, we investigate the channel codes which are used throughout the studies for the MIMO-BICM systems. In the first place, we introduce the convolutional codes and quantify the complexities. The recursive systematic convolutional codes and the non-systematic convolutional codes

are compared. Afterwards, the iterative decoding for a turbo code and a stopping criterion based on cross entropy are studied.

We start the Chapter 3 with the description of MIMO systems and space-time coding techniques. The iterative receiver with a MAP detector are studied and we see how a list sphere detector (LSD) [8] can provide a performance close to that of a MAP detector but with significantly reduced complexity. Subsequently, we present an iterative receiver with PIC-DSC, and derive a performance bound on its bit error probability. After that, a summary of this chapter is given.

In chapter 4, we present the approaches for tracking the convergence behaviors of the iterative receivers. We introduce two empirical measurements which are the mutual information [10] and variance [14]. The convergence behaviors of the decoders are presented via variance exchange graphs. After that, we derive the variance transfer function of PIC and depict that for LSD. Later, the convergence behaviors of the iterative receivers for MIMO-BICM are investigated via variance exchange graphs. Subsequently, we re-visit the complexity issue for the MIMO detection and propose a detection switching. The switching criterion based on cross entropy is derived. Finally, we present the simulation results and discuss the complexities of various schemes.

In chapter 5, we investigate the scheduling for the iterative receivers with more than two components. A periodic scheduling and a master-slave scheduling are presented. Afterward, the applications in the iterative receivers are investigated.

In chapter 6, we summarized the results and make suggestions for the future works.

Chapter 2

Error Control Channel Coding

In 1940s, Shannon showed that for any given channel it is possible to transmit information at a rate, which is known as the capacity of the channel, with an arbitrarily small error rate. Moreover, he showed that one method to achieve the capacity is by adding redundant digits to the transmitted data.

Nowadays, error control coding techniques are widely used in digital communications and it is one of the main advantages of digital systems over analog systems. In wireless systems, the channel influences cause errors in the received signal. By assigning each message of k bits a codeword with n digits ($n > k$), the channel encoder introduces redundancy so as to reduce the reception errors quantified as *bit error rate* (BER), where $R_c = \frac{k}{n} < 1$ is called the *code rate*. The number of places in which two codewords differ is referred to as the *distance* which is useful to reflect the error-correction capability of the channel code.

The primary purpose of employing error control coding in wireless communications is to increase the reliability of transmission within the constraints of signal power and system bandwidth. As a result, the same BER can be achieved with a smaller SNR in a coded system than in an un-coded system. The improved power efficiency by employing a coded system is measured by *coding gain.* Generally, a coded system yields a larger coding gain at lower BERs (or higher SNRs). At a very low SNR,

however, negative coding gains are found for coded systems and this phenomenon is due to the threshold effect [3].

In this chapter, we begin our study with convolutional codes. The non-systematic convolutional (NSC) codes and recursive systematic convolutional (RSC) codes are described and compared. After that, the popular turbo codes (TC) are narrated. The complexity issue of the turbo decoder is discussed and a stopping criterion for iterative decoders is introduced.

2.1 Convolutional Codes

The distinguishing feature of a convolutional code over a block code [1]-[4] is that its current output block depends on one or more previous input blocks. For a convolutional code, it is no longer possible to divide the code stream into distinct codewords. Thus, we must consider the distance between the code sequences. The term *free distance*, which is defined as the smallest distance between any pair of code sequences commencing and finishing on the same states [3, 4], is frequently used in the study of convolutional codes.

2.1.1 Encoder

NSC Codes

Let us consider a rate $R_c = \frac{1}{2}$ NSC encoder as shown in Figure 2.1. The binary un-coded message (or information) sequence is given by

$$\mathbf{u} = (u_1, u_2, u_3, \ldots, u_t, \ldots, u_\tau), u_t \in \{0, 1\} \tag{2.1}$$

where t is the index for a time instant and τ is the length of the message sequence. The output coded digits are denoted by

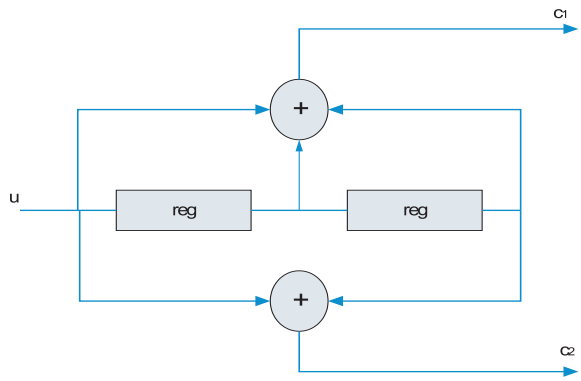

Figure 2.1: A code rate R_c=1/2, memory order $m = 2$ NSC encoder with generator $[7, 5]_8$.

$$\begin{aligned} \mathbf{c}^{(1)} &= (c_1^{(1)}, c_2^{(1)}, c_3^{(1)}, \ldots, c_t^{(1)}, \ldots, c_\Gamma^{(1)}) \\ \mathbf{c}^{(2)} &= (c_1^{(2)}, c_2^{(2)}, c_3^{(2)}, \ldots, c_t^{(2)}, \ldots, c_\Gamma^{(2)}) \end{aligned} \tag{2.2}$$

where $c_t^{(1)}$ and $c_t^{(2)}$ are the encoded digits from the first and second output branch of the encoder. The relation of the encoded digits and the input message bits are

$$\begin{aligned} c_t^{(1)} &= u_t + u_{t-1} + u_{t-2} \\ c_t^{(2)} &= u_t + u_{t-2} \end{aligned} \tag{2.3}$$

where "+" stands for a modulo-2 addition. We see that the encoder stores two most recent message bits, so we say that the *memory order* of this encoder is $m = 2$ and the *constraint length* of the code is $\upsilon = m + 1$. Each branch of the encoder has a coded sequence which consists of $\Gamma = \tau + m$ binary coded digits. We may describe the connections between the shift register elements and the modulo-2 adders by the following two *generator sequences*

$$\begin{aligned} \mathbf{g}^{(1)} &= (g_1^{(1)}, g_2^{(1)}, g_3^{(1)}) = (111) \\ \mathbf{g}^{(2)} &= (g_1^{(2)}, g_2^{(2)}, g_3^{(2)}) = (101) \end{aligned} \tag{2.4}$$

where $\mathbf{g}^{(1)}$ corresponds to the upper connections and $\mathbf{g}^{(2)}$ is for the lower connections. The equivalent octal representations of the two generator sequences are 7_8 and 5_8. For brevity, we refer to this code as NSC $[7, 5]_8$.

By convolving the input message sequence and the generator sequences, we obtain the output sequences which can be written as

$$\begin{aligned} \mathbf{c}^{(1)} &= \mathbf{u} * \mathbf{g}^{(1)} \\ \mathbf{c}^{(2)} &= \mathbf{u} * \mathbf{g}^{(2)} \end{aligned} \tag{2.5}$$

where "$*$" denotes the convolution operation. The input and output sequences can be represented as $\mathbf{u}(D)$, $\mathbf{c}^{(1)}(D)$, $\mathbf{c}^{(2)}(D)$. Then, we have

$$\begin{aligned} \mathbf{u}(D) &= u_1 + u_2 D + u_3 D^2 \\ \mathbf{c}^{(1)}(D) &= c_1^{(1)} + c_2^{(1)} D + c_3^{(1)} D^2 \\ \mathbf{c}^{(2)}(D) &= c_1^{(2)} + c_2^{(2)} D + c_3^{(2)} D^2 \end{aligned} \tag{2.6}$$

where the multiplication by D corresponds to delay by one input block period. The shift register of length m can be represented by polynomials as follows:

$$\begin{aligned} \mathbf{g}^{(1)}(D) &= 1 + D + D^2 \\ \mathbf{g}^{(2)}(D) &= 1 + D^2 \end{aligned} \tag{2.7}$$

which are called the *generator polynomials*. By arranging the generator polynomials of a convolutional code into a matrix, we get

$$\mathbf{G}(D) = \left[1 + D + D^2, 1 + D^2\right] \tag{2.8}$$

which is called the *generator matrix*. Then, the encoding operation can be simplified

as:

$$\mathbf{C}(D) = \mathbf{u}(D)\mathbf{G}(D) \tag{2.9}$$

RSC Codes

In a *systematic* convolutional code [3, 4], the first output sequence is the replica of the information sequence. The generator matrix can then be represented as

$$\mathbf{G}(D) = [\mathbf{I}, \mathbf{P}(D)] \tag{2.10}$$

where $\mathbf{I}$ is a identity matrix. It is shown [3] that if the generator matrix is represented as

$$\mathbf{G}(D) = [\mathbf{T}(D), \mathbf{S}(D)] \tag{2.11}$$

the equivalent systematic generator matrix is

$$\mathbf{G}_{sys}(D) = \left[\mathbf{I}, \mathbf{T}^{-1}(D)\mathbf{G}(D)\right] \tag{2.12}$$

The equivalent systematic encoder is shown in Figure 2.2. The encoded digits from

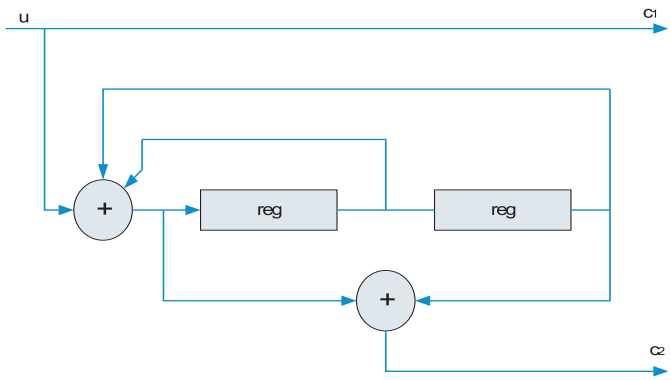

Figure 2.2: A code rate R_c=1/2, memory order $m = 2$ RSC encoder with generator $[1, 5/7]_8$.

the first output branch are the replica of the input message bits and we refer to it as *systematic bits*. The code is called a *recursive systematic convolutional* (RSC) code in

that there are feedback connections in the structure of the encoder. For brevity, we denote this code by RSC $[1, 5/7]_8$.

The encoding operation can also be modelled as a discrete time finite-state Markov process [1] begins at the initial state $S_0 = 0$ and and finishes at the terminal state $S_\Gamma = 0$, where the number of states in the trellis diagram [4] is M_s.

2.1.2 Decoder

System Model

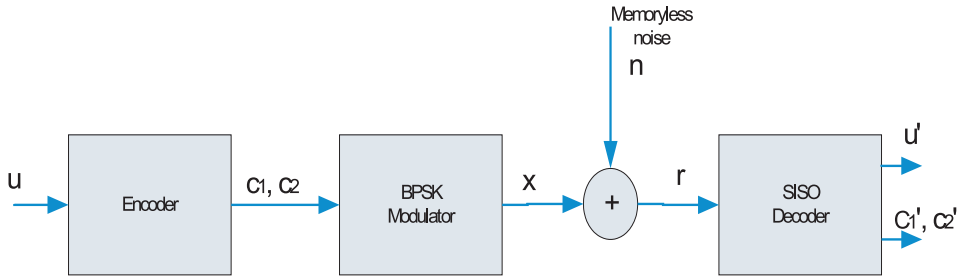

Figure 2.3: A model of a coded system with BPSK on a AWGN channel.

The model of a coded system is shown in Figure 2.3. The encoded sequence is modulated by a binary-phase-shift-keying (BPSK) modulator and the modulated sequence is denoted by

$$\mathbf{x}_1^\Gamma = (\mathbf{x}_1, ...\mathbf{x}_t, ..., \mathbf{x}_\Gamma) \tag{2.13}$$

where $\mathbf{x}_t = [x_t^{(0)}, x_t^{(1)}, ..., x_t^{(n-1)}]$. The modulated sequence $\mathbf{x}_1^\Gamma$ is corrupted by AWGN and the received sequence is $\mathbf{r}_1^\Gamma = (\mathbf{r}_1, ...\mathbf{r}_t, ..., \mathbf{r}_\Gamma)$ where $\mathbf{r}_t = [r_t^{(0)}, r_t^{(1)}, ..., r_t^{(n-1)}]$. By examining the received sequence $\mathbf{r}_1^\Gamma$, the soft-input-soft-output (SISO) decoder yields an estimate of the input message sequence as well as the estimate of the coded sequence .

Decoding Operation

In this dissertation, we consider the SISO maximum a posteriori probability (MAP) algorithm for decoding. The MAP algorithm minimizes the bit error probability by estimating the soft output in the form of the a posteriori probability (APP). Based on the received sequence $\mathbf{r}$, the decoder computes the log-likelihood ratio (LLR) of a bit given by

$$\Lambda(u_t) = \log \frac{P\left(u_t = 1|\mathbf{r}_1^\Gamma\right)}{P\left(u_t = 0|\mathbf{r}_1^\Gamma\right)} \tag{2.14}$$

and makes a hard decision on that bit by

$$\widetilde{u}_t = \begin{cases} 1 & \text{if } \Lambda(u_t) \geq \mathbf{0} \\ 0 & \text{if } \Lambda(u_t) < \mathbf{0} \end{cases} \tag{2.15}$$

We denote the transition probabilities as

$$P(\mathbf{r_1^\Gamma}|\mathbf{x_1^\Gamma}) = \prod_{t=1}^{\Gamma} R(\mathbf{r}_t|\mathbf{x}_t) \tag{2.16}$$

where

$$R(\mathbf{r}_t|\mathbf{x}_t) = \prod_{i=0}^{n-1} p(r_t^{(i)}|x_t^{(i)}) \tag{2.17}$$

For an AWGN channel with variance σ_w^2, we have

$$p(r_t^{(i)}|x_t^{(i)} = j) = \frac{1}{\sqrt{2\pi}\sigma_w} e^{-\frac{(r_t^{(i)}-j)^2}{2\sigma_w^2}} \tag{2.18}$$

where $j \in \{0, 1\}$. The APP of a message bit can be computed by

$$P(u_t = j|\mathbf{r_1^\Gamma}) = \sum_{(s',s)\in B_t^j} P\left(S_{t-1} = s', S_t = s|\mathbf{r}_1^\Gamma\right) = \sum_{(s',s)\in B_t^j} \frac{P\left(S_{t-1} = s', S_t = s, \mathbf{r}_1^\Gamma\right)}{P\left(\mathbf{r}_1^\Gamma\right)} \tag{2.19}$$

where $0 \leq s', s \leq M_s - 1$ are the states in the trellis. B_t^j is the set of transitions $s\prime \rightarrow s$ that are caused by input bit $u_t = j$. We define $\varphi_t(s', s) = P\left(S_{t-1} = s', S_t = s, \mathbf{r}_1^{\Gamma}\right)$. Then, the LLR can be written as

$$\Lambda(u_t) = \log \frac{\sum\limits_{(s',s)\in B_t^1} \varphi_t(s', s)}{\sum\limits_{(s',s)\in B_t^0} \varphi_t(s', s)} \tag{2.20}$$

To compute the joint probability $\varphi_t(s', s)$, we make the following definitions

$$\alpha_t(s) = P\left(S_t = s, \mathbf{r_1^t}\right) \tag{2.21}$$

$$\beta_t(s) = P\left(\mathbf{r_{t+1}^{\Gamma}} | S_t = s\right) \tag{2.22}$$

and

$$\gamma^j(s', s) = P\left(u_t = j, S_t = s, \mathbf{r}_t | S_{t-1} = s'\right) \tag{2.23}$$

Then, the LLR can be given as

$$\Lambda(u_t) = \log \frac{\sum\limits_{(s',s)\in B_t^1} \alpha_{t-1}(s')\gamma^1(s', s)\beta_t(s)}{\sum\limits_{(s',s)\in B_t^0} \alpha_{t-1}(s')\gamma^0(s', s)\beta_t(s)} \tag{2.24}$$

The definitions in (2.21)-(2.23) are derived as follows. We may write

$$\gamma_t^j(s', s) = \begin{cases} p_t(j) \exp\left(-\frac{\sum_{i=0}^{n-1}\left(r_t^{(i)} - x_{t,j}^{(i)}(s)\right)^2}{2\sigma_w^2}\right) & \text{for } (s', s) \in B_t^j \\ 0 & \text{otherwise} \end{cases} \tag{2.25}$$

where $p_t(j)$ is the a priori probability of $u_t = j$, $j \in \{0, 1\}$ and $x_{t,j}^{(i)}(s)$ is the encoder output associated with the transition $s\prime \rightarrow s$ and input $u_t = j$.

The $\alpha_t(s)$ can be written as

$$\alpha_t(s) = P(S_t = s, \mathbf{r_1^\Gamma}) = \sum_{s'=0}^{M_s-1} \alpha_{t-1}(s') \sum_{j\in\{0,1\}} \gamma_t^j(s', s) \tag{2.26}$$

which can be computed via a *forward recursion* [3]. The initial conditions are $\alpha_0(0) = 1$ and $\alpha_0(s) = 0, s \neq 0$.

The $\beta_t(s)$ can be written as

$$\beta_t(s) = P(\mathbf{r_{t+1}^\Gamma}|S_t = s) = \sum_{s'=0}^{M_s-1} \beta_{t+1}(s') \sum_{j\in\{0,1\}} \gamma_{t+1}^j(s, s') \tag{2.27}$$

and it can be computed via a *backward recursion.* The conditions for $t = \Gamma$ are $\beta_\Gamma(0) = 1$ and $\beta_\Gamma(s) = 0, s \neq 0$.

2.1.3 Performance

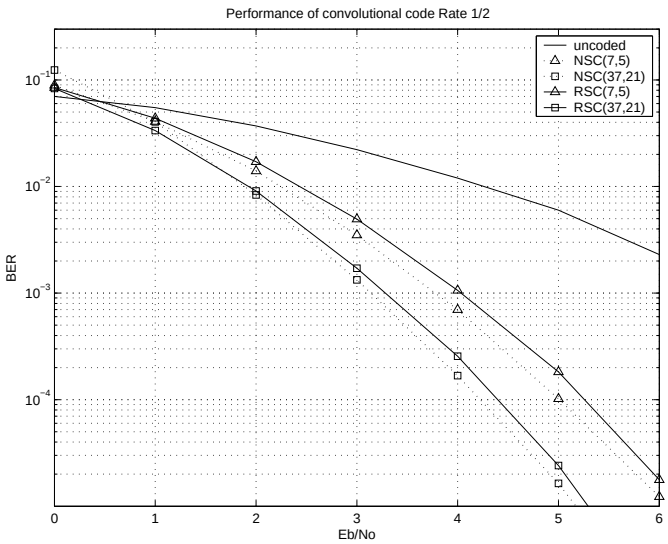

Figure 2.4: Performance of NSC $[7, 5]_8$ and RSC $[1, 5/7]_8$ with code rate R_c=1/2.

To illustrate the performance of convolutional codes, the BERs of NSC codes and RSC codes with $R_c = \frac{1}{2}$ on an AWGN channel are plotted in Figure 2.4. (Throughout the thesis, the E_b/N_o in dB is used to specify the SNR.) We observe that the coding

gain by applying the NSC $[37, 21]_8$ ($m = 4$) is about 0.8dB larger than that with NSC $[7, 5]_8$ ($m = 2$), at a BER=10^{-5}. Thus, we may say that a NSC code with a larger memory order outperforms a NSC code with a smaller memory order at a high SNR (or low BER). At a low SNR, on the other hand, we see that the coded systems have negative coding gains over the un-coded systems. Also, the NSC code with smaller memory order outperforms that with a larger memory order. The same phenomena are observed for the RSC decoders. Moreover, we observe that a NSC code performs better than its equivalent RSC ("equivalent" means that the NSC and RSC are of the same generator polynomial) at SNRs whereas it performs worse than its equivalent RSC code at low SNRs.

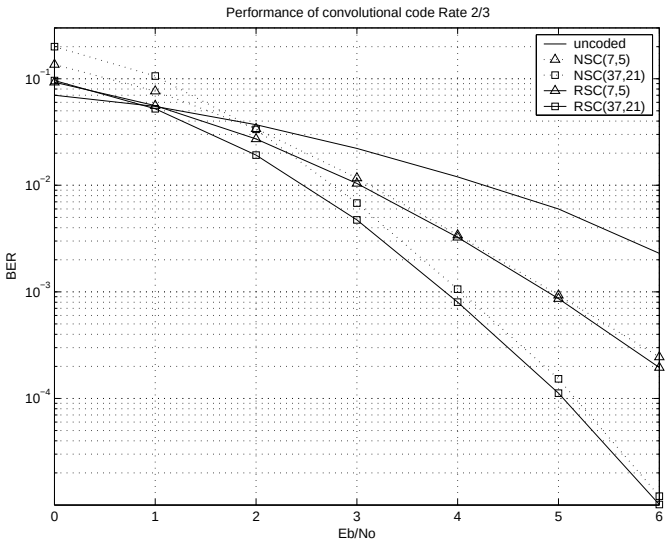

Figure 2.5: Performance of NSC $[7, 5]_8$ and RSC $[1, 5/7]_8$ with code rate R_c=2/3.

The performance of the codes of rate $R_c = 2/3$ are plotted in Figure 2.5, where the higher rate codes are acquired by puncturing [3][4] the codes with $R_c = 1/2$. It is observed that a RSC code with $R_c = 2/3$ performs better than its equivalent NSC code at all SNRs. This observation holds for the codes with $R_c \geq 2/3$ and that is the major reason why the NSC constituent codes are not adopted for turbo codes [6].

2.1.4 Complexity

In the evaluation of the overall complexity of the MAP decoder, we omit the complexity of conducting the exponential operation in (2.25) by assuming that prior to the MAP decoding, the received soft values have already been converted into probabilities via exponential operations. (We assume that part of complexity belongs to the detector or demodulator.) The complexity of a MAP decoder for one time unit is shown in Table. 2.1 [3]. From this table, we see that the complexity of a MAP decoder is exponential to the memory order of the code.

Addition	Multiplication
$2 \cdot 2^k \cdot 2^m + 6$	$5 \cdot 2^k \cdot 2^m + 8$

Table 2.1: Complexity of MAP decoding.

Let us assume that an addition operation costs the same computation as a multiplication operation. Hence, we may say that an addition (or a multiplication) costs 1 *computation unit* (CU). Considering an encoder with $R_c = 1/2$ and one input branch ($k = 1$), the complexity per time unit of MAP decoding is quantified as $14(2^m + 1)$ CUs.

2.2 Turbo Codes

In the last section, the convolutional codes are studied. We see that the performance of a convolutional code can be improved by increasing the memory order. However, the performance of convolutional codes of high memory orders are still several dBs away from the channel capacity [1][4].

In 1993, significant excitement was aroused by a paper which presented codes that were claimed to be only 0.5dB away from the Shannon bound. These codes were named as "turbo codes" and they have become a major focus of coding research and applications.

2.2.1 Encoder

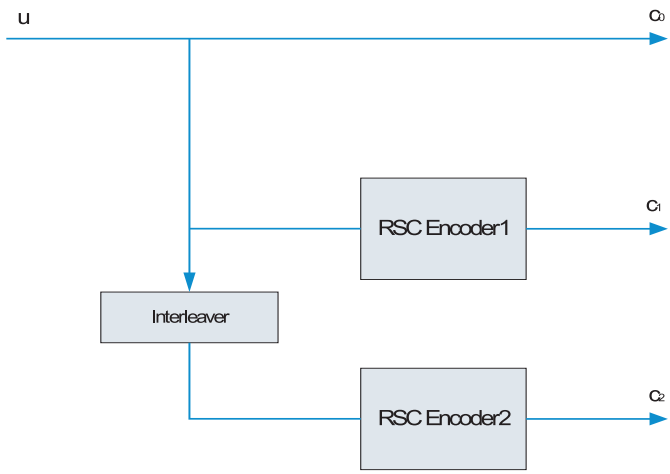

Figure 2.6: A parallel concatenated convolutional code (turbo code) encoder.

The encoder of a turbo code is virtually a parallel concatenated convolutional code (PCCC) encoder which is shown in Figure 2.6. Each of the two RSC encoders is of $R_c = \frac{1}{2}$ and the overall code rate of the turbo code is 1/3. A rate 1/2 turbo code can be obtained by puncturing the parity check digits of the constituent RSC codes [3][4][6]. For brevity, we denote the turbo code which consists of two identical RSC [1, 5/7]$_8$ constituent codes as TC [7, 5]$_8$. The asymmetric turbo code [30] which employs different RSC components are not studied in this dissertation.

Again, the un-coded binary message sequence is denoted by $\mathbf{u} = (u_1, u_2, u_3, \ldots, u_\tau)$, the output sequences from the first encoder are

$$\begin{aligned} \mathbf{c}^{(0)} &= (c_1^{(0)}, c_2^{(0)}, c_3^{(0)}, \ldots, c_t^{(0)}, \ldots, c_\Gamma^{(0)}) \\ \mathbf{c}^{(1)} &= (c_1^{(1)}, c_2^{(1)}, c_3^{(1)}, \ldots, c_t^{(1)}, \ldots, c_\Gamma^{(1)}) \end{aligned} \tag{2.28}$$

The first encoded stream is the replica of the input sequence followed by m tail digits which are used for the trellis termination [3, 4]. The second encoded stream is made up of the parity-check digits of the first encoder.

The interleaved message sequence, denoted by $\widetilde{\mathbf{u}}$, serves as the input to the second

RSC encoder. The encoded stream is made up of the parity-check digits of the second encoder, written as

$$\mathbf{c}^{(2)} = (c_1^{(2)}, c_2^{(2)}, c_3^{(2)}, \ldots, c_t^{(2)}, \ldots, c_\Gamma^{(2)}) \tag{2.29}$$

2.2.2 Iterative MAP Decoding of Turbo Codes

Let us assume the BPSK modulated sequence $\mathbf{x}_1^\Gamma = (\mathbf{x}_1, \mathbf{x}_2, ..., \mathbf{x}_\Gamma)$, where $\mathbf{x}_t = [x_t^{(0)}, ..., x_t^{(n-1)}]$, is corrupted by an AWGN channel and the received sequence is $\mathbf{r}_1^\Gamma = (\mathbf{r}_1, ...\mathbf{r}_t, ..., \mathbf{r}_\Gamma)$, where $\mathbf{r}_t = [r_t^{(0)}, r_t^{(1)}, ..., r_t^{(n-1)}]$.

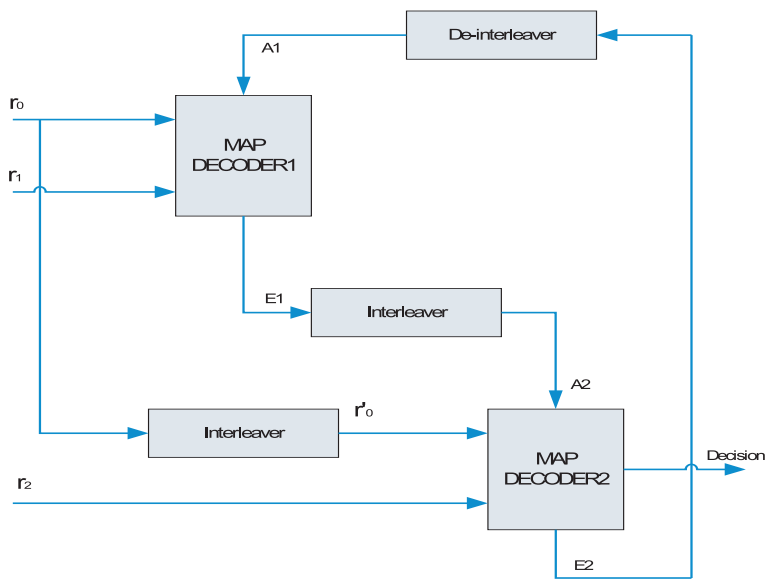

Figure 2.7: Structure of an iterative MAP decoder for turbo codes.

The iterative MAP decoder for turbo decoding is shown in Figure 2.7. The input sequence to the first decoder is denoted by

$$\mathbf{r}' = \left\{ (r_1^{(0)}, r_1^{(1)}), \cdots, (r_t^{(0)}, r_t^{(1)}), \cdots, (r_\Gamma^{(0)}, r_\Gamma^{(1)}) \right\} \tag{2.30}$$

The input sequence to the second decoder is

$$\mathbf{r}'' = \left\{ (\widetilde{r}_1^{(0)}, r_1^{(2)}), \cdots, (\widetilde{r}_t^{(0)}, r_t^{(2)}), \cdots, (\widetilde{r}_\Gamma^{(0)}, r_\Gamma^{(2)}) \right\} \tag{2.31}$$

where $\widetilde{\mathbf{r}}^{(0)} = (\widetilde{r}_1^{(0)}, \cdots, \widetilde{r}_t^{(0)}, \cdots, \widetilde{r}_\Gamma^{(0)})$ is the interleaved version of the systematic bits stream.

The turbo decoder involves two component RSC decoders which are concatenated via an interleaver and a de-interleaver. The first RSC decoder takes the input $\mathbf{r}'$ to produce a soft output. This output is interleaved and used to produce an improved estimate of the a priori probabilities (APRs) of the systematic bits for the second decoder. The second decoder takes the input $\mathbf{r}''$ as well as the APRs from the first decoder to yield another soft output sequence. The de-interleaved soft sequence is feedback to the first decoder and serves as the a priori information to improve the soft output of the first decoder, for the next decoding iteration. Subsequently, the second decoder takes the refined a priori probabilities to improve its soft output ... The iteration continues until the maximum number of iterations is reached.

At the kth decoding iteration, the LLR of the APP (a posteriori LLR) from the first MAP decoder is given by [3]

$$\Lambda_1^k(u_t) = \log \frac{\sum\limits_{(s',s)\in B_t^1} \alpha_{t-1}^k(s') p_t^{1,k}(1) \exp\left(-\frac{\sum_{i=0}^{n-1}\left(r_t^{(i)} - x_{t,1}^{(i)}(s)\right)^2}{2\sigma_w^2}\right) \beta_t^k(s)}{\sum\limits_{(s',s)\in B_t^0} \alpha_{t-1}^k(s') p_t^{1,k}(0) \exp\left(-\frac{\sum_{i=0}^{n-1}\left(r_t^{(i)} - x_{t,0}^{(i)}(s)\right)^2}{2\sigma_w^2}\right) \beta_t^k(s)} \tag{2.32}$$

where $p_t^{1,k}(j)$ is the a priori probabilities for $u_t = j$ acquired from the output of the second MAP decoder in the $(k-1)$th decoding iteration. The initial values for the a priori probabilities are $p_t^{1,k=1}(1) = p_t^{1,k=1}(0) = 0.5, t \in \{1, ..., \Gamma\}$. To extract the a priori information from the APP, we rewrite (2. 32) as the following

$$\begin{aligned}
\Lambda_1^k(u_t) &= \log \frac{p_t^{1,k}(1)}{p_t^{1,k}(0)} + \log \frac{\sum\limits_{(s',s)\in B_t^1} \alpha_{t-1}^k(s') \exp\left(-\frac{\left(r_t^{(0)} - x_{t,0}^{(0)}\right)^2 + \sum_{i=1}^{n-1}\left(r_t^{(i)} - x_{t,1}^{(i)}(s)\right)^2}{2\sigma_w^2}\right) \beta_t^k(s)}{\sum\limits_{(s',s)\in B_t^0} \alpha_{t-1}^k(s') \exp\left(-\frac{\left(r_t^{(0)} - x_{t,1}^{(0)}\right)^2 + \sum_{i=1}^{n-1}\left(r_t^{(i)} - x_{t,0}^{(i)}(s)\right)^2}{2\sigma_w^2}\right) \beta_t^k(s)} \\
&= \log \frac{p_t^{1,k}(1)}{p_t^{1,k}(0)} + \frac{2}{\sigma_w^2} r_t^0 + \Lambda_{1e}^k(u_t) \qquad (2.33)
\end{aligned}$$

where

$$\Lambda_{1e}^{k}(u_t)= \log\frac{\sum\limits_{(s',s)\in B_t^1} \alpha_{t-1}(s')\exp\left(-\frac{\sum_{i=1}^{n-1}\left(r_t^{(i)}-x_{t,1}^{(i)}(s)\right)^2}{2\sigma_w^2}\right)\beta_t(s)}{\sum\limits_{(s',s)\in B_t^0} \alpha_{t-1}(s')\exp\left(-\frac{\sum_{i=1}^{n-1}\left(r_t^{(i)}-x_{t,0}^{(i)}(s)\right)^2}{2\sigma_w^2}\right)\beta_t(s)} \tag{2.34}$$

$\Lambda_{1e}(u_t)$ is referred to as the LLR value of the *extrinsic information* (EXT) or the extrinsic LLR value. We see that the extrinsic LLR generated by the first decoder is a function of its parity check digits and does not correlate with the systematic bits. Therefore, the $\widetilde{\Lambda}_{1e}(u_t)$**,** which is the interleaved version of $\Lambda_{1e}(u_t)$, does not correlated with $\widetilde{\mathbf{r}}_0$ and it can be used as a priori knowledge by the second MAP decoder.

The a priori probabilities to the second decoder can be obtained from the extrinsic LLR as

$$p_t^{2,k}(1) = \frac{e^{\widetilde{\mathbf{\Lambda}}_{1e}^{k}(u_t)}}{1+e^{\widetilde{\mathbf{\Lambda}}_{1e}(u_t)}},\ p_t^{2,k}(0) = \frac{1}{1+e^{\widetilde{\mathbf{\Lambda}}_{1e}^{k}(u_t)}} \tag{2.35}$$

In the second decoding stage, the a posteriori LLR is computed as

$$\begin{aligned}\Lambda_2^k(u_t) &= \log\frac{p_t^{2,k}(1)}{p_t^{2,k}(0)} + \frac{2}{\sigma_w^2}\widetilde{r}_t^{(0)} + \Lambda_{2e}^k(u_t)\\ &= \widetilde{\Lambda}_{1e}^k(u_t) + \frac{2}{\sigma_w^2}\widetilde{r}_t^{(0)} + \Lambda_{2e}^k(u_t)\end{aligned} \tag{2.36}$$

where $\Lambda_{2e}^k(u_t)$ is used to update the a priori information to the first decoder for the $(k+1)$th iteration, that

$$p_t^{1,k+1}(1) = \frac{e^{\widetilde{\Lambda}_{2e}^{k}(u_t)}}{1+e^{\widetilde{\Lambda}_{2e}(u_t)}},\ p_t^{1,k+1}(0) = \frac{1}{1+e^{\widetilde{\Lambda}_{2e}^{k}(u_t)}} \tag{2.37}$$

2.2.3 Performance

The performance of the turbo codes of $R_c = 1/2$ and various memory orders is illustrated in Figure 2.8. For $E_b/N_o \in [0.6, 0.8]$, the BER of TC $[37,\ 21]_8$ promptly drops and this region is referred to as the *waterfall region* [30]. At BER=10^{-5}, the performance of TC $[37,\ 21]_8$ is less than 0.6dB away from the capacity limits. In addition, a

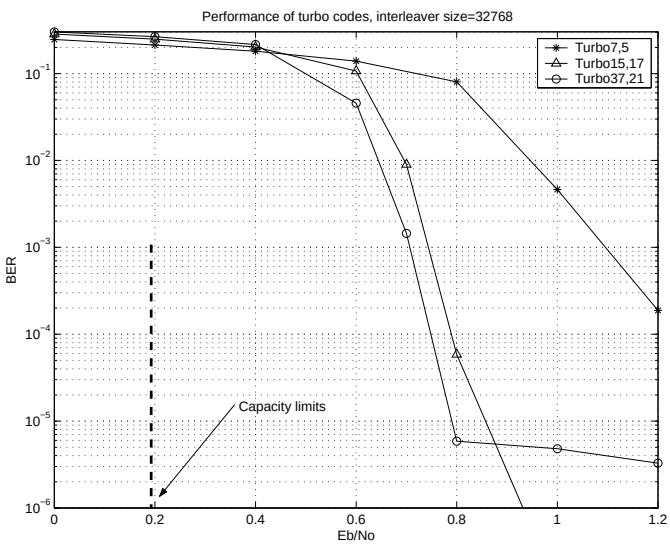

Figure 2.8: Performance of R_c=1/2 turbo codes with interleaver size=32768, the number of decoding iterations I_C=18.

significant error floor [30] is observed at BER between 10^{-5} and 10^{-6} and this region is referred to as the *error-floor region*. The performance of TC $[15, 17]_8$ is about 0.1dB worse than that of TC $[37, 21]_8$ at BER=10^{-5} and no error floor is observed at BER$\geq$ 10^{-6}. The performance of TC $[7, 5]_8$ is about 0.5dB worse than that of TC $[37, 21]_8$ at BER=10^{-4}.

From the above observations, we may conclude that at high SNRs ($E_b/N_o > 0.5$dB), a turbo code with a larger memory order has a superior performance compared to that with a smaller memory order. This phenomenon is explained in [3] that increasing the memory order of component codes usually brings about increased free distance and effective free distance which dictate the behavior of the code at high SNRs.

At the low SNRs, it is observed that a turbo code with a smaller memory order works better than that with a larger memory order. This phenomenon is explained in [3] that the performance of turbo codes at low SNRs are dominated by error coefficients which are generally higher for codes with larger memory orders. In Chapter. 4, this phenomenon will be explained by the analysis of convergence behavior of the iterative decoding.

The performance of TC $[37, 21]_8$ with various interleaver sizes are shown in Figure

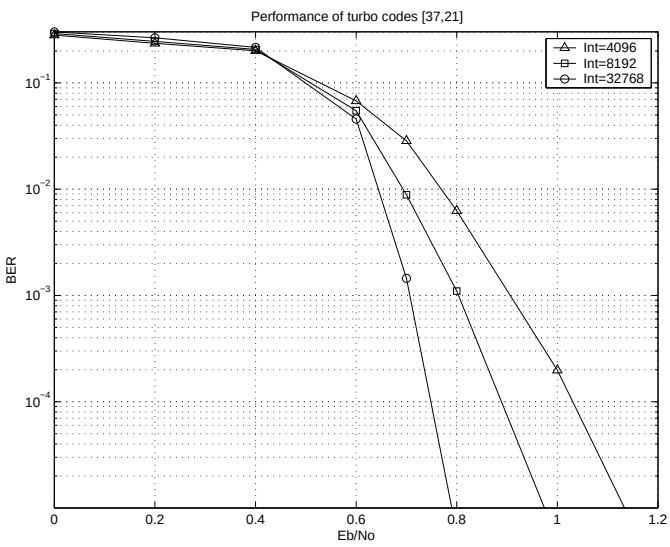

Figure 2.9: Performance of a R_c=1/2 turbo code $[37,21]_8$ with various interleaver sizes, the number of decoding iterations I_C=18.

2.9. At high SNRs, a TC with a larger interleaver size tends to bring about better performance. At low SNRs, the BERs of TC $[37, 21]_8$ with interleaver sizes larger than 4096 are almost identical.

2.2.4 Complexity

To evaluate the complexity of the iterative MAP decoding for the turbo codes, we omit the computations of the interleaving and de-interleaving operations so that the complexity of each turbo decoding iteration can be approximated as twice the complexity of a MAP decoding. Thus, the overall complexity is about $2I_C$ times of the MAP decoding, where I_C is the total number of iterations for each transmission frame. Therefore, the complexity of the turbo decoder is approximated as $28(2^m + 1)I_C$ CUs per time unit.

2.2.5 Stopping Criterion

For a turbo coded system, a fixed number I_C is often selected and each frame is decoded with I_C turbo decoding iterations. Generally, I_C is set according to the worst frame

examined. However, most frames do not need that many turbo decoding iterations to converge. In practice, a stopping criterion is adopted to avoid the unnecessary iterations of turbo decoding. To date, many stopping criteria are proposed in literature and a criterion based on cross-entropy (CE) [21] is of great interests in this thesis. Apart from the application in turbo decoding, this stopping criterion is also applicable to other concatenated systems which employ iterative processing.

Let us denote the extrinsic information of the systematic bits from the two RSC decoders at the kth decoding iteration by $q^{1,k}(u_t)$ and $q^{2,k}(u_t)$. The CE between the output extrinsic information of the two RSC decoders is represented as

$$T(k) = E_{q^{2,k}(u_t)}\left\{\log \frac{q^{2,k}(u_t)}{q^{1,k}(u_t)}\right\} \tag{2.38}$$

For a turbo code, we may assume that the extrinsic stream from the first RSC decoder and that from the second RSC decoder are statistical independent. Thus, the CE can be approximated as

$$\begin{aligned} T(k) &\approx \sum_t \log \frac{q_t^{2,k}(u_t)}{q^{1,k}(u_t)} = \sum_t \left\{ q^{2,k}(u_t=1)\log\frac{q^{2,k}(u_t=1)}{q^{1,k}(u_t=1)} + q_t^{2,k}(u_t=0)\log\frac{q^{2,k}(u_t=0)}{q^{1,k}(u_t=0)}\right\} \\ &= \sum_t \left\{ -\triangle\,\Lambda^k(u_t)\frac{1}{1+\exp(\Lambda_2^k(u_t))} + \log\frac{1+\exp(-\Lambda_1^k(u_t))}{1+\exp(-\Lambda_2^k(u_t))}\right\} \end{aligned} \tag{2.39}$$

where $\triangle\Lambda^k(u_t) = \Lambda_1^k(u_t) - \Lambda_2^k(u_t)$. If the decoding converges, we can make the following assumptions:

1) The sign of the LLR values are not likely to change anymore.

2) The magnitude of the LLR values are very large (so we have $log(1+x) \approx x$).

3) $\triangle\Lambda^k(u_t)$ has the same sign as u_t and it is of a small value.

Consider 1) and 3), (2.39) can be approximated as [21]

$$T(k) \approx \sum_t \left\{ -\widetilde{u}_t^k \triangle\,\Lambda^k(u_t)\frac{1}{1+\exp(\left|\Lambda_2^k(u_t)\right|)} + \log\frac{1+\exp(-\left|\Lambda_1^k(u_t)\right|)}{1+\exp(-\left|\Lambda_2^k(u_t)\right|)}\right\} \tag{2.40}$$

Consider 2), the CE can be finally simplified as

$$T(k) \approx \sum_t \frac{\left|\triangle\Lambda^k(u_t)\right|^2}{e^{(\left|\Lambda_1^k(u_t)\right|)}} \tag{2.41}$$

The BER performance of the TC $[37, 21]_8$ with stopping criterion is shown in Figure 2.10. In the simulations, we stop the decoding iterations once $T(k) \leq 0.001T(1)$. We see that the resultant performance degradation is very small.

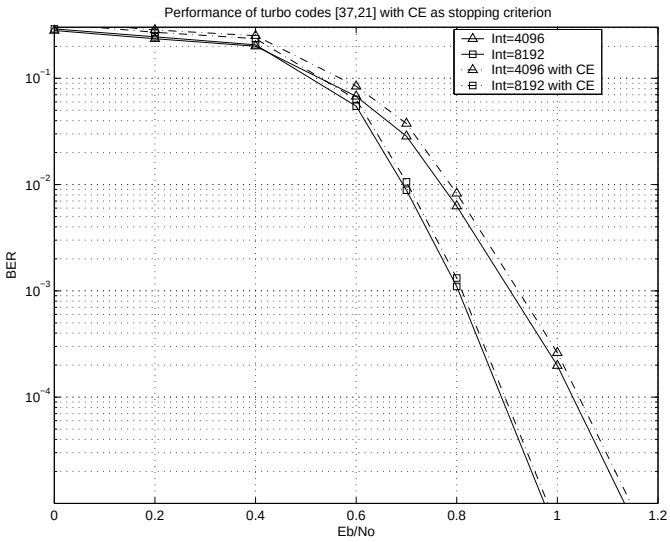

Figure 2.10: Performance of a R_c=1/2 turbo code $[37,21]_8$ with and without stopping criterion, maximum number of decoding iterations=18.

2.3 Summary

In this chapter, convolutional codes and turbo codes are briefly reviewed. We see that a stronger code performs better than a weaker code at high SNRs whereas it is another way round at low SNRs. While the performance of channel codes at high SNRs are of greater interests, the behaviors of the channel codes at all SNRs are required to be considered in concatenated systems such as MIMO-BICM systems. In the next chapter, we will explore the application of the channel codes in MIMO cases and investigate the methods to approach the capacities of MIMO channels.

Chapter 3

Iterative Receivers for the MIMO systems

3.1 Introduction to MIMO Systems

3.1.1 System Model and Capacity

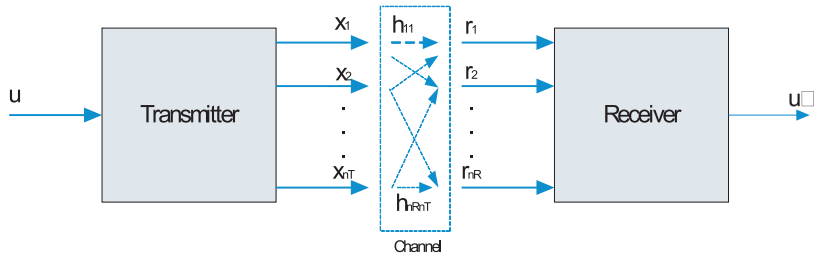

Figure 3.1: Block diagram of a MIMO system

System Model

Let us consider a complex baseband and discrete time MIMO system with n_T transmit and n_R receive antennas, as shown in Figure 3.1. Omitting the index of the time instant, the transmitted complex symbol at the ith transmit antenna is represented as x^i, $i \in \{1, 2, ..., n_T\}$. The transmitted symbols from all the transmit antennas

are represented by an column vector $\mathbf{x} = [x^1, x^2, ..., x^{n_T}]^T$ ($[\bullet]^T$ denotes the transpose operation) which can be referred to as a *hyper-symbol*. The entries of the symbols are chosen from a complex constellation with 2^M possible signal points, where $M \geq 1$ is called the *level* of digital modulation.

The channel is represented by a matrix $\mathbf{H}$ with size $n_R \times n_T$. The ji-th element of $\mathbf{H}$, denoted by h_{ji}, is the complex channel fading coefficient for the ith transmit to the jth receiver antenna, where $j \in \{1, 2, ..., n_R\}$ and $i \in \{1, 2, ..., n_T\}$. We assume that the received power for each antenna is equal to the total transmitted power so that the channel coefficients are constraint by $E[\sum_{i=1}^{n_T} |h_{ji}|^2] = n_T$.

The noise at the receiver is described by an $n_R \times 1$ column vector written as $\mathbf{n} = [n^1, ..., n^{n_R}]^T$. Its components are statistically independent complex zero-mean Gaussian variables and with independent real and imaginary parts. The variance per dimension is σ_w^2.

The received signals are represented by an $n_R \times 1$ column vector $\mathbf{r} = [r^1, ..., r^{n_R}]^T$. After coherent detection [1], the received vector can be written as

$$\mathbf{r} = \mathbf{H}\mathbf{x} + \mathbf{n} \tag{3.1}$$

In this dissertation, we assume that perfect knowledge of the channel coefficients, or channel state information (CSI) [3], is available to the receiver and the random channel coefficients follow the Rayleigh distribution [1]-[4]. Moreover, we assume that there are no antenna correlations so that each element in $\mathbf{H}$ is statistically independent from any other element.

Definition of SNR

Let us use ρ to denote the physically measured SNR that $\rho = E_s/2\sigma_w^2$ where E_s is the energy of a hyper symbol $\mathbf{x}$. We use the convention $N_o = 2\sigma_w^2$ and thus the SNR can be written as $\rho = E_s/N_o$. The average signal energy per transmitted complex symbol

from one antenna is E_s/n_T. The receive antennas collect a total energy of $n_R E_s$ on average and it is the energy for $n_T M$ coded digits or $n_T M R_c$ transmitted message (or information) bits. Therefore, the energy of one information bit is $E_b = \frac{n_R}{n_T M R_c} E_s$. The relation between E_b/N_o and E_s/N_o can be given as

$$E_b/N_o = \frac{n_R}{n_T M R_c} E_s/N_o \tag{3.2}$$

and to which we shall adhere throughout this dissertation.

Capacity

The system capacity is defined as the maximum possible spectral efficiency such that the probability of error is arbitrarily small. The instantaneous capacity [5][8] is given by

$$C = \log_2 \det\left(\mathbf{I}_n + \frac{\rho}{n_T}\mathbf{H}\mathbf{H}^H\right) = \log_2 \det\left(\mathbf{I}_n + \frac{E_s}{2n_T\sigma_w^2}\mathbf{H}\mathbf{H}^H\right) \tag{3.3}$$

where $\mathbf{I}_n$ is the identity matrix with $n = \min(n_R, n_T)$. For a fast fading channel, the capacity can be represented as the mean value of the instantaneous capacity, which is written as

$$C_f = E\left[\log_2 \det\left(\mathbf{I}_n + \frac{E_s}{2n_T\sigma_w^2}\mathbf{H}\mathbf{H}^H\right)\right] \tag{3.4}$$

For a slow fading channel, we use the term *outage probability*, denoted by P_o, to specify the probability of not achieving a certain capacity C_H. The outage probability is written as

$$P_o = P\left\{\log_2 \det\left(\mathbf{I}_n + \frac{E_s}{2n_T\sigma_w^2}\mathbf{H}\mathbf{H}^H\right) < C_H\right\} \tag{3.5}$$

The capacity of a 4 by 4 MIMO channel is plotted in Figure 3.2. On the left of this figure, we see that the capacity of a fast fading channel is an increasing function of the SNR. Moreover, the capacity with 4-QAM constraint [4][48] is smaller than the capacity of the MIMO channel and this difference becomes larger as the SNR increases.

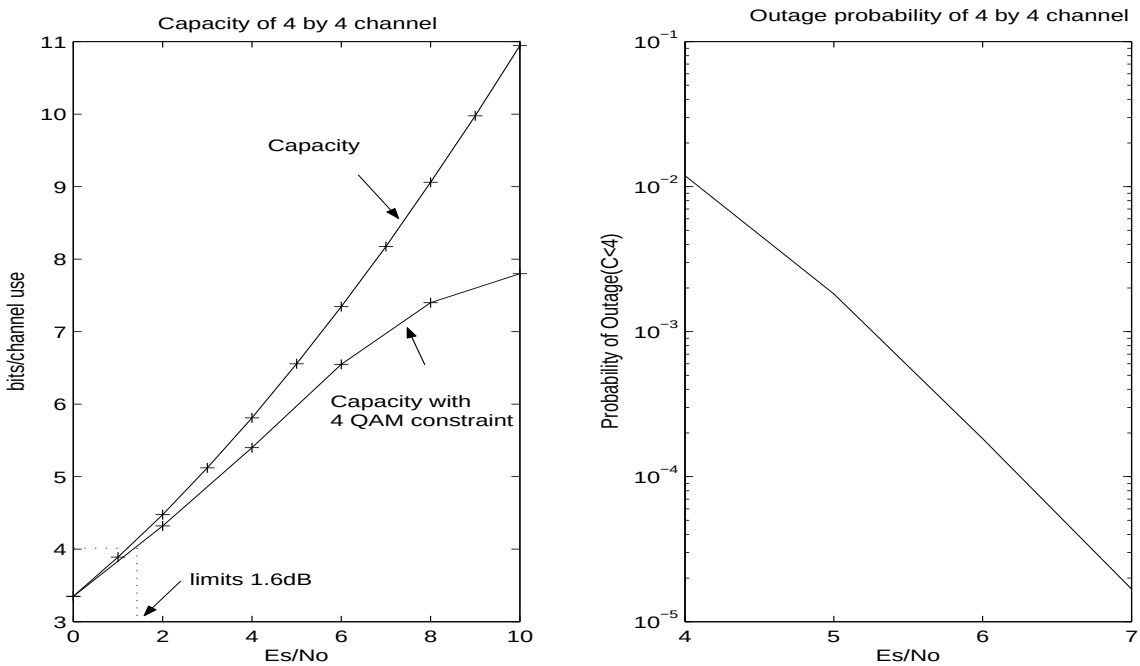

Figure 3.2: The left is the capacity of a 4 by 4 fast fading channel. The right is the probability that the capacity is smaller than 4 for a 4 by 4 slow fading channel.

For a 4 by 4 MIMO system with 4-QAM, we see that the minimum SNR for achieving a capacity of 4 bits per channel use is about 1.6dB. The outage capacity probability of a 4 by 4 slow fading MIMO channel is plotted on the right of this figure.

3.1.2 Space-Time Coding Approaches for MIMO Systems

Space-Time Trellis Codes

In order to approach the capacity of a MIMO channel, error control channel coding techniques are necessarily adopted. In the earlier stage, joint designing of error control coding, modulation, transmit and receive diversity was widely explored. Tarokh, Seshadri and Calderbank [25] introduced the space-time trellis codes (STTCs) and showed that the STTCs are able to simultaneously provide a substantial coding gain and diversity improvement.

Figure 3.2 and Figure 3.3 are the encoder and decoder architectures of a system with STTC. Binary message sequence is sent to the STTC encoder and a complex

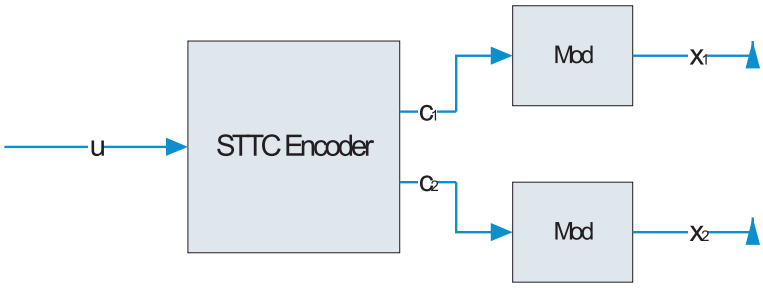

Figure 3.3: The architecture of an STTC encoder.

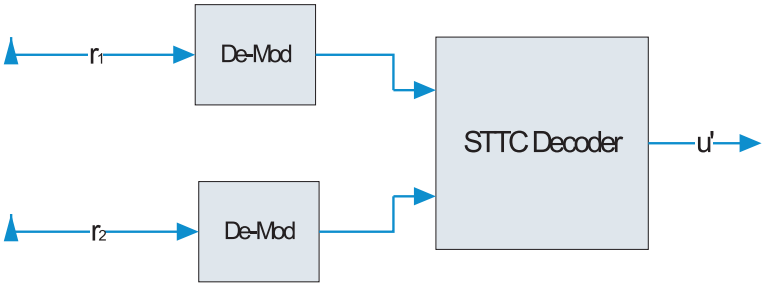

Figure 3.4: The architecture of an STTC decoder.

symbol for each antenna is generated from a code trellis. The encoding process is trying to maximize the diversity as well as the coding gain. The STTC decoder operates on the received signal and estimate the most likely transmitted information sequence.

The STTC schemes are designed specifically for operation in a quasi-static fading (slow fading) environment, where the channel remains constant for the whole frame while differing over frames. However, the assumption of slow fading conditions does not hold for the scenarios such as communication with high mobility and orthogonal-frequency-division-multiplexing (OFDM) with frequency domain interleaving, where the channel is more appropriately to be modelled as a fast fading channel. Unfortunately, the STTCs are signal-space codes and it is likely to give rise to poor performance in fast fading scenarios [9].

MIMO Bit-Interleaved-Coded-Modulation

The bit-interleaved-coded-modulation (BICM) systems are proposed in favor of a SISO system which undergoes fast fading [26]. This idea is now widely explored in MIMO cases as well. The transmitter architecture of a MIMO-BICM system is shown in Figure 3.5. The encoded sequence $\mathbf{c}$ is de-multiplexed into n_T streams and a cyclic-shifter

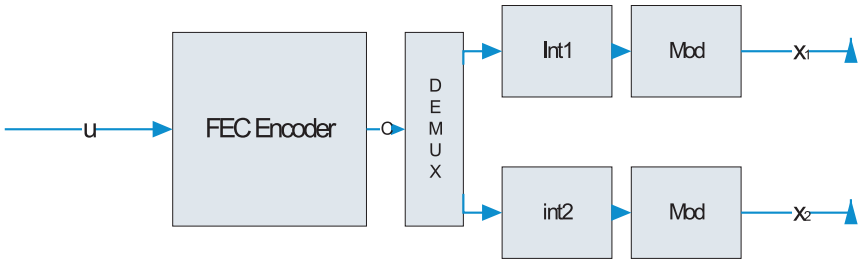

Figure 3.5: Transmitter architecture for MIMO-BICM systems.

is employed at the de-multiplexer for spatial interleaving [9]. Then, each stream is independently interleaved, modulated (with M-ary digital modulation) and transmitted by a separate antenna. Each hyper-symbol carries Mn_T coded digits which are written as $\mathbf{c} = [c_1, c_2, ..., ..., c_l, ..., c_{Mn_T}]^T$, $c_l \in \{-1, 1\}$. The modulator in Figure 3.5 is modelled by $\mathbf{x}$ =map($\mathbf{c}$) which maps the coded digits into constellation symbols.

At the receiver side, the best solution is to use a joint detector/decoder which computes the likelihood of each bit given all the knowledge of received complex signal vector $\mathbf{r}$ and the constraints imposed by the channel code. Such a receiver is referred to as a maximum likelihood (ML) receiver with which the MIMO-BICM systems are shown to outperform the STTCs for fast fading channels [9].

Unfortunately, the complexity of a ML receiver is prohibitive even for a channel code with moderate block length. Therefore, iterative receivers which decouple the detection and decoding are widely exploited. In such an iterative receiver, the MIMO detector incorporates soft information provided by the channel decoder to perform processing in spatial domain. The channel decoder operates with the soft information given by the MIMO detector to carry out time-domain processing. The soft information is exchanged between the detector and decoder in an iterative manner and

the operation of the receiver is usually referred to as *iterative detection and decoding* (IDD). Although there is no strict theoretical proof that the iterative receiver is necessarily converged to the optimal solution, the application of "turbo principle" in this scenario is tested to work very well.

A Preview of Iterative MIMO Receivers

An optimal iterative MIMO receiver should involve a MAP detector and a MAP decoder. For every time instant, the MAP detector computes the a posteriori probability (APP) of the coded digits conditioned on the received signal vector. Omitting the index of the time instant, the a posteriori LLR value from the MAP detector can be written as

$$\Lambda_D(c_l|\mathbf{r}) = \log \frac{p(c_l = 1|\mathbf{r})}{p(c_l = -1|\mathbf{r})} \tag{3.6}$$

where c_l is the lth coded digits in a hyper symbol. Considering the bit interleaver in Figure 3.5, we may assume that the bits within a hyper symbol are statistically independent of one another. Using the Bayes' theorem, (3.6) can be written as

$$\Lambda_D(c_l|\mathbf{r}) = \log \frac{\sum\limits_{\mathbf{c}\in\mathbb{C}_l,+1} p\left[\mathbf{r}|\mathbf{x} = \text{map}(\mathbf{c})\right] p(\mathbf{c})}{\sum\limits_{\mathbf{c}\in\mathbb{C}_l,-1} p\left[\mathbf{r}|\mathbf{x} = \text{map}(\mathbf{c})\right] p(\mathbf{c})} = \log \frac{\sum\limits_{\mathbf{c}\in\mathbb{C}_l,+1} p\left[\mathbf{r}|\mathbf{x} = \text{map}(\mathbf{c})\right] \exp \sum\limits_{j\in\mho} \Lambda_A(c_j)}{\sum\limits_{\mathbf{c}\in\mathbb{C}_l,-1} p\left[\mathbf{r}|\mathbf{x} = \text{map}(\mathbf{c})\right] \exp \sum\limits_{j\in\mho} \Lambda_A(c_j)} \tag{3.7}$$

where $\mathbb{C}_l, +1$ is the set of 2^{Mn_T-1} bit vectors $\mathbf{c}$ having $c_l = +1$ and $\mathbb{C}_l, -1$ is that with $c_l = -1$ ($\mathbb{C}$ is the set of 2^{Mn_T} bit vectors $\mathbf{c}$). $\mho$ is the set of indices j satisfies $\mho = \{j|j = 1, 2, .., Mn_T,\ c_j = 1\}$. $\Lambda_A(c_j)$ is the a priori LLR value provided by the MAP decoder in the previous receiver iteration. The likelihood function used in (3.7) is written as

$$p[\mathbf{r}|\mathbf{x} = \text{map}(\mathbf{c})] = \frac{\exp[-\frac{1}{2\sigma_w^2} \cdot |\mathbf{r} - \mathbf{H}\mathbf{x}|^2]}{(2\pi\sigma_w^2)^{n_R}} \tag{3.8}$$

To generate $\Lambda_D(c_l|\mathbf{r})$ in (3.7), the detector needs to compute the a priori probabilities for all the 2^{Mn_T} candidates. Therefore, the complexity of the MAP detector

is exponential to the number of transmit antennas n_T and the modulation level M. Thus, the complexity of an iterative receiver with MAP detector is still prohibitive for a MIMO system with a relatively large number of antennas and high-order modulations, although the complexity is no longer exponential to the block length of the channel code.

In this background, some computationally efficient detectors based on the MAP algorithm have been proposed [8][22][23]. Among those, list sphere detection (LSD) is of great interests in this dissertation. Instead of exhaustively computing the bit metrics, the LSD provide soft information by searching over a list of candidates where the size of the list determines the complexity of the detector. This kind of detector is also referred to as an "APP based detector" [22] and it is non-linear.

Some linear detectors such as parallel interference canceller (PIC) [5][19], minimum mean-square-error filter (MMSE) [18] and zero forcing detector (ZF) [17] for the MIMO-BICM systems are proposed. The complexity of these detectors are generally lower than the APP based detector due to their linearity. Since these detectors operate by performing interference suppression or cancellation (ISC), we refer to them as "ISC based detectors". The performance of ISC based receiver can be improved with some complexity increase, such as the MMSE detector with successive interference cancellation (MMSE-SIC) [45]. In this chapter, we consider the iterative receivers with a MAP detector, a LSD and a PIC.

3.2 Iterative receiver with a MAP detector

3.2.1 Architecture and Algorithm

The architecture of the iterative receiver with a MAP detector is shown in Figure 3.6 (which is also applicable to the iterative receivers with APP based detectors). In order to simplify the illustration, the multiplexing/de-multiplexing and spatial interleaving/spatial de-interleaving are included in the block of interleaving/de-interleaving.

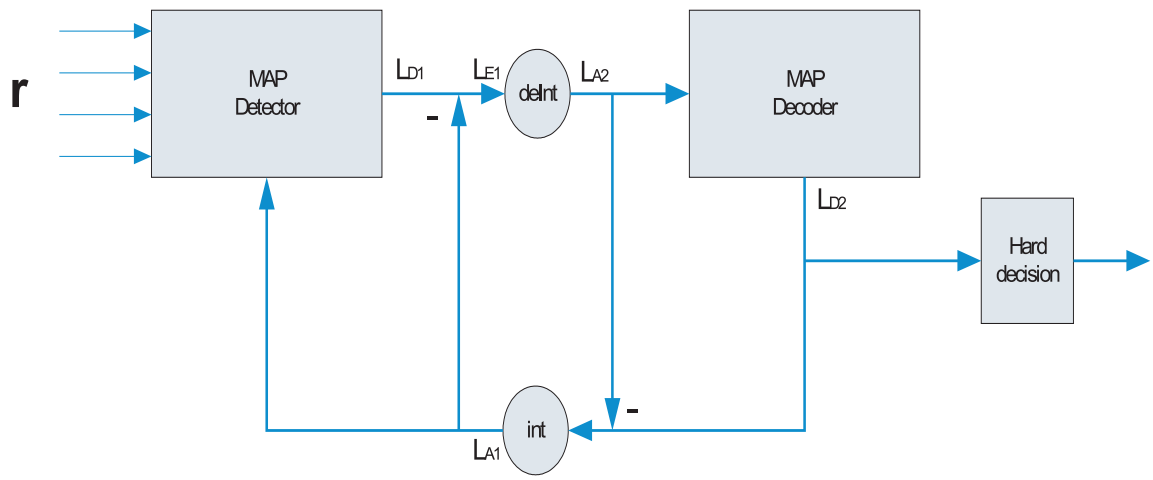

Figure 3.6: An iterative receiver with a MAP detector for a MIMO-BICM system.

Generally, the MAP detector can be viewed as an inner decoder and hence the architecture of the iterative receiver with MAP detector and a MAP decoder is analogous to the turbo decoder described in the previous chapter. Here, we call an iteration between the detector and decoder as a *receiver iteration* and use I_D to denote the total number of receiver iterations.

To distinguish the soft values of the detector and that of the decoder, we use Λ_{D1}^k to denote the a posteriori LLR value yielded by the detector and let Λ_{A1}^k represent the a priori LLR (which are provided by the decoder at the $(k-1)$th iteration) available at the detector, in the kth receiver iteration. We use Λ_{D2}^k to denote the a posteriori LLR generated by the decoder and let Λ_{A2}^k represent the a priori LLR available to the decoder.

By separating the a priori knowledge from the APP, the soft output of the MAP detector at kth receiver iteration can be written as

$$\Lambda_{D1}^k(c_l|\mathbf{r}) = \Lambda_{A1}^k(c_l) + \log \frac{\sum\limits_{\mathbf{c}\in\mathbb{C}_l,+1} p[\mathbf{r}|\mathbf{x} = \text{map}(\mathbf{c})] \exp \sum\limits_{j\in\mathcal{O}_l} \Lambda_{A1}^k(c_j)}{\sum\limits_{\mathbf{c}\in\mathbb{C}_l,-1} p[\mathbf{r}|\mathbf{x} = \text{map}(\mathbf{c})] \exp \sum\limits_{j\in\mathcal{O}_l} \Lambda_{A1}^k(c_j)} \tag{3.9}$$

where $\mathcal{O}_l$ is the set of indices j satisfies $\mathcal{O} = \{j|j = 1, 2, .., Mn_T,\ j \neq l,\ c_j = 1\}$. Let us defined $\mathbf{c}_{[l]}$ the sub-vector of $\mathbf{c}$ obtained by removing its lth element c_l. Also, we define

$\mathbf{\Lambda}_{A1,[l]}$ the column vector made up by all the Λ_{A1} values excluding that for c_l and the vector can be represented as $\mathbf{\Lambda}_{A1,[l]} = [\Lambda_{A1}(c_1), ..., \Lambda_{A1}(c_{l-1}), \Lambda_{A1}(c_{l+1}), ..., \Lambda_{A1}(c_{Mn_T})]^T$. Then, the a posteriori LLR value of the bit of interest can be represented by a sum of the a priori LLR value and the extrinsic LLR value. By multiplying the numerator and denominator with $\exp[-\frac{1}{2}\sum_{l=1}^{Mn_T}\Lambda_{A1}^k(c_l)]$, (3.9) can be written as

$$\begin{aligned}\Lambda_{D1}^k(c_l|\mathbf{r}) &= \Lambda_{A1}^k(c_l) + \log\frac{\sum\limits_{\mathbf{c}\in\mathbb{C}_l,+1} p[\mathbf{r}|\mathbf{x}=\text{map}(\mathbf{c})]\exp\left[\sum\limits_{j\in\mho_l}\frac{1}{2}\Lambda_{A1}^k(c_j) - \sum\limits_{j\in\overline{\mho}_l}\frac{1}{2}\Lambda_{A1}^k(c_j)\right]}{\sum\limits_{\mathbf{c}\in\mathbb{C}_l,-1} p[\mathbf{r}|\mathbf{x}=\text{map}(\mathbf{c})]\exp\left[\sum\limits_{j\in\mho_l}\frac{1}{2}\Lambda_{A1}^k(c_j) - \sum\limits_{j\in\overline{\mho}_l}\frac{1}{2}\Lambda_{A1}^k(c_j)\right]} \\ &= \Lambda_{A1}^k(c_l) + \log\frac{\sum\limits_{\mathbf{c}\in\mathbb{C}_l,+1} p[\mathbf{r}|\mathbf{x}=\text{map}(\mathbf{c})]\exp\left(\frac{1}{2}\mathbf{c}_{[l]}^T\cdot\mathbf{\Lambda}_{A1,[l]}^k\right)}{\sum\limits_{\mathbf{c}\in\mathbb{C}_l,-1} p[\mathbf{r}|\mathbf{x}=\text{map}(\mathbf{c})]\exp\left(\frac{1}{2}\mathbf{c}_{[l]}^T\cdot\mathbf{\Lambda}_{A1,[l]}^k\right)} \qquad (3.10)\end{aligned}$$

where $\overline{\mho} = \{j|j = 1, 2, .., Mn_T, j \neq l, c_j = -1\}$ and the likelihood function $p[\mathbf{r}|\mathbf{x}=\text{map}(\mathbf{c})]$ is computed by (3.8). Also, we have

$$\Lambda_{E1}^k(c_l|\mathbf{r}) = \log\frac{\sum\limits_{\mathbf{c}\in\mathbb{C}_l,+1} p[\mathbf{r}|\mathbf{x}=\text{map}(\mathbf{c})]\exp\left(\frac{1}{2}\mathbf{c}_{[l]}^T\cdot\mathbf{\Lambda}_{A1,[l]}^k\right)}{\sum\limits_{\mathbf{c}\in\mathbb{C}_l,-1} p[\mathbf{r}|\mathbf{x}=\text{map}(\mathbf{c})]\exp\left(\frac{1}{2}\mathbf{c}_{[l]}^T\cdot\mathbf{\Lambda}_{A1,[l]}^k\right)} \qquad (3.11)$$

which denotes the extrinsic LLR value provided by the detector. In line with the turbo principle, this interleaved extrinsic information can be used as the a priori information at the decoder.

The decoder takes the a priori knowledge of all the coded digits and the constraints imposed by the channel code to generate new APP of a coded bit, written as $\Lambda_{D2}^k(c_l)$. The extrinsic information on the coded digits is computed as $\Lambda_{E2}^k(c_l) = \Lambda_{D2}^k(c_l) - \Lambda_{A2}^k(c_l)$. The interleaved version of this extrinsic LLRs will be served as the new a priori knowledge for the detector in the next iteration.

3.2.2 Performance

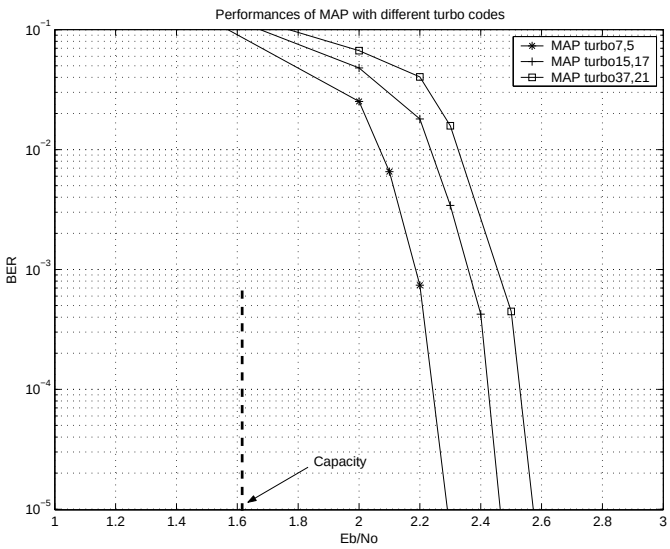

Figure 3.7: Performance of MIMO-BICM iterative receiver with a MAP detector on a fast fading 4 by 4 MIMO channel (where 4-QAM with grey mapping is used). The number of receiver iterations $I_D = 10$ and the number of turbo decoding iterations $I_C = 10$.

The performance of the iterative receivers with a MAP detector and turbo codes with different memory orders are shown in Figure 3.7. The channel is modelled as a 4×4 fast fading MIMO channel and 4-QAM with grey mapping is employed. The frame length is set to 8192. 10 receiver iterations ($I_D = 10$) and 10 turbo decoding iterations ($I_C = 10$) per receiver iteration are used. At BER=10^{-5}, we observe that the performance of the receiver with TC $[7, 5]_8$ is only 0.7dB away from the capacity limit. The performance degradation by replacing the TC $[7, 5]_8$ with TC $[15, 17]_8$ is about 0.15dB and that with TC $[37, 21]_8$ is about 0.3dB.

It is shown that the iterative receiver with a turbo code of a higher memory order does not necessarily perform better than that with a lower memory order. As we will see later in this chapter, similar phenomena are also observed for the iterative receivers with LSD and PIC, over either fast fading channels or slow fading channels.

3.3 Iterative Receiver with A List Sphere Detector

The iterative receiver with a list sphere detector shares the same structure as that with a MAP detector, as shown in Figure 3.6. In this section, we start with presenting the sphere decoding algorithm (SDA). After that, we proceed to the application of the SDA in the MIMO-BICM iterative receivers.

3.3.1 Sphere Decoding Algorithm

At a time instant, the sphere decoder (SD) finds the ML estimate of the transmitted signal by

$$\begin{aligned} \widetilde{\mathbf{x}} &= \arg\min_{\mathbf{x}\in\Delta} ||\mathbf{r}-\mathbf{H}\mathbf{x}||^2 \\ &= \arg\min_{\mathbf{x}\in\Delta} \left[(\mathbf{x}-\widehat{\mathbf{x}})^H\mathbf{H}^H\mathbf{H}(\mathbf{x}-\widehat{\mathbf{x}}) + \mathbf{r}^H(\mathbf{I}-\mathbf{H}(\mathbf{H}^H\mathbf{H})^{-1}\mathbf{H}^H)\mathbf{r}\right] \end{aligned} \tag{3.12}$$

where $\widehat{\mathbf{x}} = [x^1, x^2, ..., x^{n_T}]$ is the center of the search sphere acquired via ZF filtering [17][23], which is computed by $\widehat{\mathbf{x}} = (\mathbf{H}^H\mathbf{H})^{-1}\mathbf{H}^H\mathbf{r}$. Δ is the set which consists of the 2^{Mn_T} hyper-symbols (which are also referred to as candidates or hypotheses). Each entry of the n_T-dimensional vector $\mathbf{x}$ are taken from a constellation of 2^M points. Since $\mathbf{r}^H(\mathbf{I}-\mathbf{H}(\mathbf{H}^H\mathbf{H})^{-1}\mathbf{H}^H)\mathbf{r}$ is independent to the decision on $\mathbf{x}$, (3.12) can be written as

$$\widetilde{\mathbf{x}} = \arg\min_{\mathbf{x}\in\Delta}(\mathbf{x}-\widehat{\mathbf{x}})^H\mathbf{H}^H\mathbf{H}(\mathbf{x}-\widehat{\mathbf{x}}) \tag{3.12b}$$

Generally, the solution can be found without computing (3.12b) for all the hyper-symbols. Especially, SD only examines the hypotheses that lie within a sphere

$$(\mathbf{x}-\widehat{\mathbf{x}})^H\mathbf{H}^H\mathbf{H}(\mathbf{x}-\widehat{\mathbf{x}})^2 \leq R^2 \tag{3.13}$$

with a radius R large enough to contain the solution. By using the complex Cholesky factorization [1][8], we acquire $\mathbf{V}$ which is an upper triangular $n_T \times n_T$ matrix satisfying

$\mathbf{V}^H\mathbf{V} = \mathbf{H}^H\mathbf{H}$. Let us denote the entries of the matrix $\mathbf{V}$ as $\mathbf{v}_{ij}$, $i \leq j = 1, ..., n_T$ so that equation (3.13) becomes

$$(\mathbf{x} - \widehat{\mathbf{x}})^T\mathbf{V}^T\mathbf{V}(\mathbf{x} - \widehat{\mathbf{x}}) = \sum_{i=1}^{n_T} \mathbf{v}_{ii}^2 \left[x^i - \widehat{x}^i + \sum_{j=i+1}^{n_T} \frac{\mathbf{v}_{ij}}{\mathbf{v}_{ii}} (x^j - \widehat{x}^j) \right]^2 \leq R^2 \tag{3.14}$$

If the summation in (3.14) is smaller than R^2, every component in the summation has to be less than R^2. Starting from layer $i = n_T$, we get

$$\mathbf{v}_{n_T n_T}^2 (x_t^{n_T} - \widehat{x}_t^{n_T})^2 \leq R^2 \tag{3.15}$$

The SD chooses a candidate for x^{n_T} which satisfies (3.15) and continues with layer $i = n_T - 1$. Then, we get

$$\mathbf{v}_{n_T-1,n_T-1}^2 \left[x_t^{n_T-1} - \widehat{x}_t^{n_T-1} + \frac{\mathbf{v}_{n_T-1,n_T}}{\mathbf{v}_{n_T,n_T}} (x_t^{n_T} - \widehat{x}_t^{n_T}) \right]^2 + \mathbf{v}_{n_T n_T}^2 (x_t^{n_T} - \widehat{x}_t^{n_T})^2 \leq R^2 \tag{3.16}$$

Now, the SD chooses a candidate for $x_t^{n_T-1}$ within the range of equation (3.16). If a candidate is found, SD proceeds to the next layer $i = n_T - 2$ and finds a candidate for $x_t^{n_T-2}$. Otherwise, it goes back to the previous layer and search for another hypothesis which is within the range.

If SD reaches the last layer ($i = 1$) and at least one candidate is within the corresponding radius, it chooses the one with the smallest value of (3.13) as the final estimate. Otherwise, a larger radius has to be used and the same operations will be repeated.

Obviously, the performance of the algorithm is closely related to the setting of the initial radius. Choosing a too small initial radius may result in the failure of locating the best solution, whereas choosing a too large initial radius will lead the SD to search too many hypotheses, resulting a high computational complexity. There are many discussions on choosing the initial radius for SDA [46, 47]. In our works, however, a good initial radius is assumed to be empirically acquired.

3.3.2 List Sphere Detection

The SDA is efficient for searching the ML symbol estimates. To be applicable in the MIMO iterative receivers, the SD is revised to generate a list of candidates $\pounds$ which contains the ML estimate and its $N-1$ neighbors of smallest value in (3.13). This revised SD is referred to as list sphere detection (LSD) and N is called the *list size* of LSD. The extrinsic LLRs of the detector output in the kth iteration can be approximated as [8]

$$\begin{aligned}\Lambda_{E1}^{k}(c_l|\mathbf{r}) \approx & \frac{1}{2}\max_{\mathbf{c}\in\pounds\cap\mathbb{C}_{l,+1}}\left\{-\frac{1}{\sigma_w^2}||\mathbf{r}-\mathbf{H}\mathbf{x}||^2+\mathbf{c}_{[l]}^T\cdot\mathbf{\Lambda}_{A1,[l]}^k\right\} \\ & -\frac{1}{2}\max_{\mathbf{c}\in\pounds\cap\mathbb{C}_{l,-1}}\left\{-\frac{1}{\sigma_w^2}||\mathbf{r}-\mathbf{H}\mathbf{x}||^2+\mathbf{c}_{[l]}^T\cdot\mathbf{\Lambda}_{A1,[l]}^k\right\} \end{aligned} \tag{3.17}$$

where $\mathbf{x}$ =map($\mathbf{c}$). $\mathbf{c}_{[l]}$ and $\mathbf{\Lambda}_{A1,[l]}^k$ are defined in Section 3.2.1.

The performance and complexity of the LSD is also tied to the choice of the initial radius. If the initial radius is too small, the target list size N cannot be met and there will be a considerable difference between (3.17) and (3.11). If the radius is set to be too large, on the other hand, too many hypotheses will be evaluated and the computational efficiency will be greatly contaminated. Generally, the initial radius of LSD is larger than that of SDA and it depends on the target list size.

3.3.3 Performance

Fast Fading Channels

The BER performance of the iterative receivers with LSD are shown in Figure 3.8, where the channel is modelled by a 4×4 fast fading MIMO channel. The settings of the simulation are the same as in Section 3.2.2 and 4-QAM with grey mapping is employed. The channel code is TC $[7, 5]_8$ and the number of turbo decoding iterations is set to $I_C = 10$. At BER=10^{-5}, a 0.2dB performance degradation is observed by replacing the MAP detector with a LSD of list size $N = 128$, where the total number

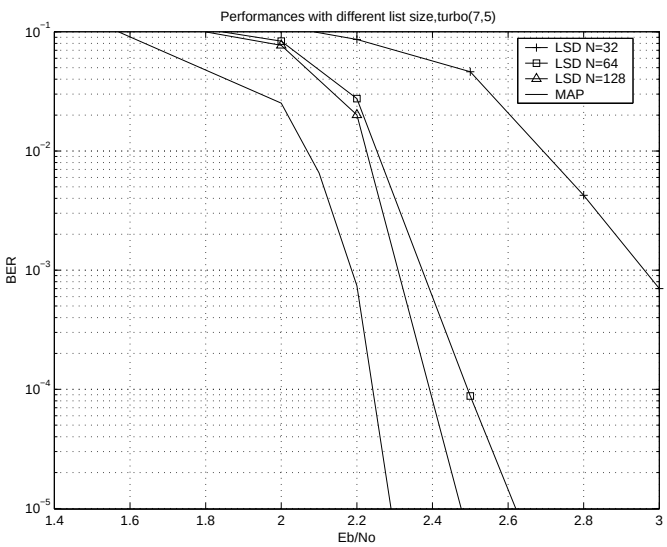

Figure 3.8: Performance of MIMO-BICM iterative receiver with LSD of various list sizes on fast fading channels. 4-QAM. Frame length=8192, $I_D = 10$ and $I_C = 10$.

of candidates is 256. The performance of the iterative receiver with LSD ($N = 64$) is 0.15dB worse than that with LSD ($N = 128$). The performance of the iterative receiver with LSD ($N = 32$) is more than 1 dB away from that with a MAP detector.

Slow Fading Channels

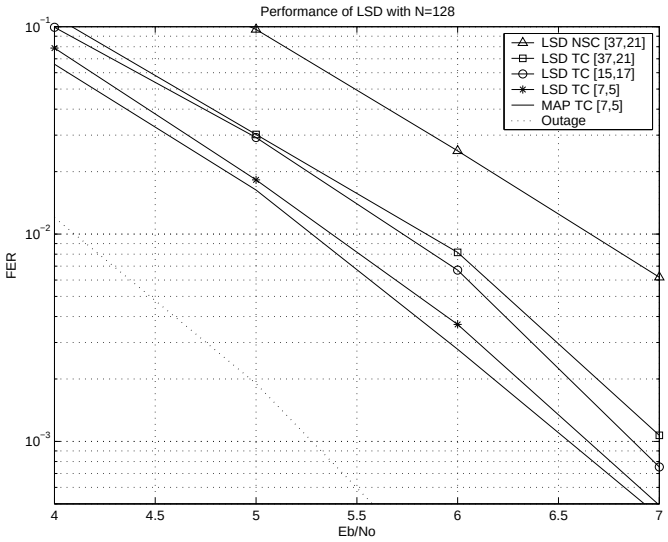

Figure 3.9: Performance of MIMO-BICM iterative receiver with LSD ($N = 128$). Frame length=1024, $I_D = 10$ and $I_C = 10$.

For a slow fading channel, the performance of the iterative receivers with LSD

($N = 128$) and a variety of channel codes are shown in Figure 3.9. The performance of the iterative receiver with a MAP detector and TC $[7, 5]_8$ is also plotted which is 1.2dB away from the outage capacity (at FER=10^{-2}). With TC $[7, 5]_8$, the performance of the iterative receiver with LSD ($N = 128$) is 0.15dB worse than that with a MAP detector (at FER=10^{-2}). The performance degradation by replacing TC $[7, 5]_8$ with TC $[15, 17]_8$ is about 0.3dB and that with TC $[37, 21]_8$ is about 0.45dB. Also, the iterative LSD receiver with NSC $[37, 21]_8$ is tested and it is 1.2dB worse than that with TC $[7, 5]_8$. In addition, no error floor is observed at FER$\geq 10^{-3}$.

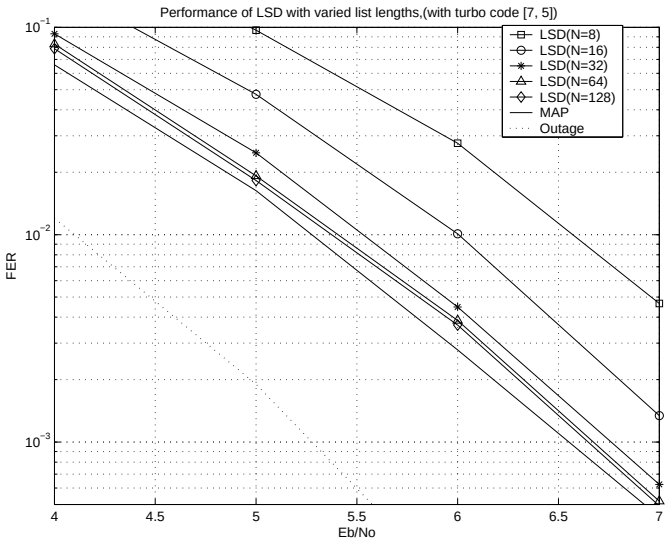

Figure 3.10: Performance of MIMO-BICM iterative receiver with LSD ($N = 8- > 128$) and a turbo code $[7,5]_8$.

The performance of the iterative LSD receivers with varied list lengths are shown in Figure 3.10 whereby the TC $[7, 5]_8$ is employed. Similar performance for the receivers with $N = 128$ and $N = 64$ are observed. At FER=10^{-2}, the performance of the iterative LSD receiver with $N = 32$ is 0.25dB worse than that with $N = 64$ and the FER of the iterative LSD receiver with $N = 16$ is 0.5dB away from that with $N = 32$. Moreover, another 0.5dB performance degradation is observed by further decreasing the list size to $N = 8$. No error floor is observed at FER$\geq 10^{-3}$.

3.3.4 Complexity

In this section, we evaluate the complexity of LSD for slow fading MIMO channels. Since the channel remains the same within one frame of transmission, the computation of the preprocessing, such as performing the Cholesky decomposition, is not taken into account.

The complexity of the LSD is determined by the complexity of 1) finding the candidate list $\pounds$ as well as 2) generating the LLR values by (3.18). To measure the complexity of the latter, let us assume that the metric $\frac{1}{\sigma_w^2}||\mathbf{r}-\mathbf{Hx}||^2$ in (3.17) can be stored before the receiver iterates. Therefore, the complexity of computing (3.17) is determined by the computation of $\mathbf{c}_{[l]}^T \cdot \mathbf{\Lambda}_{A1,[l]}^k$ (which consists of $n_T M - 1$ multiplications and $n_T M - 1$ additions) as well as the list size N. Thus, the complexity of conducting (3.17) is about $2N(n_T M - 1)$ CUs per bit and $2N\Gamma(n_T M - 1)/R_c$ CUs per frame, where Γ is the frame size defined in Chapter 2.

Now we would like to measure the complexity of finding the candidate list $\pounds$. Generally, finding a list of candidates with best metrics is slower than finding the ML solution. However, the difference in complexity is so small [8] that it is reasonable to use the complexity of SDA to roughly approximate that of generating the candidate list.

To date, many efforts have been made towards speeding up the SDA [28][29]. Here, we approximate the complexity of SDA as in [28]. For a 4 by 4 MIMO channel with 4-QAM, 4 "parallel searchers" [28] is the best choice and hence the parameter "z" in [28] is equals to 8. The parameter "K" in [28] is 4 so that the total number of multiplications required is approximated as $Kz + K(K+1) = 52$ for each channel use. Empirically, the number of additions is of the same level as the number of multiplications. Thus, the complexity of SDA can be roughly approximated by 104 CUs per channel use and $104\frac{\Gamma}{R_c M n_T}$ CUs per frame. For a system with $n_T = n_R = 4$, 4-QAM modulation ($M = 2$) and $R_c = 1/2$, the complexity of finding the candidate list $\pounds$ can be approximated as 26Γ CUs per frame. Note that this approximation is

too optimistic and the complexity in practice is moderately higher than that. From simulations (not shown), the complexity of generating the candidate list is about 4 times than we estimated (26Γ CUs per frame), for the worst case examined. Thus, we treat the complexity of generating the list as 104Γ CUs per frame.

From the above, we see that the complexity of finding the candidate list $\pounds$ is comparable to that of computing (3.17) with small list size. For LSD with large list sizes, the majority of the complexity resides in the computation of (3.17). Finally, the complexity of LSD for a 4 by 4 slow fading channel and 4-QAM is approximated as $(104 + 28NI_D)\Gamma$, where I_D is the total number of receiver iterations. The complexity of LSD is shown in Table. 3.1.

Preparing the list	Generating the LLR values
$104\frac{\Gamma}{R_c M n_T}$ CUs/Frame	$2N\Gamma(n_T M - 1)I_D/R_c$CUs/Frame

Table 3.1: Complexity of LSD.

3.4 Iterative Receiver with PIC-DSC

3.4.1 Architecture and Algorithm

In this section, we study a linear detector, namely the parallel interference canceller (PIC), for the iterative MIMO receivers. The study of PIC in MIMO systems has its origin from its application in the CDMA systems [19]. One distinguishing feature of PIC over the APP-based detectors is that the non-linear tree search methodology is replaced by performing linear transformation. Another feature of PIC is that the a posteriori LLRs on the coded digits, rather than the extrinsic LLRs, are typically used to estimate the transmitted symbols for a system with small number of interferers (number of users or antennas). For a system with large processing gain (large number of antennas or users), on the other hand, the exchanging of extrinsic probabilities performs better and is typically used [27]. In this dissertation, we concentrate on

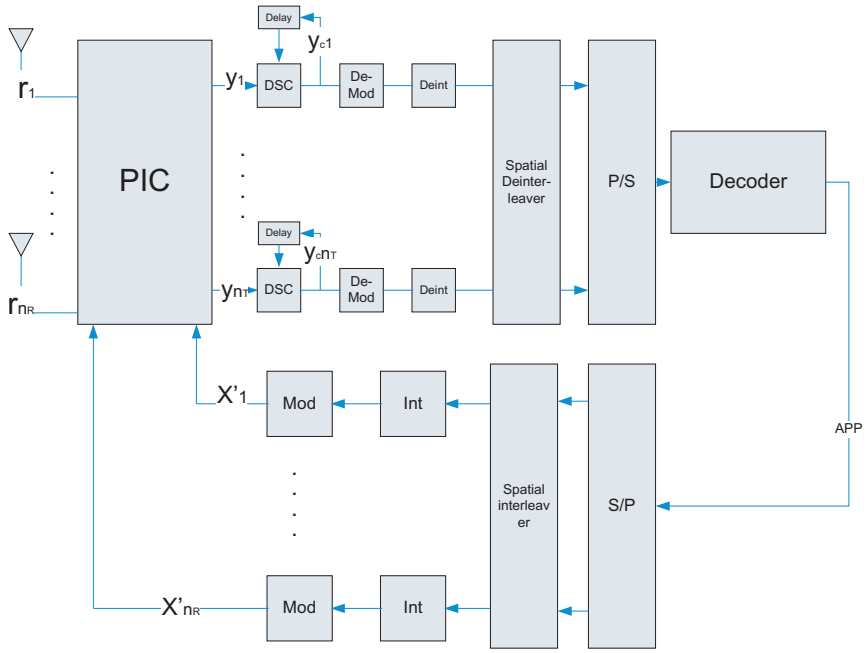

Figure 3.11: Architecture of iterative PIC-DSC receiver for MIMO-BICM.

MIMO systems with antenna number less than 8 so that APPs are chosen as the soft estimates to perform the parallel cancellation. The iterative PIC receivers are examined over slow fading channels.

The receiver architecture is shown in Figure 3.11. In the first receiver iteration, the PIC operation is equivalent to a matched filtering [1]. In the kth ($k \geq 1$) iteration, the output of the PIC is demodulated, de-interleaved, spatially de-interleaved, multiplexed and fed to the decoder. The decoder employs the SISO MAP algorithm [3] to generate the a posteriori LLRs of the coded digits, denoted by $\Lambda^k(c_t)$. Following the Bayesian principle, the estimate of a coded bit is given by

$$\widehat{c_t^k} = (+1)p(c_t^k = 1) + (-1)p(c_t^k = -1) = \frac{\exp\left[(\Lambda(c_t^k)\right] - 1}{\exp\left[\Lambda(c_t^k)\right] + 1} = \tanh\left[\frac{\Lambda(c_t^k)}{2}\right] \quad (3.18)$$

The estimated coded sequence are re-interleaved, re-modulated and served as the soft estimates of the transmitted signals. The detector use the soft estimates to perform parallel cancellation for the next iteration. The soft outputs of the PIC of the ith transmitter antenna is written as [5]

$$y^{i,k} = \mathbf{h}_i^H(\mathbf{r} - \mathbf{H}\underline{\widetilde{\mathbf{x}}}_i^{k-1}) \tag{3.19}$$

where $\mathbf{h}_i$, the ith column of channel matrix $\mathbf{H}$, denotes the channel from the ith transmitter antenna to all receiver antennas and $(\bullet)^H$ denotes Hermitian operation. $\underline{\widetilde{\mathbf{x}}}_i^{k-1}$is an estimation of signals of the all transmitter antennas excluding the ith antenna in the $(k-1)$th iteration, given by

$$\underline{\widetilde{\mathbf{x}}}_i^{k-1} = [\widetilde{x}^{1,k-1}, ..., \widetilde{x}^{i-1,k-1}, 0, \widetilde{x}^{i+1,k-1}, ..., \widetilde{x}^{n_T,k-1}]^T \tag{3.20}$$

Applying (3.20) in (3.19), we have

$$y^{i,k} = x^{i,k}\sum_{j=1}^{n_R}|h_{ji}|^2 + \sum_{\substack{m=1,\\ m\neq i}}^{n_T}(x^{m,k} - \widetilde{x}^{m,k-1})\sum_{i=1}^{n_R}h_{ji}^*h_{jm} + \sum_{j=1}^{n_R}h_{ji}^*n^j \tag{3.21}$$

From (3.21) we observe that for the ith antenna, the detector's output signal $y^{i,k}$ can be decomposed into three terms. The first term shows that the total channel gain (in amplitude) for the signal from transmit antenna i is $\alpha^i = \sum_{j=1}^{n_R}|h_{ji}|^2$. The second part shows the uncanceled (or residual) interference from other antennas. The last term is the output noise which has a variance $\alpha^i\sigma_w^2$ for each real dimension. According to the large number theorem (here $n_T \geq 4$ will suffice) [1][5], the summation of the residual interference and noise follows a Gaussian distribution with variance σ^2. Then, the probabilities on the coded digits (at the PIC output) can be computed by

$$p(y^{i,k} = l) = \frac{1}{\sqrt{2\pi}\sigma}\exp(-\frac{(y^{i,k} - l\alpha^i)^2}{2\sigma^2}),\ l \in \{-1, 1\} \tag{3.22}$$

The soft estimates from the decoder are APPs which contain the information provided by the PIC. Thus, the soft decision at the output of detector will be biased for $k > 1$. To combat the bias effect, a decision statistic combining (DSC) is proposed

[5][19] which is given by

$$y_c^{i,k} = \frac{(\sigma_c^{i,k-1})^2}{(\sigma_c^{i,k-1})^2 + (\sigma^{i,k})^2} y^{i,k} + \frac{(\sigma^{i,k})^2}{(\sigma_c^{i,k-1})^2 + (\sigma^{i,k})^2} y_c^{i,k-1} \tag{3.23}$$

where $y_c^{i,k}$ is the output of DSC and $y^{i,k}$ is the output of PIC. σ_c^2 is the variance observed at the output of DSC.

3.4.2 Performance Analysis

In this section, we derive performance bound of the receiver with a NSC on a slow Rayleigh fading MIMO channel. For perfect cancellation, (3.21) becomes

$$y^i = \alpha^i x^i + \widetilde{n_p}^i \tag{3.24}$$

where $n_p^i = \sum_{j=1}^{n_R} h_{ji}^* n^j$ is a sample of the noise observed at the PIC's output for the ith antenna and it is of a variance $\alpha^i \sigma_w^2$ for each real dimension.

Pair-wise Error Probability

We define the transmitted coded digits from the ith antenna as $\mathbf{c}^i = (c_1^i, c_2^i, ..., c_t^i, ..., c_L^i)$, $c_t^i \in \{-1, 1\}$ where L is the length of the coded sequence of each antenna in each transmission frame. The transmitted sequences from all the antenna are represented by $\mathbf{C} = [\mathbf{c}^1, ..., \mathbf{c}^{n_T}]^T$. The output signal from the interference canceller is denoted by $\mathbf{Y} = [\mathbf{y^1}, ..., \mathbf{y^{n_T}}]^T$, where $\mathbf{y}^i = (y_1^i, y_2^i, ..., y_t^i, ..., y_L^i)$.

Let us denote the energy of a hyper-symbol as E_s and assume that the transmitted symbol energy from all the antennas are of the same value. Hence, each transmitted symbol is of energy E_s/n_T. Let us consider 4-QAM and hence the energy for each coded bit is $\varepsilon_c = E_s/2n_T$.

The pair-wise error probability (PEP) $P(\mathbf{C} \rightarrow \widehat{\mathbf{C}})$ [3][4] is the probability that the decoder chooses $\widehat{\mathbf{C}} = [\widehat{\mathbf{c}}^1, \widehat{\mathbf{c}}^2, ..., \widehat{\mathbf{c}}^{n_T}]^T$ as the estimate of the coded sequence whereas

the genuine coded sequence is $\mathbf{C} = [\mathbf{c}^1, \mathbf{c}^2, ..., \mathbf{c}^{n_T}]^T$, $\mathbf{C} \neq \widehat{\mathbf{C}}$. According to the ML rule [1]-[4], error happens if the distance between $\mathbf{C}$ and $\mathbf{Y}$ are larger than that between $\widehat{\mathbf{C}}$ and $\mathbf{Y}$. For a transmission frame with channel $\mathbf{H}$, the conditional PEP is

$$P(\mathbf{C} \rightarrow \widehat{\mathbf{C}}|\mathbf{H}) = P\left(\sum_{i=1}^{n_T}\sum_{t=1}^{L}\left|y_t^i - \alpha^i\sqrt{\varepsilon_c}c_t^i\right|^2 > \sum_{i=1}^{n_T}\sum_{t=1}^{L}\left|y_t^i - \alpha^i\sqrt{\varepsilon_c}\widehat{c}_t^i\right|^2\right) \tag{3.25}$$

We denote d the Hamming distance between $\mathbf{C}$ and $\widehat{\mathbf{C}}$ and d_i the Hamming distance between $\mathbf{c}^i$ and $\widehat{\mathbf{c}}^i$.

Referring [12][13] and for a slow fading channel, we have

$$P(\mathbf{C} \rightarrow \widehat{\mathbf{C}}|\mathbf{H}) = Q\left(\sqrt{\sum_{i=1}^{n_T}\frac{\varepsilon_c\alpha^i}{\sigma_w^2}d_i}\right) = Q\left(\sqrt{\sum_{i=1}^{n_T}\frac{E_s\alpha^i}{2n_T\sigma_w^2}d_i}\right) \tag{3.26}$$

By using $E_b = \frac{n_R}{n_T R_c \log_{2M}} E_s$ and for 4-QAM, we have

$$P(\mathbf{C} \rightarrow \widehat{\mathbf{C}}|\mathbf{H}) = Q\left(\sqrt{\sum_{i=1}^{n_T}2R_c\frac{E_b\alpha^i}{n_R N_o}d_i}\right) \tag{3.27}$$

where $N_o = 2\sigma_w^2$ and $Q(\bullet)$ is the complementary error function which is given by [1] $Q(z) = \int_z^\infty \frac{1}{\sqrt{2\pi}}e^{(-\frac{x^2}{2})}dx$. Using the inequality $Q(x) \leq \frac{1}{2}e^{(\frac{-x^2}{2})}, x >> 1$, we get

$$\begin{aligned} P(\mathbf{C} \rightarrow \widehat{\mathbf{C}}|\mathbf{H}) &\leq \frac{1}{2}\exp\left(-\frac{R_c E_b}{n_R N_o}\sum_{i=1}^{n_T}\alpha^i d_i\right) \\ &= \frac{1}{2}\prod_{i=1}^{n_T}\exp\left(-\frac{R_c E_b}{n_R N_o}\alpha^i d_i\right) \end{aligned} \tag{3.28}$$

Since each antenna is assumed to be independent from other antennas, we have

$$P(\mathbf{C} \rightarrow \widehat{\mathbf{C}}|\mathbf{H}) = \prod_{i=1}^{n_T}P(\mathbf{c}^i \rightarrow \widehat{\mathbf{c}}^i|\mathbf{H}^i) \tag{3.29}$$

To compute the unconditional PEP, we average (3.29) over the random variable α^i

which yields

$$P(\mathbf{C} \rightarrow \widehat{\mathbf{C}}) = \prod_{i=1}^{n_T} \int P(\mathbf{c}^i \rightarrow \widehat{\mathbf{c}}^i | \mathbf{H}^i) P(\alpha^i) d\alpha^i \tag{3.30}$$

where $\alpha^i = \sum_{j=1}^{n_R} |h_{ji}|^2$ is of a chi-square distribution with $2n_R$ degree of freedom [1]. The of the channel gain α is written as [1]

$$P(\alpha) = \frac{\alpha^{(n_R-1)} e^{\left(-\frac{\alpha}{2\sigma_h^2}\right)}}{(2\sigma_h^2)^{n_R} (n_R-1)!}, 0 \leq \alpha \leq \infty \tag{3.31}$$

By applying (3.28)(3.31) into (3.30) and letting $2\sigma_h^2 = 1$ (since $E[|h_{ji}|^2] = 1$ is assumed), we get:

$$\begin{aligned} P(\mathbf{C} \rightarrow \widehat{\mathbf{C}}) &\leq \frac{1}{2} \prod_{i=1}^{n_T} \int_0^\infty \frac{e^{\left(-\frac{RE_b}{n_R N_o} d_i \alpha^i\right)} (\alpha^i)^{(n_R-1)} e^{\left(-\alpha^i\right)}}{(n_R-1)!} d\alpha^i \\ &= \frac{1}{2} \prod_{i=1}^{n_T} \int_0^\infty \frac{e^{\left(-R(\frac{E_b}{n_R N_o}+1) d_i \alpha^i\right)} (\alpha^i)^{(n_R-1)}}{(n_R-1)!} d\alpha^i \end{aligned} \tag{3.32}$$

Considering $\int_{\mathbf{o}}^\infty e^{(-Ax)} x^N dx = \frac{N!}{A^{N+1}}$, we have

$$P(\mathbf{C} \rightarrow \widehat{\mathbf{C}}) \leq \frac{1}{2} \prod_{i=1}^{n_T} \left(\frac{RE_b}{n_R N_o} d_i + 1 \right)^{-n_R} \tag{3.33}$$

Assume that an ideal space interleaver is employed at the transmitter, which means that the error bits are evenly distributed among n_T transmitter antennas. That is

$$d_i = \begin{cases} \lfloor \frac{d}{n_T} \rfloor + 1, & i = 1, ..., a \\ \lfloor \frac{d}{n_T} \rfloor, & i = a+1, ..., n_T \end{cases} \tag{3.34}$$

where $a \equiv (d \bmod n_T)$ and $\lfloor x \rfloor$ means the integer part of x.

In the following analysis, we consider two cases depending on the value of Hamming distance d.

- The case $d \geq n_T$.

In this case, d_i is not equal to zero for all the transmitter antennas. At a high SNR, the pair-wise error probability can be simplified as

$$\begin{aligned}\mathbf{P}(\mathbf{C} \rightarrow \widehat{\mathbf{C}}) &\leq \frac{1}{2}\left(\frac{RE_b}{n_R N_o}\right)^{-n_R n_T}\left(\prod_{i=1}^{n_T} d_i^{-n_R}\right)^{-n_R} \\ &= \frac{1}{2}\left(\frac{RE_b}{n_R N_o}\right)^{-n_R n_T} \cdot \left(\left\lfloor \frac{d}{n_T} \right\rfloor + 1\right)^{-a n_R} \cdot \left(\left\lfloor \frac{d}{n_T} \right\rfloor\right)^{-(n_T - a) n_R}\end{aligned} \tag{3.35}$$

We can see that with a constituent code which has a free distance greater than or equal to the number of transmitter antennas, the scheme achieves a full diversity order of $n_T n_R$. The coding gain of the scheme is given by

$$\mathbf{G}_c = \frac{\left(\left\lfloor \frac{d}{n_T} \right\rfloor + 1\right)^{a/n_T}\left(\left\lfloor \frac{d}{n_T} \right\rfloor\right)^{(n_T - a)/n_T}}{d_u^2} \tag{3.36}$$

where d_u^2 is the squared Euclidean distance of the reference un-coded system.

- The case $d \leq n_T$.

In this case, we have

$$d_i = \begin{cases} 1, & i = 1, ..., d \\ 0, & i = d+1, ..., n_T \end{cases} \tag{3.37}$$

At a high SNR, the pair-wise error probability can be simplified as

$$\mathbf{P}(\mathbf{C} \rightarrow \widehat{\mathbf{C}}) \leq \frac{1}{2}\left(\frac{RE_b}{n_R N_o}\right)^{-d n_R} \tag{3.38}$$

From the above equation, we show that in this scenario the scheme can only achieve a diversity order of $d n_R$.

The above two cases can be summarized as that the diversity order of the scheme on a slow Rayleigh fading channel is determined by $\min(d, n_T)\, n_R$.

ABS Bound on the Bit Error Probability

The standard bound, which is also referred to as the average-before-summation (ABS) bound [20], on the BEP can be acquired by truncating the code distance spectrum [3][4]. We denote B_d as the error coefficient which is the average number of bit errors associated with error events of Hamming weight d. The BEP bound can be represented by

$$P_b(\mathbf{e}) \leq \sum_{d=d_{free}}^{\infty} B_d P_d(\mathbf{C} \rightarrow \widehat{\mathbf{C}}) \tag{3.39}$$

where $P_d(\mathbf{C} \rightarrow \widehat{\mathbf{C}})$ is the PEP when the Hamming distance between the events of the two sequences is d.

LBA Bound on the Bit Error Probability

It is reported in [20] that a tighter upper bound can be obtained by limiting the conditional union upper bound on the BEP before averaging (LBA) over the fading vector. Hence, the BEP upper bound by applying LBA is modified as

$$P_b(\mathbf{e}) \leq \int \min \left[\frac{1}{2}, \sum_{d=d_{free}}^{\infty} B_d \prod_{i=1}^{n_T} P(\mathbf{c}^i, \widehat{\mathbf{c}}^i | \mathbf{H}^i) \right] P(\boldsymbol{\alpha}) \mathbf{d}\boldsymbol{\alpha} \tag{3.40}$$

where $\boldsymbol{\alpha} = (\alpha^1, ..., \alpha^{n_T})$. A close-form representation of the above expression requires n_T-fold integration which is complicated. However, we can use numerical techniques to evaluate the above performance bound.

Numerical Results

In the simulations, we consider the BEP performance of an iterative receiver with PIC-DSC. To ensure full diversity order, a $R_c = 1/2$ NSC with generator $[23, 35]_8$ and minimum free distance 7 is used for systems with $n_T = n_R = 2$ and $n_T = n_R = 4$. An NSC with generator $[133, 171]_8$ and minimum free distance 10 is used for a system with $n_T = n_R = 8$. Moreover, a simple 4-QAM with Grey mapping is employed.

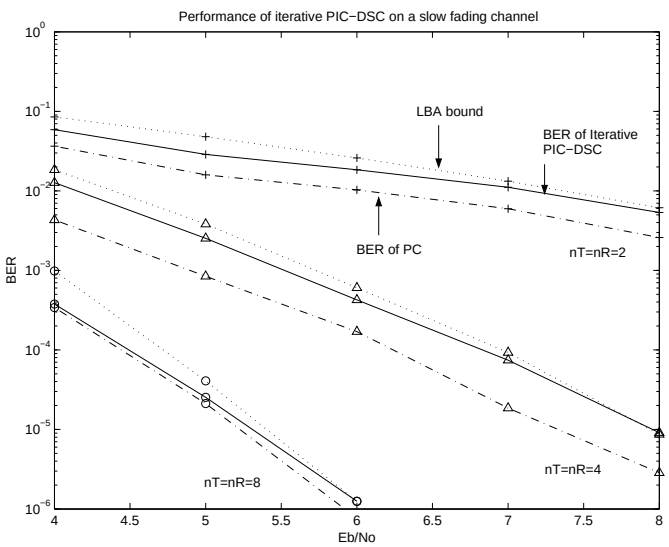

Figure 3.12: Performance of iterative receiver with PIC-DSC ($I_D = 10$) and a NSC $[7, 5]_8$ for 2 by 2, 4 by 4, 8 by 8 slow Rayleigh fading MIMO channels. The frame length is 1024 and 4-QAM with grey mapping is used.

Figure 3.12 shows the performance of the iterative PIC-DSC receivers with 10 receiver iterations and the LBA bounds. The solid curves are the BERs of iterative PIC-DSC receivers and the dotted curves are the LBA bounds. The dotted-dashed curves are the performance with perfect cancellation (PC), which can be viewed as lower bounds for the performance of the iterative receivers with PIC-DSC. From this plot, we see that the BERs of iterative receivers with PIC-DSC are nicely upper-bounded by the LBA bounds. For a system with $n_T = n_R = 8$, the LBA bound is about 0.1 dB away from the BER of the iterative receiver with PIC-DSC.

Figure 3.13 shows the performance of the scheme with perfect cancellation and its comparison with the performance bound. The solid curves are the BERs of systems with perfect cancellation. The dotted curves are the LBA bounds and the dotted-dashed curves are the ABS bound. For a system with $n_T = n_R = 2$, we observe that the LBA bound is tighter to the performance of PC than the ABS bounds. For a system with $n_T = n_R = 4$ or $n_T = n_R = 8$, the LBA bound almost coincides with the ABS bound. For a system with $n_T = n_R = 8$, the LBA bound is about 0.15 dB away from the BEP of PC.

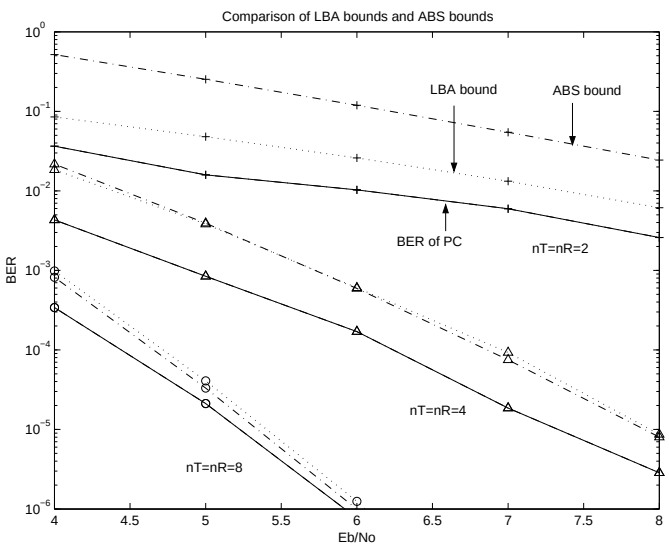

Figure 3.13: The comparison of the LBA bounds and ABS bounds, for 2 by 2, 4 by 4 and 8 by 8 slow Rayleigh fading MIMO channels. The frame length is 1024 and 4-QAM with grey mapping is used..

3.4.3 Performance of Iterative Receiver with PIC-DSC and Various Channel Codes

The performance of iterative receivers with PIC-DSC and turbo codes are presented in Figure 3.14. The sub-figure on the left hand side shows the FER performance of the iterative receiver with 10 receiver iterations. The sub-figure on the right hand side shows the FERs of the receiver with perfect cancellation. From the sub-figure on the left, we observe that the iterative receiver with TC $[7, 5]_8$ yields the best performance whereas the TC $[37, 21]_8$ results in the worst performance at FER$\leq$0.003. Moreover, error floors are observed for the iterative receiver with TC $[37, 21]_8$ and TC $[15, 17]_8$ at FER$\leq$0.001. From the sub-figure on the right, we witness that the TC $[37, 21]_8$ and TC $[15, 17]_8$ are of the best interference-free performance.

The performance of iterative receivers with PIC-DSC and their interference-free counter-parts are compared for a variety of channel codes in Figure 3.15. The solid curves are for the performance of the iterative receivers while the dotted curves are that with perfect cancellation. We observe that the iterative receiver with PIC-DSC and convolutional code $[37, 21]_8$ is able to approach its interference-free performance

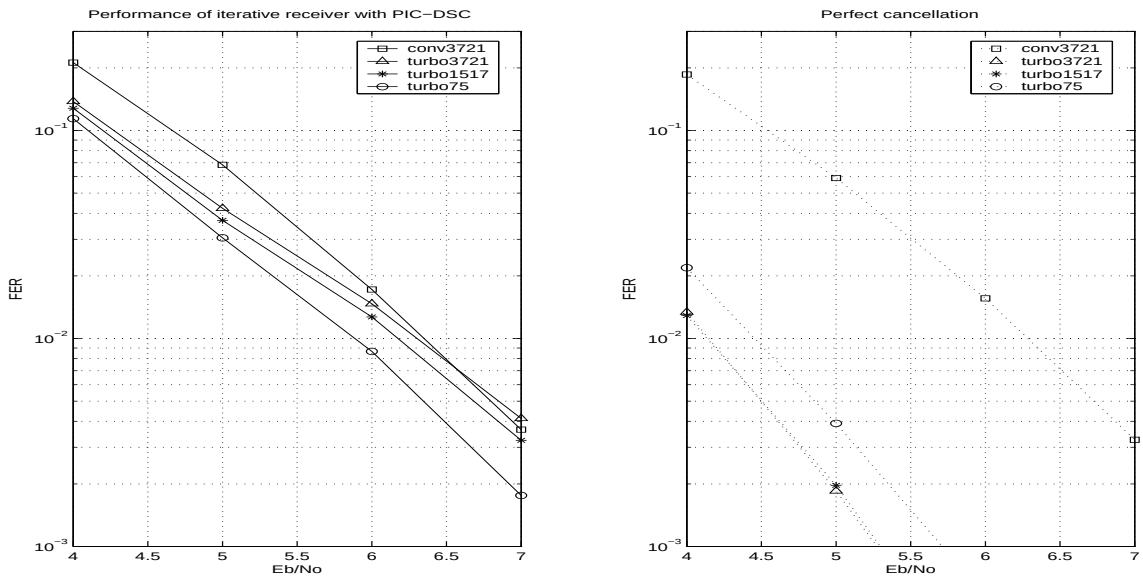

Figure 3.14: FERs of iterative receives with PIC-DSC ($I_D = 10, I_C = 10$) and with perfect cancellation. The frame length is 1024 and 4-QAM with grey mapping is used.

whereas the iterative receivers with turbo codes cannot. At FER=0.01, the iterative receiver with TC $[37,\ 21]_8$ is observed to be 2.2dB away from its interference-free performance.

The observed error floors as well as the huge differences from their interference-free performance lead to the undesirable performance of the iterative receivers with TC $[15{,}17]_8$ and TC $[37,\ 21]_8$. In fact, the error floor is also observed for the iterative receiver with a weaker channel code such as TC $[7,\ 5]_8$ or an NSC code with $m = 4$.

3.4.4 Complexity

We evaluate the complexity of PIC-DSC by (3.20), (3.23) and (3.24) over slow fading channels. The operation of (3.20) consists of $n_T n_R$ complex multiplications as well as $n_T n_R - 1$ complex additions, for each channel use. Each complex multiplication consists of four multiplications as well as two addition and each complex addition consists of two additions. Therefore, the complexity of the operation of (3.20) can be measured by $6n_T n_R + 2(n_T n_R - 1) = (8n_T n_R - 1)$CUs, for each channel use. In (3.23), four multiplications and 3 additions are required for one bit. Hence, the

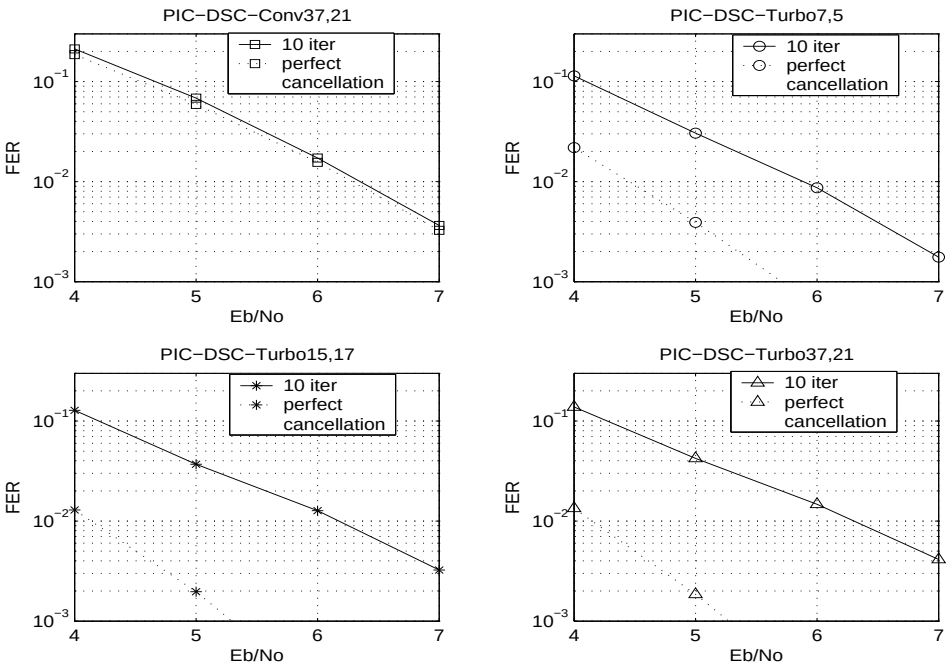

Figure 3.15: The FERs of iterative receivers with PIC-DSC (and the FERs of receivers with perfect cancellation) and various channel codes. The frame length is 1024 and 4-QAM with grey mapping is used.

complexity by computing (3.24) is measured by 7 CUs for each bit. The computing of (3.23) consists of one addition, 3 multiplication and 1 exponential operation. Since one exponential operation is tested to cost about 5 CUs, the complexity of computing (3.23) is measured by 9 CUs for each bits.

The overall complexity of the PIC-DSC is $(8n_T n_R - 1)\frac{\Gamma}{R_c M n_T} + 7\frac{\Gamma}{R_c} + 9\frac{\Gamma}{R_c} \approx \left(\frac{8n_R}{R_c M} + \frac{16}{R_c}\right)\Gamma$. Obviously, the complexity of PIC-DSC is linear with the antenna numbers. For the simple case that $n_R = n_T = 4$, 4-QAM ($M = 2$) and $R_c = 1/2$, the complexity of PIC operation per frame can be approximated as $64\Gamma I_D$ CUs per frame where I_D is the total number of receiver iterations. Moreover, we find that the PIC-DSC is faster than LSD with moderate list size ($N \geq 4$).

3.5 Performance Comparison of Various Iterative Receivers

The performance of the iterative receivers with MAP, LSD ($N \in \{8, 16, 32, 64\}$) and PIC-DSC over slow-fading MIMO channels are plotted in Figure 3.16 where TC $[7, 5]_8$ is used. An error floor is observed for the iterative receiver with PIC-DSC whereas

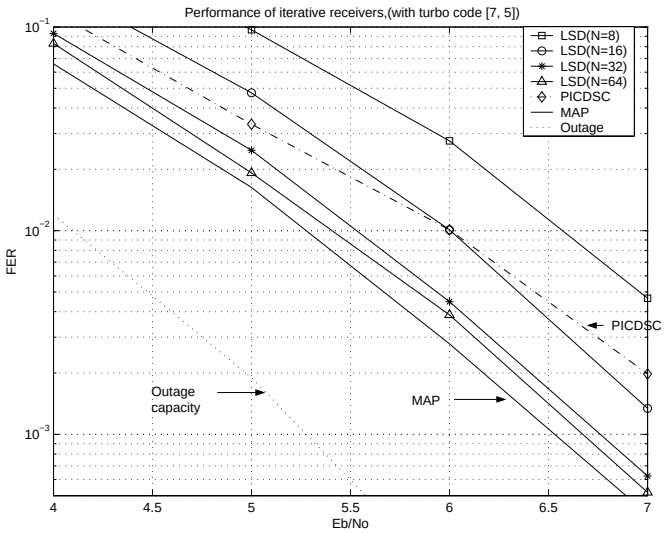

Figure 3.16: Comparison of the FERs of iterative receivers with various detectors.The frame length is 1024 and 4-QAM with grey mapping is used.

no error floors are observed for those with MAP detectors and LSD detectors. We see that the FER of iterative receiver with PIC-DSC is about 0.75 dB worse than the that with a MAP detector at FER=10^{-2} and larger performance differences are observed for lower FERs. The performance of the iterative receiver with PIC-DSC is similar to that with LSD ($N = 16$) at FER=10^{-2} whereas the iterative receiver with LSD ($N = 16$) outperforms that with PIC-DSC at FER>10^{-2}.

3.6 Summary

In this chapter, the iterative receivers with various detectors and different channel codes are examined and we see that capacity of a MIMO channel can be approached

by a MIMO-BICM system with iterative detection and decoding. However, explicit explanations for some observations are required such as 1) the error floor observed for the iterative PIC-DSC receiver and 2) the performance degradation by employing stronger turbo codes. These questions will be investigated in the following chapters.

Chapter 4

Convergence Analysis and Detection Switching for Iterative Detection and Decoding

In the previous chapter, we show that an analytical performance bound is able to predict the performance of an iterative receiver with PIC-DSC and a NSC decoder. For turbo-coded MIMO-BICM systems, however, there is significant probability with that the iterative process does not converge to successful decoding, as shown in Section 3.4.3. In this case, people have commenced to investigate the convergence behavior of iterative processing via empirical measures. The analysis of convergence is useful to find good component codes which can be matched to the MIMO detectors, as shown later in this chapter.

4.1 Empirical Measures

4.1.1 Mutual Information

The most notable methodology for the convergence analysis of a turbo-like system is the extrinsic information transfer (EXIT) chart in which *mutual information* (MI) is

used to measure the reliability of the exchanged information between the components. The performance of iterative decoding can be predicted by solely looking at the input-output relations of individual constituent decoders.

In [10], it is assumed that the a priori soft input to the decoder is closely approximated as an output of AWGN channel, represented by

$$A = \mu_A \cdot x + n_A \tag{4.1}$$

where x is the unknown transmitted systematic bits and n_A is the AWGN with variance σ_A^2. In addition, the Gaussian consistent condition [10] must be fulfilled so that $\mu_A = \frac{\sigma_A^2}{2}$. The conditional PDF of A is written as

$$P_A(\xi|X = x) = \frac{e^{-((\xi-x)^2/2\sigma_A^2)}}{\sqrt{2\pi}\sigma_A} \tag{4.2}$$

where X is the random transmitted systematic bits.

The mutual information between the transmitted systematic bits X and the a priori LLR value A is defined as [10]

$$\mathbf{I}_A = \mathbf{I}(X; A) = \frac{1}{2} \sum_{x=-1,1} \int_{-\infty}^{\infty} P_A(\xi|X = x) \log_2 \left[\frac{2P_A(\xi|X = x)}{P_A(\xi|X = 1) + P_A(\xi|X = -1)} \right] d\xi$$

$$0 \leq \mathbf{I}_A \leq 1 \tag{4.3}$$

Combining (4.2) and (4.3), we have

$$\mathbf{I}_A = 1 - \int_{-\infty}^{\infty} \frac{e^{-\frac{(\xi-\sigma_A^2/2)^2}{2\sigma_A^2}}}{\sqrt{2\pi\sigma_A^2}} \log_2(1 + e^{-\xi}) d\xi \tag{4.4}$$

At the output of the decoder, mutual information is also used to quantify the extrinsic

output $\mathbf{I}_E = \mathbf{I}(X;E)$ computed by

$$\mathbf{I}_E = \mathbf{I}(X;E) = \frac{1}{2}\sum_{x=-1,1}\int_{-\infty}^{\infty} P_E(\xi|X=x)\log_2\left[\frac{2P_E(\xi|X=x)}{P_E(\xi|X=1)+P_E(\xi|X=-1)}\right]d\xi \tag{4.5}$$

where E stands for the extrinsic LLR at the decoder's output.

By measuring the mutual information at the input and the output of a component decode, we are able to depict its mutual information transfer function. Generally, a very large frame size is required for an accurate measurement of mutual information.

4.1.2 Variances

In [14], it is reported that the variance is as accurate as the mutual information in the study of the turbo-like systems. However, the calculation of variance is much easier than the computation of mutual information. In this dissertation, we use the evolution of variances to track the convergence behaviors of the iterative receivers for MIMO-BICM systems.

Observation Variance

The first type of variance will be used is the *observation variance* (OV) which is the normalized variance of the noisy observation of the signal [14]. This parameter can be straightforwardly used to measure the reliability of the output signal from linear detectors such as PIC and MMSE filter.

Assuming that the Gaussian consistent condition is met that $\mu_A = \frac{\sigma_A^2}{2}$ (as shown in the previous section), the observation of the signal y can be viewed as the summation of symbol c of unitary power and a Gaussian noise sample n with variance σ_{obv}^2 such

that $y = c + n$. The LLR of the signal can be calculated as

$$\begin{aligned}\Lambda(y) &= \log\left(\frac{P(y|c=1)}{P(y|c=-1)}\right) = \log\left(\frac{\exp(-\frac{(y-1)^2}{\sigma^2_{obv}})}{\exp(-\frac{(y+1)^2}{\sigma^2_{obv}})}\right) \\ &= \frac{(y+1)^2 - (y-1)^2}{2\sigma^2_{obv}} = \frac{2y}{\sigma^2_{obv}} \end{aligned} \tag{4.6}$$

Bit Variance

The application of OV in an APP based detector such as an LSD is not straightforward as the output from the detector is soft probabilities rather than values. Thus, we introduce another type of variance, namely the *bit variance* (BV). The BVs of the un-coded (or information) bits and coded digits are calculated as

$$\sigma^2_{bit}(u) = E\left[\left|u - \tanh\left(\frac{\Lambda(u)}{2}\right)\right|^2\right] \tag{4.7}$$

$$\sigma^2_{bit}(c) = E\left[\left|c - \tanh\left(\frac{\Lambda(c)}{2}\right)\right|^2\right] \tag{4.8}$$

If c is correctly decoded, its LLR $\Lambda(c) \rightarrow \pm\infty$ and hence the $\sigma^2_{bit}(c)$ approaches zero (the $\tanh(\bullet)$ converts $\pm\infty$ into ± 1). If no knowledge of c is acquired, on the other hand, the LLR $\Lambda(c) \rightarrow \pm 0$ and $\sigma^2_{bit}(c)$ approaches 1. The mapping between the BV and OV is obtained by combining (4.6) and (4.8) and it is shown in Figure 4.1.

By computing the BVs (or OVs) of the input and output signals of a decoder or a detector, we are able to depict its *variance transfer (VTR) function.*

4.2 Variance Transfer Functions of Decoders

4.2.1 VTR Function of the RSC Decoder

The RSC decoder operates on two streams of a priori LLRs which are the $\Lambda_A(u)$ (on the information bits) from the other decoder and $\Lambda_A(c)$ (on the coded digits) from the

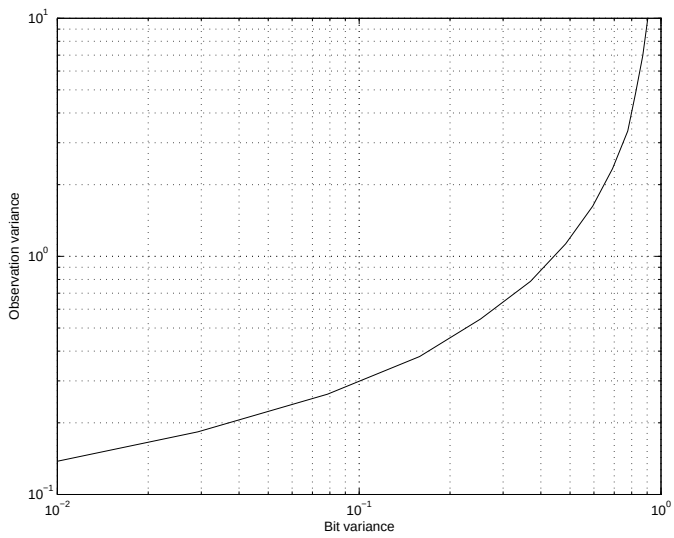

Figure 4.1: The mapping between observation variance and bit variance.

detector. Let us use $\sigma^2_{bit,in}(u_A)$ to measure the variance of the a priori information to the decoder and use $\sigma^2_{bit,out}(u_E)$ to parameterize the extrinsic information generated by the decoder. In addition, we use $\sigma^2_{bit,in}(c_A)$ and $\sigma^2_{bit,out}(c_E)$ to denote the bit variance of the stream consists of coded digits. Thus, the VTR function of an RSC decoder can be represented as

$$\sigma^2_{bit,out}(u_E) = \mathcal{F}[\sigma^2_{bit,in}(u_A), \sigma^2_{bit,in}(c_A)] \tag{4.9}$$

$$\sigma^2_{bit,out}(c_E) = \Theta[\sigma^2_{bit,in}(u_A), \sigma^2_{bit,in}(c_A)] \tag{4.10}$$

The variance transfer model of the RSC decoder is shown in Figure 4.2. For an AWGN channel with single antenna, the VTR can be written as $\sigma^2_{bit,out}(u_E) = \mathcal{F}[\sigma^2_{bit,in}(u_A), E_b/N_o]$. Since a RSC decoder is a non-linear system, a close-form representation of the transfer

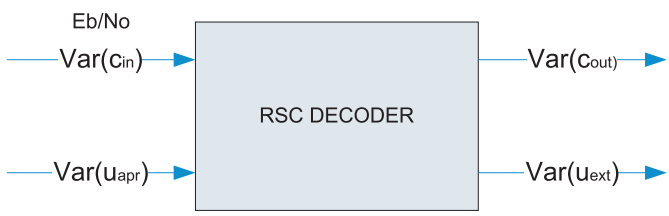

Figure 4.2: The VTR model of a RSC decoder.

function is not feasible. Hence, the transfer functions of decoders are often obtained

via simulations with very large frame sizes. (In our simulations, we set the decoding frame size to 40,000.)

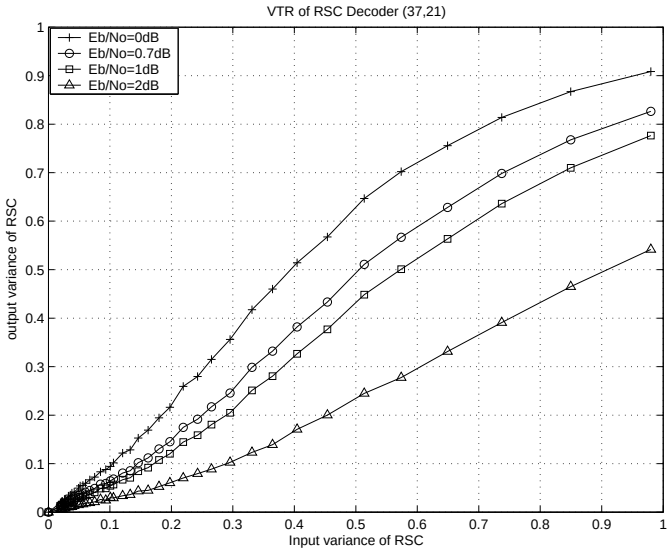

Figure 4.3: The VTR function of the RSC $[1,21/37]_8$ decoder.

The VTR functions of RSC $[1,\ 21/37]_8$ decoder ($R_c = 1/2$) with different SNRs are given in Figure 4.3 for an AWGN channel. It shows that the VTR of a decoder is an increasing function of it's input variance. For the ease of illustration, we define the reduction in the bit variance, given by $\sigma^2_{bit,in}(u_A) - \sigma^2_{bit,out}(u_E)$, as the *bit variance reduction* (BVR) of the decoder. The BVR can be used to reflect the capability of error correction and a larger BVR is invariably desirable.

The VTR functions of $R_c = 1/2$ RSC decoders with a variety of generator polynomials are depicted in Figure 4.4. Each sub-figure shows the VTR functions for various decoders and a fixed E_b/N_o. We observe that the VTR functions of a RSC $[1,\ 17/15]_8$ decoder are close to those of the RSC $[1,\ 21/37]_8$ decoder for all the E_b/N_o examined. Hence, we will focus on the RSC $[1,\ 21/37]_8$ decoder and the RSC $[1,\ 5/7]_8$ decoder for the following analysis.

At E_b/N_o =0dB, we observe that the VTR curve of RSC $[1,\ 21/37]_8$ is below that of RSC$[1,\ 5/7]_8$ for $\sigma^2_{bit,in}(u_A) < 0.4$. This observation implies that the RSC $[1,\ 21/37]_8$ decoder is able to achieve a larger BVR at $\sigma^2_{bit,in}(u_A) < 0.4$. For $\sigma^2_{bit,in}(u_A) > 0.4$, on

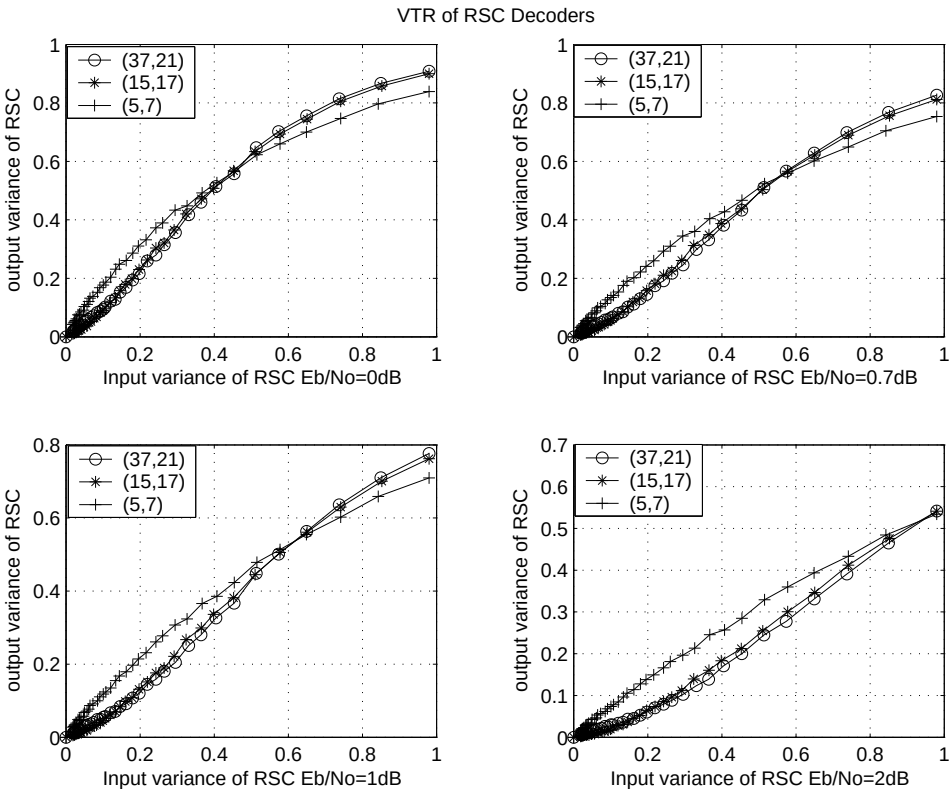

Figure 4.4: Comparison of the VTR functions of various RSC decoders.

the other hand, the curve for RSC $[1,\ 21/37]_8$ is above that for RSC$[1,\ 5/7]_8$ which means RSC $[1,\ 21/37]_8$ has a smaller BVR.

An interesting finding is that as the E_b/N_o becomes larger, the $\sigma^2_{bit,in}(u_A)$ at which the curve of RSC $[1,\ 21/37]_8$ intercepts with that of RSC$[1,\ 5/7]_8$ also becomes larger (move towards the right), and vice versa. it suggests that if the E_b/N_o is large enough, the BVR of the RSC $[1,\ 21/37]_8$ is larger than that of the RSC$[1,\ 5/7]_8$ for all the $\sigma^2_{bit,in}(u_A)$ values (as shown in the sub-figure of $E_b/N_o = 2$dB). If the E_b/N_o is small enough, on the other hand, the BVR of the RSC $[1,\ 21/37]_8$ is smaller than that of RSC$[1,\ 5/7]_8$ for all the $\sigma^2_{bit,in}(u_A)$ values.

4.2.2 VEG of the Turbo Decoder

The variance transfer model of a turbo decoder can be obtained by concatenating two RSC decoders, as shown in Figure 4.5. We see that the output extrinsic information

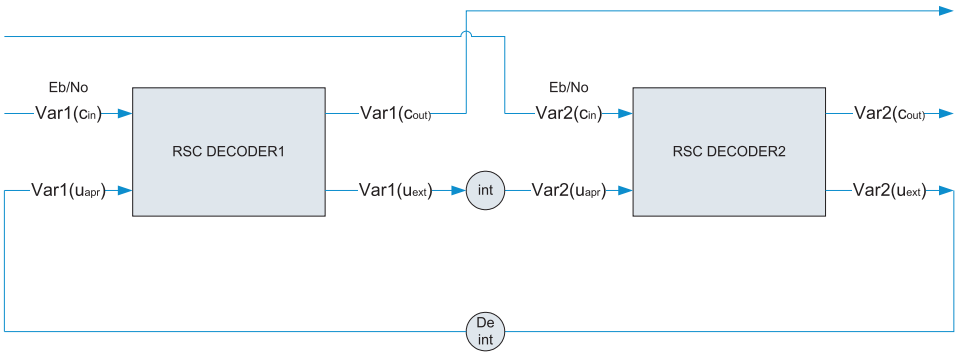

Figure 4.5: The VEG model of a turbo decoder.

of the first decoder is used as the a priori information for the second decoder, and the output extrinsic information of the second decoder is used as the a priori information for the first decoder. In order to narrate the iterative nature of the decoding operation, both of the decoder VTR curves are plotted into a single graph (Figure 4.6), namely *variance exchange graph* (VEG), where the axes of the second decoder are swapped.

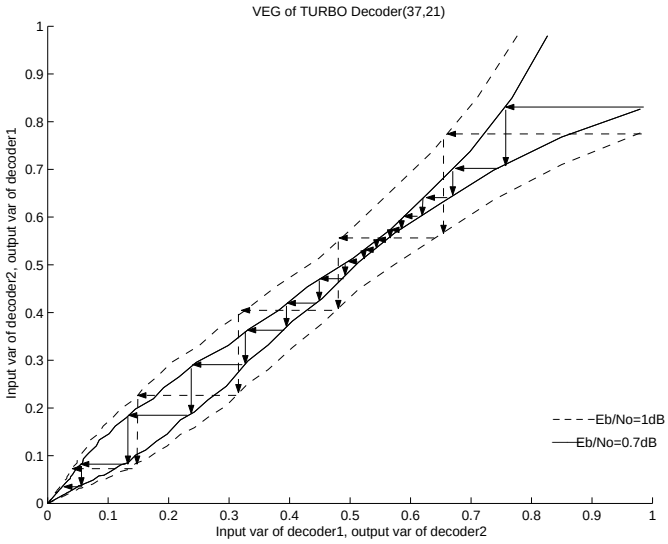

Figure 4.6: The VEG and trajectory of a turbo decoder $[37, 21]_8$.

In the first iteration of the turbo decoding, there is no a priori information to the first RSC decoder and hence the $\sigma^2_{bit,in,k=1}(u_A) = 1$, where k is the index of the decoding iteration. At iteration k, the output extrinsic information from the first decoder is forwarded to the second decoder. After that, the output extrinsic information from the second decoder is feedback to the first decoder. The iteration proceeds as long as

$\sigma^2_{bit,out,k+1}(u_E) < \sigma^2_{bit,out,k}(u_E)$. The condition of $\sigma^2_{bit,out,k+1}(u_{ext}) = \sigma^2_{bit,out,k}(u_{ext})$ can be visualized as the intersection of the two VTR curves in the VEG.

If the intersection is found to be at a very low variance value close to zero, the turbo decoding is likely to converge to a successful decoding and we can see a tunnel between the two VTR curves, as shown in Figure 4.6. If the intersection happens at a relative large variance value (we refer to it as an *early intersection*), on the other hand, there is no tunnel between the two VTR curves, as shown in Figure 4.7. In such a case, the turbo decoding is not able to converge to successful decoding.

In Figure 4.6 where $E_b/N_o = 0.7$dB, we observe that the curves of the two RSC $[1, 21/37]_8$ decoders do not but almost get in touch with each other. This observation suggests that the TC $[37, 21]_8$ is likely to converge to successful decoding at $E_b/N_o = 0.7$dB. Therefore, we see that the waterfall region of a turbo code, shown in Figure 2.8, is predicted by VEG.

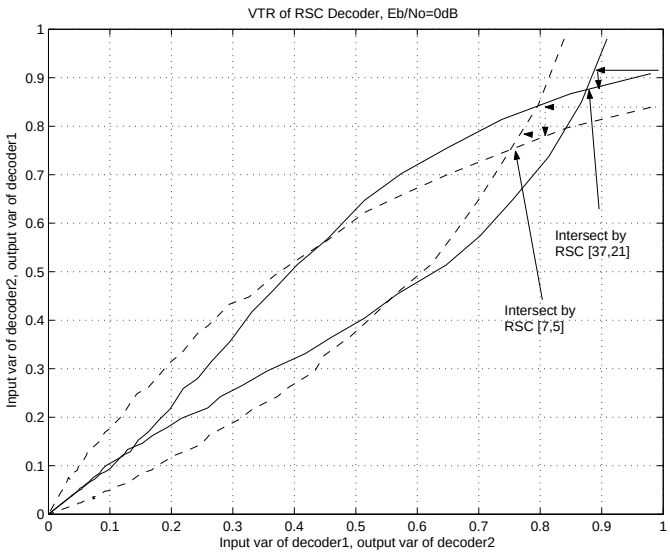

Figure 4.7: VEGs and trajectories of turbo decoders at $E_b/N_o = 0$dB.

For comparison, the VEG of TC $[37, 21]_8$ and that of TC $[7, 5]_8$ are plotted in Figure 4.7 where $E_b/N_o = 0$dB. The solid curves are the VTR functions of RSC $[1, 21/37]_8$ and the dashed curves are the VTR functions of RSC $[1, 5/7]_8$. We observe that although both of the two turbo decoders cannot converge to successful decoding

(a tunnel does not exist), the TC $[7, 5]_8$ stops at a smaller $\sigma^2_{bit,out}(u_{ext})$ compared to the TC $[37, 21]_8$. This observation can be regarded as another explanation of why the TC $[7, 5]_8$ performs better than TC $[37, 21]_8$ at a low SNR.

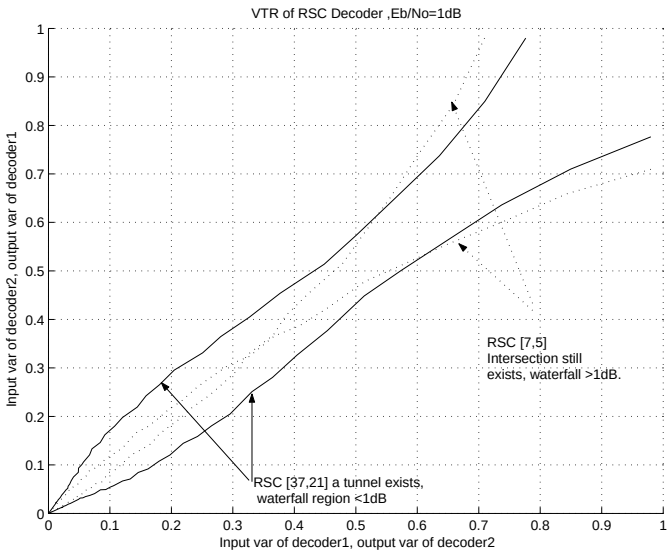

Figure 4.8: VEGs and trajectories of turbo decoders at $E_b/N_o = 1$dB.

At $E_b/N_o = 1$dB (Figure 4.8), we see a tunnel between the VTR curves of RSC $[37, 21]_8$ decoders whereas the intersection between the curves of the RSC $[1, 5/7]_8$ decoders is still there. This observation implies that at $E_b/N_o = 1$dB, the TC $[37, 21]_8$ is able to converge to a successful decoding whereas the TC $[7, 5]_8$ cannot. Consequently, the TC $[7, 5]_8$ requires a larger E_b/N_o to approach its waterfall region.

4.2.3 VTR Function of the Turbo Decoder

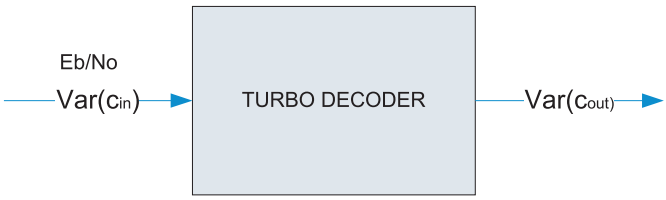

Figure 4.9: The VTR model of a turbo decoder

In the previous section, the convergence behavior of a turbo code is examined by VTR functions and VEG. In a concatenated system employing a turbo code (such

as an turbo-coded BICM system), the turbo decoder is usually treated as a single component rather than two RSC decoders. The soft information about the coded digits c is exchanged between the turbo decoder and the other component (such as a MIMO detector). In Figure 4.9, we show the VTR model of a turbo decoder where

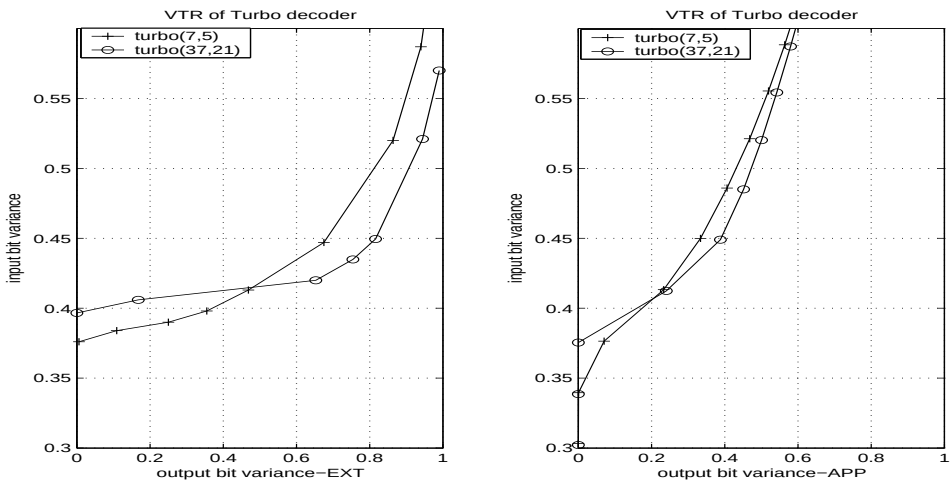

Figure 4.10: VTR functions of turbo decoders. The left is with APP output and the right is with extrinsic output.

only the coded digits are considered.

The VTR function of TC $[37,\ 21]_8$ and that of TC $[7,\ 5]_8$ are depicted in Figure 4.10. The figure on the left employs the extrinsic LLRs on the coded digits as the output (which is applicable for a MAP detector or an LSD). We observe that for $\sigma^2_{bit,in}(c) > 0.5$, the TC $[37,\ 21]_8$ yields a larger BVR than TC $[7,\ 5]_8$ does. For $\sigma^2_{bit,in}(c) > 0.5$, however, the TC $[7,\ 5]_8$ is able to yield larger BVR. The figure on the left uses the a posteriori LLRs on the coded digits as the output (which is applicable for PIC or MMSE filter). We observe that for $\sigma^2_{bit,in}(c) > 0.25$, the TC $[37,\ 21]_8$ yields a larger BVR than TC $[7,\ 5]_8$ does. For $\sigma^2_{bit,in}(c) > 0.25$, however, the TC $[7,\ 5]_8$ is able to yield a larger BVR. The observations are align with the results obtained in Figure 2.8. For a conclusion, we may say that the TC $[37,\ 21]_8$ has a better transfer property at low variances (or high SNRs) whereas TC $[7,\ 5]_8$ has a preferable transfer property at high variances (or low SNRs).

4.3 Variance Transfer Functions of Detectors

The transfer functions of decoders are relatively standard and not changeable for a variety of channels. However, the transfer functions of MIMO detectors are closely related to the properties of channel. In this section, we investigate the variance transfer functions of MIMO detectors on both fast fading and slow fading channels. Unlike a decoder which have two streams of a priori knowledge (which are $\Lambda_A(u)$ from other decoder and $\Lambda_A(c)$ from the detector), a detector operates with the a priori knowledge on the coded digits only.

4.3.1 VTR Function of the PIC

Since the operation of PIC is virtually performing linear transformation, it is feasible to derive the VTR function of the PIC based on (3.21).

VTR Function of PIC on a Slow Fading Channel

From the definition in Chapter 3, each complex symbol x^i is of energy $\frac{E_s}{2n_T}$ in each real dimension. In the following derivation, we use $\sqrt{\frac{E_s}{2n_T}}x^i$ to denote the complex symbol from the ith transmit antenna, where $\mathrm{Re}(x^i) \in \{-1, 1\}$ and $\mathrm{Im}(x^i) \in \{-1, 1\}$. Then, (3.21) is written as

$$y^{i,k} = \sqrt{\frac{E_s}{2n_T}} \left\{ x^{i,k} \sum_{j=1}^{n_R} |h_{ji}|^2 + \sum_{m=1, m\neq i}^{n_T} \Delta_x^{m,k} \sum_{i=1}^{n_R} h_{ji}^* h_{jm} \right\} + \sum_{j=1}^{n_R} h_{ji}^* n^j \tag{4.11}$$

where $\Delta_x^{m,k} = x^{m,k} - \widetilde{x}^{m,k-1}$ is the difference between the estimated symbol and the genuine transmitted symbol in the kth iteration.

Virtually, (4.11) is a symbol-level representation of the received signal where the OVs and BVs cannot be straightforwardly employed. Since the variance for the real part and that for the imaginary part is identical (because there is a single decoder employed at the receiver, as shown in Figure 3.6 and Figure 3.11), we may perform

the derivation of the VTR by purely considering the real part of (4.11), written as

$$\mathrm{Re}\left(y^{i,k}\right) = \sqrt{\frac{E_s}{2n_T}}\left[\mathrm{Re}\left(x^{i,k}\right)\sum_{j=1}^{n_R}|h_{ji}|^2 + \mathrm{Re}\sum_{m=1,m\neq i}^{n_T}\Delta_x^{m,k}\sum_{i=1}^{n_R}h_{ji}^*h_{jm}\right] + \mathrm{Re}\left(\sum_{j=1}^{n_R}h_{ji}^*n^j\right) \tag{4.12}$$

where we assume QPSK modulation. For normalization, we divide both sides of (4.11) with $\sqrt{\frac{E_s}{2n_T}}\sum_{j=1}^{n_R}|h_{ji}|^2$ and obtain the bit-level normalized output signal from PIC, written as

$$\mathrm{Re}\left(y_{nor}^{i,k}\right) = \mathrm{Re}\left(x^{i,k}\right) + \left(\sum_{j=1}^{n_R}|h_{ji}|^2\right)^{-1}\cdot\mathrm{Re}\left(\sum_{m=1,m\neq i}^{n_T}\Delta_x^{m,k}\sum_{i=1}^{n_R}h_{ji}^*h_{jm} + \sqrt{\frac{2n_T}{E_s}}\sum_{j=1}^{n_R}h_{ji}^*n^j\right) \tag{4.13}$$

Thus, the difference between the normalized PIC output signal and genuine digit is

$$\mathrm{Re}(y_{nor}^{i,k} - x^{i,k}) = \mathrm{Re}\left(\sum_{m=1,m\neq i}^{n_T}\Delta_x^{m,k}\sum_{i=1}^{n_R}h_{ji}^*h_{jm} + \sqrt{\frac{2n_T}{E_s}}\sum_{j=1}^{n_R}h_{ji}^*n^j\right)\cdot\left(\sum_{j=1}^{n_R}|h_{ji}|^2\right)^{-1} \tag{4.14}$$

The expectation of the squared value of (4.14) is

$$E\left[\mathrm{Re}(y_{nor}^{i,k} - x^{i,k})\right]^2 = E\left\{\left(\sum_{j=1}^{n_R}|h_{ji}|^2\right)^{-1}\mathrm{Re}\left(\sum_{m=1,m\neq i}^{n_T}\Delta_x^{m,k}\sum_{i=1}^{n_R}h_{ji}^*h_{jm} + \sqrt{\frac{2n_T}{E_s}}\sum_{j=1}^{n_R}h_{ji}^*n^j\right)\right\}^2$$

For MIMO-BICM systems, we assume that an ideal interleaver is employed so that Δ_x^m and Δ_x^n are independent for $m \neq n$. Then, we have

$$E\left[\mathrm{Re}(y_{nor}^{i,k} - x^{i,k})\right]^2 = \frac{1}{\left(\sum_{j=1}^{n_R}|h_{ji}|^2\right)^2}\left\{\sum_{m=1,m\neq i}^{n_T}\left[\left(\mathrm{Re}\sum_{i=1}^{n_R}h_{ji}^*h_{jm}\right)^2 E\left(\mathrm{Re}\,\Delta_x^{m,k}\right)^2\right.\right. \tag{4.15}$$

$$\left.\left. + \left(\mathrm{Im}\sum_{i=1}^{n_R}h_{ji}^*h_{jm}\right)^2 E\left(\mathrm{Im}\,\Delta_x^{m,k}\right)^2\right] + \frac{2n_T}{E_s}\sum_{j=1}^{n_R}\left[\left(\mathrm{Re}\,h_{ji}^*\right)^2\left(\mathrm{Re}\,n^j\right)^2 + \left(\mathrm{Im}\,h_{ji}^*\right)^2\left(\mathrm{Im}\,n^j\right)^2\right]\right\}$$

As shown in Figure 3.11, there is a single decoder in the iterative receiver. Therefore,

the input bit variances from all the antennas to the PIC are assumed to be identical that $\sigma_{bit}^2(x^{m,k}) = \sigma_{bit}^2(x^{n,k}), m \neq n$. For brevity, we denote it by $\sigma_{bit}^2(x^k)$. Moreover, the bit variance of the real part is the same as that of the imaginary part so that $E\left(\mathrm{Re}\,\Delta_x^{m,k}\right)^2 = E\left(\mathrm{Im}\,\Delta_x^{m,k}\right)^2 = \sigma_{bit}^2(x^k)$. Consequently, we have

$$E\left[\mathrm{Re}(y_{nor}^{i,k} - x^{i,k})\right]^2 = \frac{\sum_{m=1,m\neq i}^{n_T}\left\{\left|\sum_{i=1}^{n_R} h_{ji}^* h_{jm}\right|^2 \sigma_{bit}^2(x^k)\right\} + \frac{n_T}{E_s}2\sigma_w^2\sum_{j=1}^{n_R}\left|h_{ji}^*\right|^2}{\left(\sum_{j=1}^{n_R}|h_{ji}|^2\right)^2} \tag{4.16}$$

Finally, let us denote the normalized observation variance for the real part (or imaginary part) of the detected signal by $\sigma_{obv}^2(y^{i,k})$ and we have $\sigma_{obv}^2(y^{i,k}) = E\left[\mathrm{Re}(y_{nor}^{i,k} - x^{i,k})\right]^2 = E\left[\mathrm{Im}(y_{nor}^{i,k} - x^{i,k})\right]^2$. Then, we get the variance transfer function of PIC as the following

$$\sigma_{obv}^2(y^{i,k}) = \sum_{m=1,m\neq i}^{n_T}\left|\sum_{j=1}^{n_R} h_{ji}^* h_{jm}\right|^2\left(\sum_{j=1}^{n_R}|h_{ji}|^2\right)^{-2}\cdot\sigma_{bit}^2(x^k) + \left[\frac{E_s}{n_T}\sum_{j=1}^{n_R}|h_{ji}|^2\right]^{-1}\cdot 2\sigma_w^2 \tag{4.17}$$

The expression of (4.18) implies that the output OV of PIC is linear with the input BV of the estimated signal which is obtained from the decoder. Moreover, (4.17) suggests that if the feedback from the decoder is completely reliable that $\sigma_{bit}^2(x^k) = 0$, the output signal of PIC has a normalized observed variance $2\sigma_w^2 / \left(\frac{E_s}{n_T}\sum_{j=1}^{n_R}|h_{ji}|^2\right)$ and the physically measured SNR is $\rho = \frac{E_s}{N_o}\sum_{j=1}^{n_R}|h_{ji}|^2 / n_T$. For slow fading channels, we see that the VTR of the PIC is a variable of the channel matrix $\mathbf{H}$ and hence the transfer function of PIC differs over frames.

VTR Function of PIC on a Fast Fading Channel

For a fast fading channel, the expectation of the squared value of (4. 13) is written as

$$\sigma^2_{obv}(y^{i,k}) = E\left\{\left[\sum_{m=1,m\neq i}^{n_T} \mathrm{Re}\left(\Delta_x^{m,k}\sum_{i=1}^{n_R} h^*_{ji}h_{jm}\right) + \sqrt{\frac{2n_T}{E_s}}\,\mathrm{Re}\sum_{j=1}^{n_R} h^*_{ji}n^j\right]\left(\sum_{j=1}^{n_R}|h_{ji}|^2\right)^{-1}\right\}^2 \tag{4.18}$$

Assuming the independent conditions are applicable, the above equation can be written as:

$$\sigma^2_{obv}(y^{i,k}) = \sum_{\substack{m=1,\\ m\neq i}}^{n_T} E[\mathrm{Re}\,\Delta_x^{m,k}]^2 E\left[\frac{\mathrm{Re}\sum_{i=1}^{n_R} h^*_{ji}h_{jm}}{\sum_{j=1}^{n_R}|h_{ji}|^2}\right]^2 + \sum_{\substack{m=1,\\ m\neq i}}^{n_T} E[\mathrm{Im}\,\Delta_x^{m,k}]^2 E\left[\frac{\mathrm{Re}\sum_{i=1}^{n_R} h^*_{ji}h_{jm}}{\sum_{j=1}^{n_R}|h_{ji}|^2}\right]^2$$
$$+\frac{2n_T}{E_s}\sum_{j=1}^{n_R} E\left[\frac{\mathrm{Re}(h^*_{ji})}{\sum_{j=1}^{n_R}|h_{ji}|^2}\right]^2 E[\mathrm{Re}(n^j)]^2 + E\left[\frac{\mathrm{Im}(h^*_{ji})}{\sum_{j=1}^{n_R}|h_{ji}|^2}\right]^2 E[\mathrm{Im}(n^j)]^2 \tag{4.19}$$

and finally it can be simplified as

$$\sigma^2_{obv}(y^{i,k}) = E\left[\left(\sum_{\substack{m=1\\ m\neq i}}^{n_T}\left|\sum_{j=1}^{n_R} h^*_{ji}h_{jm}\right|^2\right)\left(\sum_{j=1}^{n_R}|h_{ji}|^2\right)^{-2}\right]\sigma^2_{bit}(x^k) + E\left[\left(\frac{E_s}{n_T}\sum_{j=1}^{n_R}|h_{ji}|^2\right)^{-1}\right]2\sigma^2_w \tag{4.20}$$

The derived VTRs of PIC are shown in Figure 4.11. The expression of (4.21) shows that the VTR of PIC for a fast fading channel is also a linear function and it is related to the statistics of the channel coefficients. For Rayleigh fading channels, we have $E\left[\left(\frac{E_s}{n_T}\sum_{j=1}^{n_R}|h_{ji}|^2\right)^{-1}\right] = \frac{n_T}{n_R E_s}$. If the feedback from the decoder is completely reliable (perfect feedback) that $\sigma^2_{bit}(x^k) = 0$, the output SNR of each antenna is $\frac{E_s n_R}{N_o n_T}$. For a system with $n_T = n_R$ and at $\sigma^2_{bit}(x^k) = 0$, in particular, the SNR at the output of PIC is exactly $\frac{E_s}{N_o}$ (which means PIC is optimal if input $\sigma^2_{bit}(x^k) = 0$).

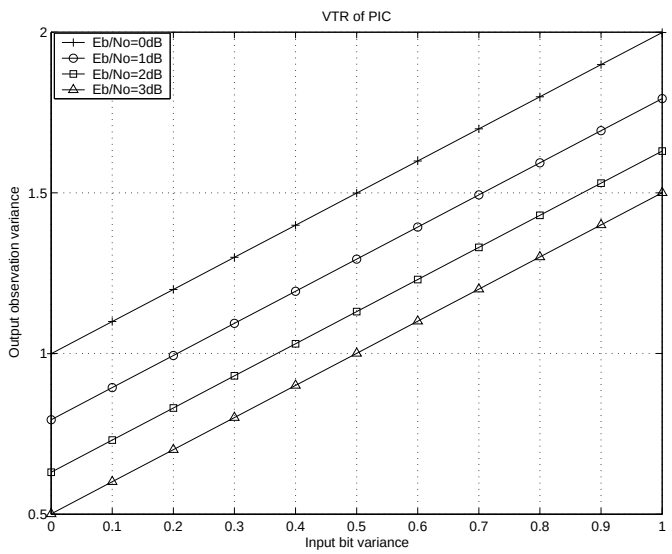

Figure 4.11: VTR functions of PIC, 4 by 4 fast fading channel, 4-QAM.

4.3.2 VTR Function of the LSD

For the ML detection, Matthew R. McKay and Iain B. Collings show that deriving a tight bound for the performance is not possible [17]. Also, there are no theoretical developments for the transfer functions of APP based detections in literature. In this section, the variance transfer function for the LSD is obtained by simulations with very large frame size.

In the previous analysis of the transfer characteristics of PIC, we show that the transfer function of a detector is a variable of the channel coefficients for a slow fading channel. For a fast fading channel, however, the average transfer property is fixed and it only relies on the statistics of the channel coefficients.

Figure 4.12 presents the derived VTR function of PIC (where the output OV is transformed into BV according to (4.6) and (4.8)) and the simulated VTR curves of LSD with varied list sizes. The channel is modelled as a 4 by 4 fast fading channel and the E_b/N_o is 2.5dB. For accuracy, the frame size is set to be 16384. 4-QAM is employed and the full list size of LSD is $2^{n_T M} = 256$. Similarly to that in Section 4.2.1, we define the reduction in the bit variance, given by $\sigma^2_{det,in}(c) - \sigma^2_{det,out}(c)$, by the *bit variance reduction* (BVR) of the detector.

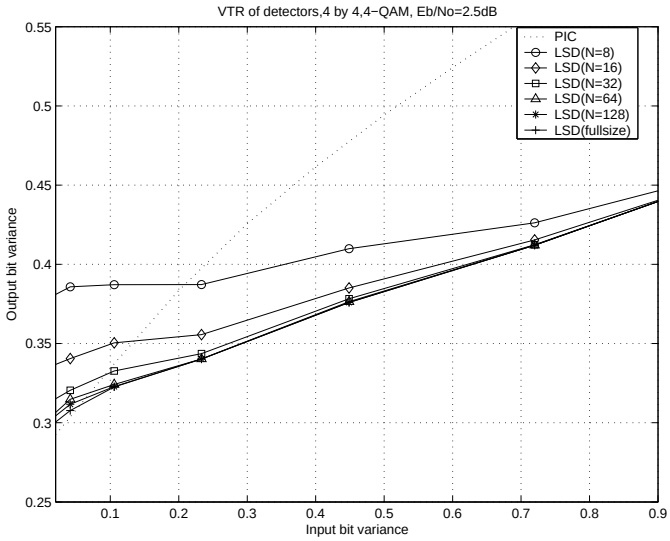

Figure 4.12: VTR functions of detectors,Tx=Rx=4,4-QAM

4.3.3 Comparison of the VTR Functions of LSD and PIC

Variance Transfer Characteristics at a High Variance Region

At a high variance region (e.g. $\sigma^2_{det,in}(c) > 0.8$), we have the following observations:

a) A LSD with list size $N \geq 8$ has a larger BVR than the PIC.

It suggests that the LSD may perform better than PIC when strong interferences between antennas are in presence. The philosophy behind could be found from (3.17). At a high input variance region, the soft information from the decoder is not reliable so that the a priori LLR values to the LSD are very small. Hence, the summation of $\mathbf{c}^T_{[l]} \cdot \mathbf{\Lambda}^k_{A1,[l]}$ in (3.17) is not significant so that the detector is close to a an optimal MAP detector.

For PIC, on the other hand, the term of uncanceled interference, given by $\sum_{m=1,m\neq i}^{n_T} (x^{m,k} - \widetilde{x}^{m,k-1}) \sum_{i=1}^{n_R} h^*_{ji} h_{jm}$ in (3.21), is very large at a high input variance region. Thus, the PIC operation is close to a matched filtering [1]. However, the performance of the matched filtering is shown [44] to be far from that of the optimal MAP detector.

b) The differences between the LSD with various list size is small.

At a high variance region, the a priori LLR values to the LSD are so small that

incomplete list sizes do not significantly impair the accuracy of searching in (3.17). Thus, the BVR of LSD with different list sizes is very similar at this region. As the LLR values become larger (and the input variance decreases), the gap between the VTR of the LSD with a smaller list size and that with a larger list size becomes significant.

Variance Transfer Characteristics at a Low Variance Region

At a very low input variance region (e.g. $\sigma^2_{bit}(x^k) < 0.05$) we obtain the following observations

a) The PIC has a larger BVR than a LSD with a full list size.

b) As the input variance approaches zero, the VTR of a LSD with a small list size stray away from that with a full list size.

In the scenario with a low input variance, the a priori LLR values to the LSD are so large that the summation of $\mathbf{c}^T_{[l]} \cdot \mathbf{\Lambda}^k_{A1,[l]}$ dominates the computation of (3.18). Thus, the accuracy of the generated extrinsic output is largely related to the list size of LSD. *(*This argument is valid since we consider that a priori information is not used in improving the center of the sphere*).*

On the other hand, we see from last section that the PIC is able to approach the optimal performance as the input variance approaches zero. We may also say that the PIC has a better transfer property than LSD with incomplete list size at a low input variance region.

The above observations and analysis motivate a *detection switching* in the iterative receiver which will be presented in section 4.5.

4.4 VEG of Iterative Detection and Decoding

4.4.1 VEG of IDD on Fast Fading Channels

By plotting the VTR function of a detector and that of a decoder in a single graph where the axes for the decoder are swapped, we obtain the VEG of the IDD scheme. The input variance and the output variance of decoder are denoted as $\sigma^2_{dec,in}$ and $\sigma^2_{dec,out}$. The input variance and the output variance of detector are denoted as $\sigma^2_{det,in}$ and $\sigma^2_{det,out}$. In the VEG of the IDD shown in Figure 4.13, the horizontal axis is for $\sigma^2_{dec,out}$ and $\sigma^2_{det,in}$ and the vertical axis is for $\sigma^2_{dec,in}$ and $\sigma^2_{det,out}$. The solid curves are

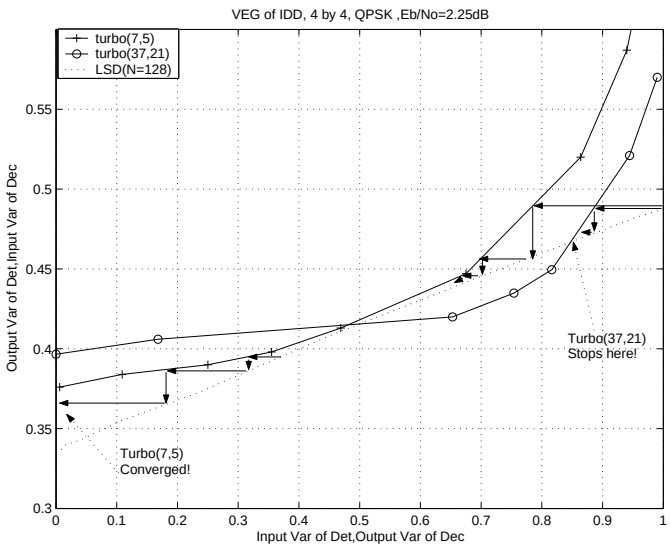

Figure 4.13: VEG of IDD,Tx=4,Rx=4, 4-QAM, R_c=1/2,E_b/N_o = 2.25dB.

the VTRs of decoders and the dashed curve is the VTR of the LSD(N = 128) where E_b/N_o = 2.25dB. We observe that the curve of LSD intercepts with that of TC [37, 21]$_8$ at $\sigma^2_{dec,in}$ = 0.85 and the trajectory stops at this intersection point. Since this intersection happens before the IDD converges to a very small variance, we refer the intersection as an *early inter**c**eption* (EC) between the VTR curves of the detector and the decoder. From the VEG in Figure 4.13, it is obvious that the iterative receiver with TC [37, 21]$_8$ requires a higher E_b/N_o to remove the EC and achieve its waterfall region.

On the other hand, we observe that the VTR curve of LSD does not intercept the VTR curve of TC $[7,\ 5]_8$ at $E_b/N_o = 2.25$dB. Thus, the iterative receiver with LSD($N = 128$) and turbo decoder $[7,\ 5]_8$ is likely to converge to successful decoding. For this iterative receiver, we may say that the minimum E_b/N_o at which EC does not happen is about 2.25dB. In such a manner, the waterfall region of the iterative detection and decoding (shown in Figure 3.8) can be predicted.

4.4.2 VEG of IDD on Slow Fading Channels

For slow fading MIMO channels, the capacities are not identical among different transmission frames. In light of that, outage capacity probability is adopted to characterize the capacity of a slow fading channel. For the study of the iterative detection and decoding on slow fading MIMO channels, we also have to rely on the statistics.

The concept of outage capacity probability of slow fading channels can be explained as: At a certain E_b/N_o, there is a probability with that the instantaneous capacity of the channel of a frame below the target capacity. From transfer characteristics' point of view, analogously, there is a probability with that the transfer function curve of the detector intercepts with that of the decoder before the IDD converges (EC happens) to a low variance. We refer to the probability of EC as *early interception ratio (ECR).* Apparently, the achievable FER performance of an iterative receiver on a slow fading channel is invariably larger than or equal to the ECR.

Since the transfer functions of the decoders are not regular functions, it is not feasible to obtain the ECR in a close-form. However, a precise ECR can be obtained by simulating a very large number of frames. The ECRs of iterative receivers with PIC-DSC and LSD (with $N = 8, 16, 32, 64, 128$) are shown in Figure 4.14 where a TC $[7,\ 5]_8$ is used. We observe that the iterative receiver with the PIC-DSC has a larger ECR than that with the LSD($N \geq 16$). As E_b/N_o increases, the difference between the ECR of iterative receiver with PIC-DSC and that with LSD($N \geq 16$) also becomes larger. (We observe that at FER <0.02, the ECR curve for the iterative PIC-DSC

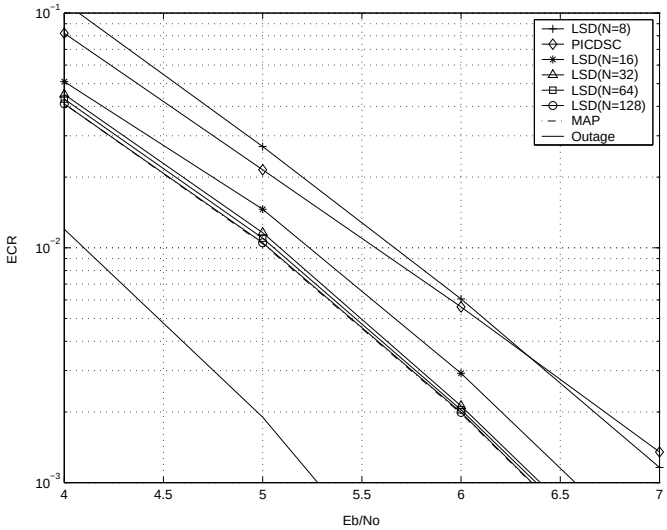

Figure 4.14: Early interception ratio of iterative receivers (of various detectors) with R_c=1/2 TC $[7,\ 5]_8$ on a 4 by 4 slow fading channel. Frame size=1024 and I_D=10. 4-QAM with Grey mapping is used.

receiver is not parallel to that for the outage capacity. The phenomenon gives rise to the error floor observed in Figure 3.14.) At $E_b/N_o = 7$dB, a smaller ECR is observed for the iterative receiver with LSD($N = 8$) than that with PIC-DSC. Moreover, we observe that as the list size of LSD approaches the full list size, the resultant ECR reduction by increasing the list size becomes marginal.

The outage probability is also plotted in Figure 4.14. We observe that the ECR of the iterative LSD receiver with full list size and TC $[7,\ 5]_8$ is about 1.1dB away from the outage capacity at FER=10^{-3}. For this reason, the FER performance of the iterative receivers are more than 1.1dB away from the outage capacity as shown in Chapter 3. To approach the outage probability, we need to reduce the ECR. One possible solution is to use some other channel codes which are of a better transfer property, such as a specially designed irregular LDPC code [34].

4.5 Detection Switching in the Iterative Detection and Decoding

4.5.1 Detection Switching

To bring down the complexity of the iterative receiver with LSD, a reduced list size is always preferable as long as a certain level of performance can be maintained. In Figure 3.10, we see that the performance of iterative receiver with LSD ($N = 32$) is only 0.2dB away from that with full list size. However, considerable performance degradation are observed if smaller list sizes (e.g. $N = 16$ and $N = 8$) are used. As unveiled in Figure 4.12, the reason for such a behavior is that as the input variance becomes low, the VTR function of LSD with incomplete list size strays away from that with full list size.

On the other hand, we notice that the PIC has a very attractive VTR function at a low variance region whereas it cannot compete with that of LSD (of small list size) at a high variance region. Thus, it is reasonable to employ an LSD at the first few iterations and replace it with PIC-DSC at later iterations where the variance is relatively low. In another word, we would like to employ a PIC-DSC in the iterative receiver as long as the IDD process works in a low variance region where the EC is not likely to happen in the subsequent iterations. Thus, LSDs with further reduced list sizes are promising to be used in the first few iterations. In this thesis, we propose a *detection switching* (DSW) from LSD to PIC in the iterative receiver.

4.5.2 Switching Criterion

Simply, the switching can be carried out as long as the variance is smaller than a pre-defined value. However, the evaluation of the BVs requires the knowledge of the transmitted signal which is practically unavailable.

As presented in Chapter 2, the cross entropy can be adopted to predict the con-

vergence of the turbo decoding. In the following, we shown that the CE can also be used to predict the convergence of IDD to determine when to carry out the DSW. And hence, it can be used to determine when to switch from the LSD detector to PIC-DSC detector.

Let us denote the APPs of coded digits from the turbo decoder at the kth receiver iteration by $q^k(c_t)$. The CE between the output APPs of coded digits from two consecutive receiver iterations is represented as

$$T(k) = E_{q^k(c_t)} \left\{ \log \frac{q^k(c_t)}{q^{k-1}(c_t)} \right\} \tag{4.21}$$

Since the correlation between the soft information of two consecutive iterations are small for the first few receiver iterations [35][39], we may assume that the soft output from the decoder at receiver iteration k is statistically independent from that at receiver iteration k' ($k' \neq k$). For the first few iterations, the cross entropy of the decoder output APPs can be approximated as

$$\begin{aligned} T(k) &\approx \sum_t \log \frac{q^k(c_t)}{q^{k-1}(c_t)} \\ &= \sum_t \left\{ q^k(c_t = 1) \log \frac{q^k(c_t = 1)}{q^{k-1}(c_t = 1)} + q^k(c_t = 0) \log \frac{q^k(c_t = 0)}{q^{k-1}(c_t = 0)} \right\} \end{aligned} \tag{4.22}$$

Let us define $\triangle\Lambda^k(c_t) = \Lambda^k(c_t) - \Lambda^{k-1}(c_t)$. Similar to (2.41), we can simplify the CE as

$$T(k) = \sum_t \frac{\left|\triangle\Lambda^k(c_t)\right|^2}{e^{\left(\left|\Lambda^{k-1}(c_t)\right|\right)}} \tag{4.23}$$

Though (4.23) is an approximation since the condition 3) made for the derivation of (2.41) may not be met, simulation shows that switching at $T(k)<0.1$ is able to yield good results. Simply, we start the iteration with LSD and switch to PIC once $T(k)<0.1$. If the condition is not met, we switch to PIC at the end of the receiver iteration.

At the first iteration with PIC, the extrinsic information from the decoder are used

for cancellation and hence the output of PIC is not biased. At later PIC iterations, the APPs from the decoder is used for cancellation and hence it is biased. Similar to Section 3.4.1, the DSC is employed after the detection switching.

4.5.3 Simulations

Frame Error Performance

In the simulations, we consider slow fading channels and all the settings are the same as in Section 3.3.3. The total number of receiver iteration I_D is 10 where the maximum number of iterations with LSD is 5. The FER of the receivers with and without DSW

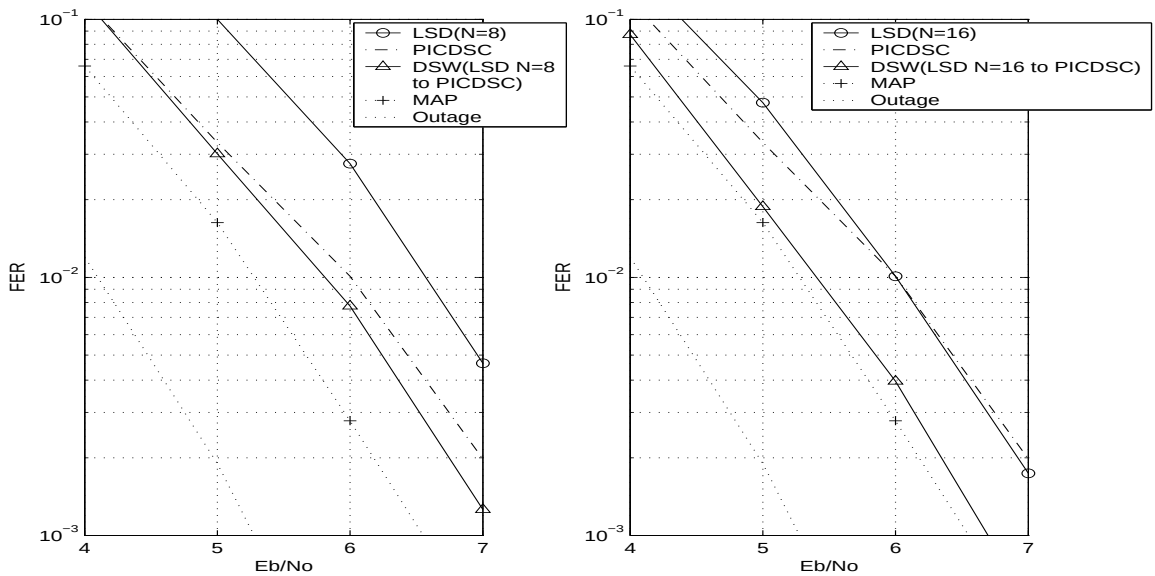

Figure 4.15: FER of iterative receiver with DSW and R_c=1/2 TC $[7, 5]_8$ on a 4 by 4 slow fading channel. Frame size=1024 and I_D=10. 4-QAM with Grey mapping.

are shown in Figure 4.15. From the left, we see that the FER of the iterative receiver with LSD ($N = 8$) is about 0.55dB worse than that with PIC-DSC at FER=10^{-2}. By employing the DSW, the iterative receiver is about 0.7dB better than that with LSD(N=8) and 0.2dB better than that with PIC-DSC. As the SNR increase, the performance gain by using DSW over the PIC-DSC becomes larger. No error floor is observed for the iterative receiver employing DSW.

From the right of Figure 4.15, we see that the FER of the iterative receiver with LSD($N = 16$) is similar to that with PIC-DSC at FER=10^{-2}. By employing the DSW, however, the iterative receiver is about 0.6dB better than that with LSD(N=16) or PIC-DSC. The performance of that scheme is only 1.2dB away from the outage capacity. Again, no error floor is observed for the iterative receiver employing DSW.

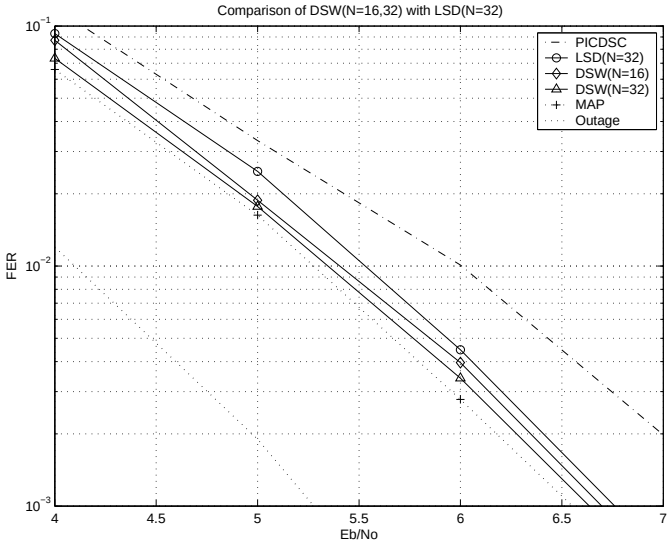

Figure 4.16: FER of iterative receiver with DSW and R_c=1/2 TC $[7, 5]_8$ on a 4 by 4 slow fading channel. Frame size=1024 and I_D=10. 4-QAM with Grey mapping.

The FERs of the iterative receivers with DSW and LSD ($N = 16, 32$) are shown in Figure 4.16. We see that the iterative receiver with DSW and a small list size ($N = 16$) outperforms that with a larger list size ($N = 32$) and no switching. (The complexities of these two schemes will be compared later on). From the above results, we see that the DSW is effective to improve the performance of the iterative receiver with LSD of a relatively small list size.

Complexity

From the above results, we see that the DSW can improve the performance of the iterative receiver with LSD($N = 8, 16, 32$). In this section, we will show that by introducing the DSW, the near-optimal performance of the iterative receiver can be achieved with a reduced complexity. The reduction in the complexity is due to the

reduced list size as well as the decreased number of iterations in which LSD operations are conducted.

In Chapter 3, the complexity of LSD and PIC-DSC is quantified with computation units (CUs). For the iterative receiver employing the switching, we use I_{LSD} to denote its average number of iterations in which the LSD is conducted. The average number of iterations with the PIC-DSC is $I_D - I_{LSD}$. The computation complexity is shown in Table 4.1 for different detection methods. We see that the complexity of the iterative receiver with DSW is also determined by the average I_{LSD} which varies with SNRs. From simulations, the average number of iterations with LSD is shown in Figure 4.17. The computation complexities quantified with CUs are also plotted. Compared to the iterative receiver with LSD($N = 32$), up to 82% (at $E_b/N_o = 7$dB) CUs of detection operations can be saved by employing the iterative receiver with DSW from LSD ($N = 16$) to PIC-DSC (and which also achieves a slightly better performance, as shown in Figure 4.16).

	complexity evaluation
LSD($N = 16$) DSW	$(104 + 28NI_{LSD})\Gamma + 64\Gamma(I_D - I_{LSD})$
LSD($N = 32$)no DSW	$(104 + 28NI_D)\Gamma$
PIC-DSC	$64\Gamma I_D$

Table 4.1: Complexity of DSW and LSD, 4-QAM and 4×4 MIMO slow fading channels.

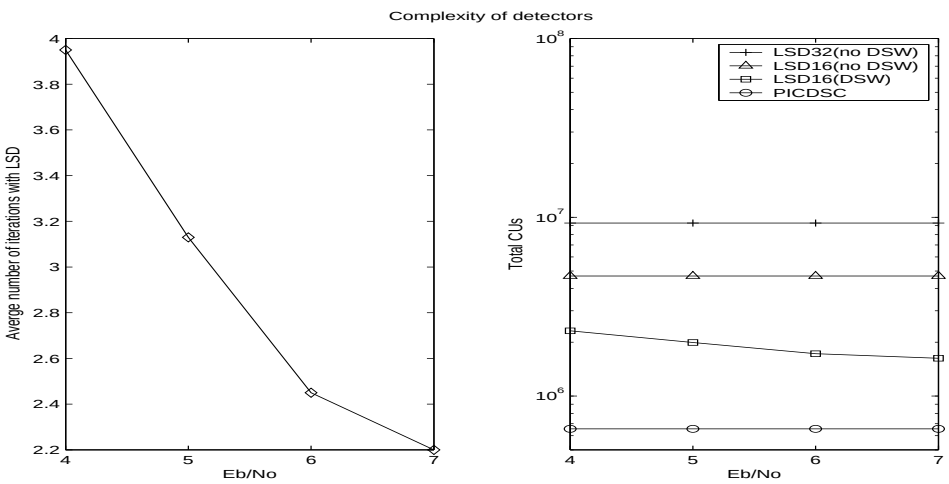

Figure 4.17: Average number of LSD detections and total CUs of detection operations.

Chapter 5

Scheduling of the Iterative Receivers for Turbo Coded MIMO Systems

In an iterative receiver with a turbo decoder, the convergence analysis involves the transfer functions of three components which are the MIMO detector, the first RSC decoder and the second RSC decoder. It is shown in [33] that the same convergence point of the iterative receiver with multiple components can be reached independent of the *iteration schedules*, provided that sufficient number of iterations are conducted. However, different schedules may have varied computational complexities. Hence, the iterations between the components in the receiver are required to be carefully scheduled to achieve a good performance and complexity trade-off.

In an iterative receiver with more than two components, the transfer function of each component has multiple inputs and hence the transfer function of that component can be multiple dimensional. In Figure 5.1, the VTR function of a RSC $[1, 5/7]_8$ is depicted as a three-dimensional surface where the output variance of the decoder is determined by the input variance from the detector as well as the input variance from the other decoder. Needless to say, the analysis of the convergence behavior of a

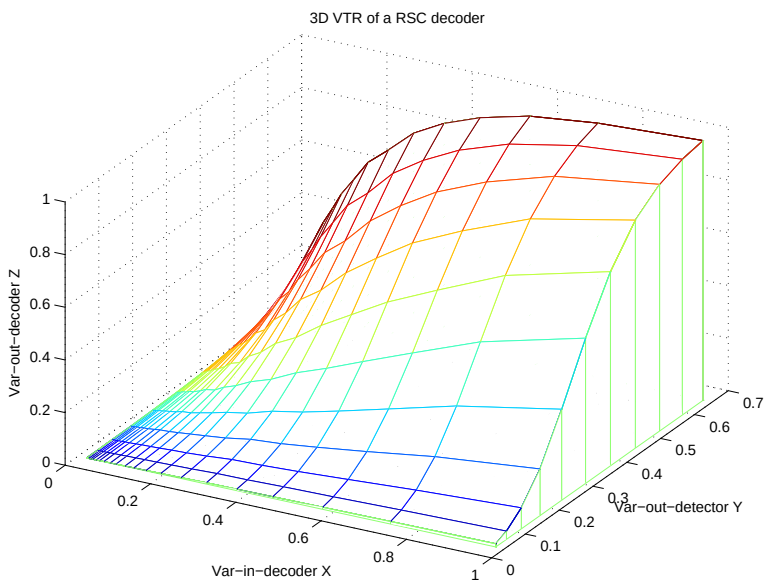

Figure 5.1: 3D VTR of RSC $[1, 5/7]_8$

three-component iterative receiver is not straightforward.

5.1 Conventional Scheduling for the Iterative Receiver

In Chapter 3 and 4, the iterative MIMO receiver with a turbo decoder is considered as a two-component concatenated system where the two RSC decoders are viewed as a single entity. Soft information is exchanged between a MIMO detector and a turbo decoder (which is called a receiver iteration or a outer iteration). In the turbo decoding of each receiver iteration, information is also passed between two RSC decoders (which is referred to as the decoding iteration or inner iteration). In this dissertation, we call this type of passing information as a *conventional scheduling*. In a receiver with such an iteration scheduling, the MIMO detector does not see the exchanging of information between the two RSC decoders.

The iterative receiver with a conventional scheduling is shown in Figure 5.2. For each frame, I_D receiver iterations are conducted and we say that the detector *activates* I_D times for each frame. In each receiver iteration, two RSC decoders of the turbo

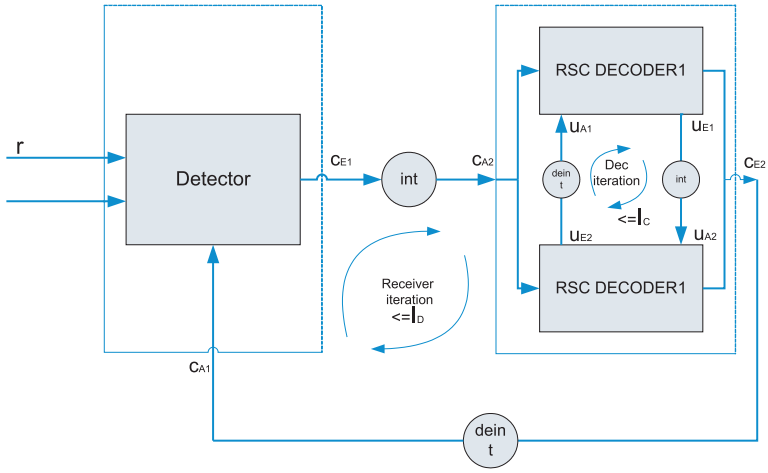

Figure 5.2: the conventional scheduling of the iterative MIMO receiver

decoder exchange soft information I_C times. Hence, a RSC decoder activates $I_D I_C$ times for each frame.

In Figure 5.3, we depict the trajectory of the iterative receiver with the conventional scheduling in a series of two-dimensional graphs where we consider a 4 by 4 fast fading MIMO channel with 4-QAM and $E_b/N_o = 3$dB. In the first iteration, the output of the detector is of a relative large variance. Hence, there is no tunnel between the VTRs of the two RSC decoders and the turbo decoding iteration stops at a high variance. In a subsequent receiver iteration, the output of the detector is improved so that the turbo decoding iteration stops at a lower variance, although a tunnel is still not observed. In the eighth receiver iteration, a tunnel between the VTRs of the two RSC decoder is obvious and the iterative receiver converges to successful decoding.

The advantage of employing such an iteration scheduling is that both the design and the convergence analysis of the iterative receiver are quite straightforward. In addition, the waterfall region of the iterative receiver can be easily and precisely predicted, as shown in Chapter 3. However, this scheduling is not necessarily optimal for a three-component iterative receiver, in terms of computational efficiency. As shown in Figure 5.3, at the first receiver iteration, the iterative decoding process stops at a point with a bit variance around 0.85, no matter how many decoding iterations are used. Therefore, a fixed number of turbo decoding iterations, for example $I_C = 10$, will

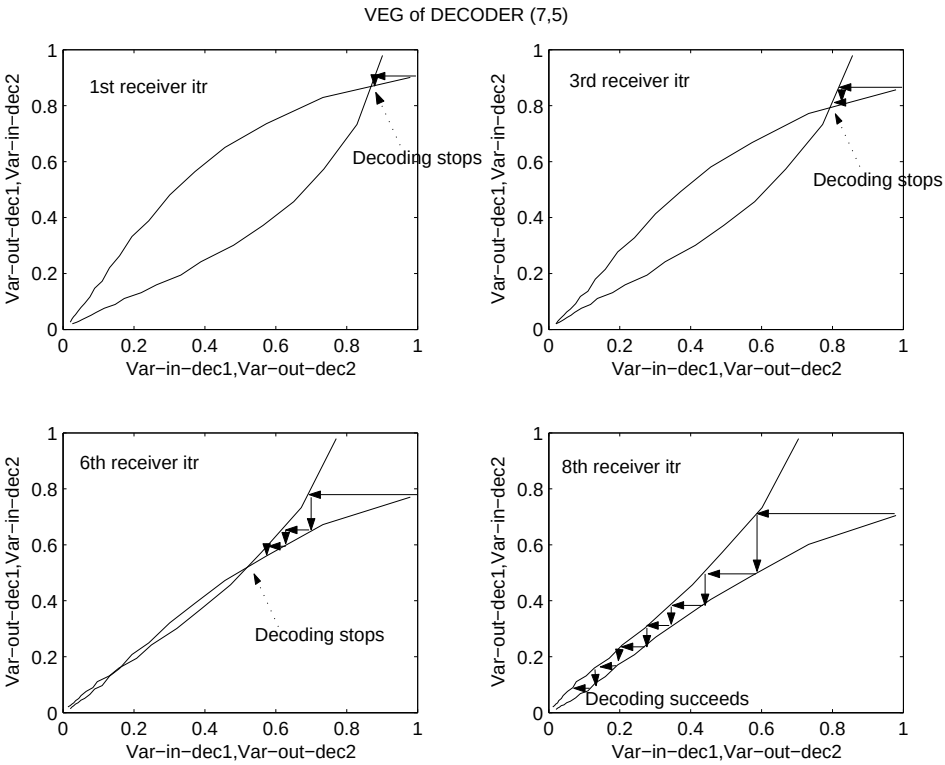

Figure 5.3: The VEG of the RSC $[7, 5]_8$ decoders in the iterative detection and decoding

give rise to a high complexity ($I_D I_C$ times of turbo decoding iterations per frame) due to the unnecessary turbo decoding iterations conducted. Although some stopping criteria can be applied to reduce the numbers of the turbo decoding operations, the overall complexity of the receiver has yet to be investigated and to be compared to the receiver with other schedules.

5.2 New Schedules for the Iterative Receiver

5.2.1 Periodic Schedule for the Iterative Receiver

In [33], it is suggested that the most recent priors should be used to generate new soft outputs upon each activation of the components. In the conventional scheduling, however, the two RSC decoders are treated as a single component so that the a priori information to the first RSC decoder is assumed to be unavailable in the first decoding

iteration of every receiver iteration.

In this section, we investigate a new scheduling, named a *periodic scheduling*, for the iterative MIMO receiver.

The periodic scheduling is of the following features:

1. The three components are activated in a periodic fashion. The activation order is

$$\underbrace{\text{Detector, RSC1, RSC2,}}_{\text{1st receiver iteration}}\ \underbrace{\text{Detector, RSC1, RSC2,}}_{\text{2nd receiver iteration}}\text{...}$$

2. When a component is in activation, it takes the most recent a priori information provided by the other two components to generate new soft information.

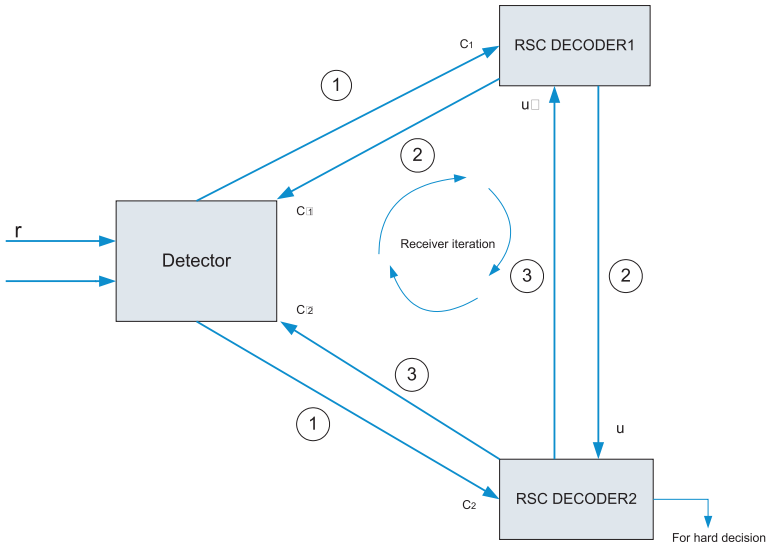

Figure 5.4: The periodic schedule for the iterative MIMO receiver.

The iterative receiver with the periodic scheduling is shown in Figure 5.4 where the operations of interleaving and de-interleaving between any two components are omitted for a simple illustration. The numbers in circles are used to denote the activation order in every receiver iteration.

Process 1. In each activation of the detector, it takes the a priori information on the coded digits from the two RSC decoders to generate new soft outputs for both RSC decoders.

Process 2. The first RSC decoder takes the a priori information on the coded digits from the detector as well as the a priori knowledge on the information bits from the second decoder (in the last receiver iteration) to yield an updated soft output of the coded digits (which will be passed to the detector) and the extrinsic information on the systematic (or message) bits (which will be passed to the second RSC decoder).

Process 3. The second RSC takes the a priori knowledge provided by the first RSC decoder as well as the a priori information on the coded digits from the detector to generate its updated soft output on the coded digits and extrinsic information on the systematic bits for the detector and the first RSC decoder, respectively.

The same operations are repeated in the next receiver iteration.

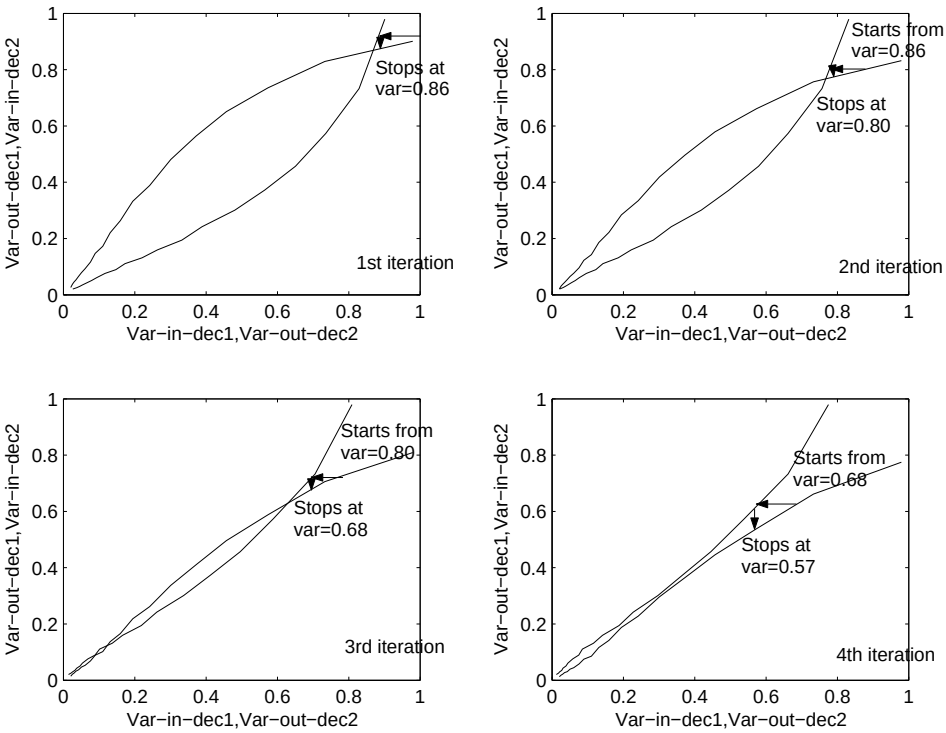

Figure 5.5: The VEG of the RSC decoders in the iterative receiver with the periodic schedule.

The variance exchange between the two RSC decoders in the iterative receiver with the periodic scheduling is shown in Figure 5.5. In comparison with Figure 5.3, we see that fewer variance exchanges (iterations) between the two RSC decoders are required to achieve the a certain bit variance (e.g $\sigma_{bit}^2 = 0.57$).

5.2.2 Master-Slave Schedule for the Iterative Receiver

In this section, we investigate another iteration scheduling named as a *master-slave* (MS) *scheduling*.

The MS scheduling is of the following features:

1. The activation order is

$$\underbrace{\text{Detector, RSC1, Detector, RSC2,}}_{\text{1st receiver iteration}}\ \underbrace{\text{Detector, RSC1, Detector, RSC2,}}_{\text{2nd receiver iteration}}\ \ldots$$

In each receiver iteration, the detector activates twice and each of the decoders activate once. We see that the detector is in a pivotal position and we may refer it as a "master" whereas the decoders are viewed as "slaves".

2. When a component is in activation, it takes the most recent a priori information provided by the other two components to generate new soft information (analogous to the periodic scheduling).

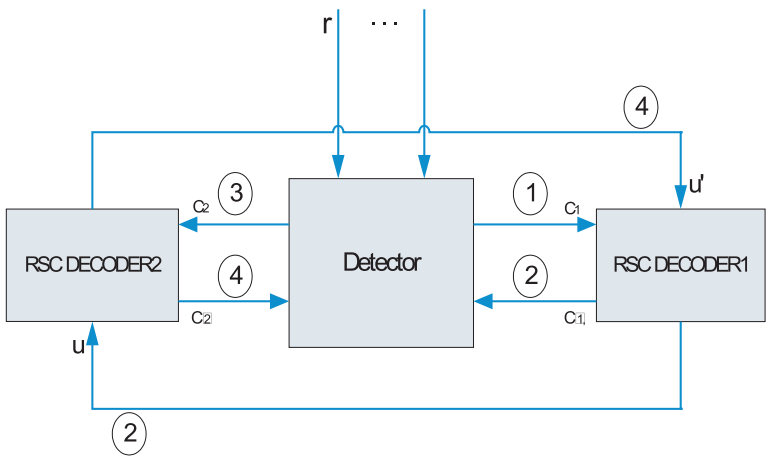

Figure 5.6: The master-slave schedule for the iterative MIMO receiver.

The iterative receiver with the MS scheduling is shown in Figure 5.6.

Process 1. In the first activation of the detector, it takes the a priori information on the coded digits from the two RSC decoders, generates soft output on the coded digits and passes it to the first RSC decoder only.

Process 2. The first RSC decoder takes the a priori information on the coded digits from the detector and the a priori information of the information bits from the second decoder (in the last receiver iteration) to yield new soft outputs of the coded digits as well as the EXT on the information bits.

Process 3. The updated soft output of the coded digits is passed back to the detector. The detector activates for the second time, generates new soft information on the coded digits and passes it to the second decoder only.

Process 4. The second RSC takes the a priori knowledge of the information bits provided by the first RSC decoder as well as the a priori information on the coded digits from the detector to generate new soft outputs.

The same operations are repeated in the subsequent receiver iterations.

5.3 Iterative Receivers with PIC-DSC and new schedules.

In this section, we evaluate the new schedules in the iterative receiver with PIC-DSC. The complexity of the PIC-DSC and that of the MAP decoder (RSC $[1, 5/7]_8$) acquired in the earlier sections are listed in Table 5.1. For a 4 by 4 MIMO system with 4-QAM,

	PIC-DSC	MAP decoder $[7, 5]_8$
Complexity per frame	64ΓCUs	70Γ CUs

Table 5.1: Complexity of PIC-DSC and MAP decoder.

we see that the complexities of these two components are comparable. Hence, we may say that the complexity of the iterative receiver is proportional to the total number of activations of the components, where the detector and decoder are regarded to be equivalent in terms of complexity. (The complexity in Table 5.1 is based on the use of a [7, 5] RSC code. For a scheme with more complex codes, a better scheduling will achieve more gains.)

Now, we compare the performance of the iterative receivers with different schedules. In order to get a fair comparison, we made some modifications for the conventional scheduling. The modifications are as follows:

a) The stopping criterion based on CE described in Chapter 2 is adopted to avoid unnecessary turbo decoding iterations.

b) In the first (inner) iteration of the turbo decoding, the first RSC decoder takes the a priori knowledge from the second RSC decoder obtained in the previous receiver (outer) iteration.

Hence, the activation order of the modified conventional scheduling is

$$\underbrace{\text{Detector,RSC1,RSC2,RSC1,RSC2,...,}}_{\text{1st receiver iteration, until } T(k)\leq 0.001T(1)}\underbrace{\text{Detector,RSC1,RSC2,RSC1,RSC2..}}_{\text{2nd receiver iteration, until } T(k)\leq 0.001T(1)}$$

The performance of the receivers is shown in Figure 5.7. In each scheduling, the iteration is terminated when the total number of activations reaches 30 (the detector and the two decoder have operated 30 times in total) or 60. We observe that the iterative receiver with the periodic scheduling clearly outperforms that with the other two schedules (30 activations). As the total number of activations increases, the performance differences become smaller. Moreover, we see that the periodic scheduling can achieve a similar performance at a much lower complexity, compared with other schedules.

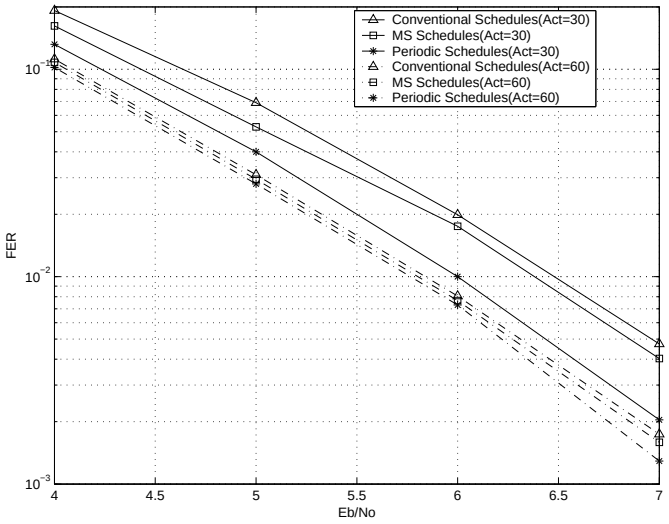

Figure 5.7: The performance of iterative receivers with various schedules. Total number of activations is 30 or 60.

Chapter 6

Conclusion

6.1 Summary of Results

The application of MIMO techniques is considered to be an attractive solution in the development of new generation wireless communications featuring very high spectral efficiency and power efficiency. For feasible implementation, iterative detection and decoding techniques for MIMO system have been well-explored.

This dissertation has studied a variety of iterative detection and decoding schemes for MIMO-BICM systems. To approach the capacity of MIMO channel with acceptable complexity, various detectors and channel codes are investigated. For a system with a linear detector and a simple convolutional code, union bounding techniques are employed to predict the performance. For an iterative receiver with a more powerful detector and a stronger channel code, we employ the variance transfer functions to analyze the iterative decoding behaviors. By following such a methodology, a good channel code (turbo code $[7, 5]_8$ in this thesis) is found for an iterative receiver.

For fast fading channels, we showed that the waterfall region of an IDD scheme can be predicted via VTR, in the same manner as the waterfall region of a turbo code. For slow fading channels, the performance of an iterative receiver is found to be restricted by the early interception ratio between the components' transfer curves.

In order to fully exploit the advantage of PIC-DSC and that of LSD while circumventing their shortages, a detection switching is proposed for the iterative receivers. Moreover, a switching criterion based on the cross entropy is introduced. For a slow fading channel, we show that considerably reduced complexity is achieved by using the detection switching, at a FER performance within 1.2dB to the outage capacity.

To reduced the overall complexity of the iterative receiver with three components, a periodic scheduling and a master-slave scheduling are studied. We see that this scheduling outperforms the conventional scheduling in terms of performance and complexity trade-off.

6.2 Future Works

The work in this dissertation can be further strengthened by the following:

1. The channel codes studied in this dissertation are convolutional codes and turbo codes. However, a code with a better shape of transfer function has yet to be investigated. By designing and employing an irregular convolutional code [37] as the constituent code of a turbo code, it is potential to improve the transfer property and hence the performance of the receiver.

2. In this dissertation, the channel is assumed to be perfectly know by the receiver which is not realistic. Thus, joint channel estimation and iterative detection and decoding is of great interests. Especially, the pilot sequence for the channel estimation can be used to modify the transfer functions of the decoders as in [38] so that a better convergence behavior can be achieved.

Bibliography

[1] J. Proakis, *Digital Communications*, 2nd edition, McGRAW HILL, 2001.

[2] S. Haykin, *Communication Systems*, 3rd Ed. John Wiley & Sons, 1994.

[3] B. Vucetic, and J. Yuan, *Turbo Codes: Principles and Applications*, Kluwer Academic Publishers, 2000.

[4] A. Burr, *Modulation and Coding for Wireless Communications,* Prentice Hall, 2003.

[5] B. Vucetic and J. Yuan, *Space-time Coding*, WILLEY, 2003.

[6] C. Berrou, A. Glavieux and P. Thitimajshima, "Near Shannon limit error-correcting coding and decoding : Turbo-codes (I)," *IEEE Int. Conf. on Comm. ICC' 93*, vol 2/3, pp. 1064-1071, May 1993.

[7] G. Foschini, "Layered space-time architecture for wireless communication in a fading environment when using multi-element antennas", *Bell Labs Technical Journal,* pp. 41-59, Autumn 1996.

[8] B. M. Hochwald and S. ten Brink, "Achieving near-capacity on a multiple-antenna channel," *IEEE Trans. Commun*, vol. 51, no. 3, pp. 389-400, Mar. 2003.

[9] S. H. M. Weinfurtner, "coding approaches for multiple antenna transmission in fast fading and OFDM," *IEEE Trans. Sig. Proc*, vol. 50, no. 10, pp. 2442-2450, Oct 2002.

[10] S. ten Brink, "Convergence behavior of iteratively decoded parallel concatenated codes," *IEEE Trans. Commun*, vol. 49, no. 10, pp. 1727-1737, Oct 2001.

[11] J. Hagenauer, E. Offer, and L. Papke, "Iterative decoding of binary block and convolutional codes," *IEEE Trans. Inform. Theory*, vol. 42, pp 429–445, March 1996.

[12] J. Yuan, W. Feng and B. Vucetic, "Performance of parallel and serial concatenated codes on fading channel", *IEEE Trans. commun,* vol. 50, no. 10, pp. 1600-1608, Oct. 2002.

[13] E. K. Hall and S. G. Wilson, "Design and analysis of turbo codes on Rayleigh fading channels," *IEEE J. Select. Areas Commun,* vol. 16, no.2 pp. 160–174, Feb. 1998.

[14] Z. Shi, "Joint iterative detection for random coded code-division-multiple-access," Ph.D dissertation, The University of Utah, May. 2003.

[15] J. Choi, "Iterative receivers with bit-level cancellation and detection for MIMO-BICM systmes," *IEEE Trans. Signal. Proc*, vol. 53, no. 12, pp. 4568-4577, Dec 2005.

[16] Z. Shi, C. Schlegel, "Joint iterative decoding of serially concatenated error control coded CDMA," *IEEE journal on selected areas in communications,* vol 19, no.8, pp. x, Aug 2001.

[17] M. R. McKay and I. B. Collings, "Capacity and performance of MIMO-BICM with zero-forcing receivers," *IEEE Trans. Commun,* vol 53, no.1, pp. 74-83, Jan 2005.

[18] F. S. Ostuni, M. R. Nakhai and A. H. Aghvami, "Iterative MMSE receivers for space–time trellis-coded CDMA systems in multipath fading channels," *IEEE Trans. Veh. Tech*, vol. 54, no. 1, pp. 163-176, Jan 2005.

[19] S. Marinkovic, B. S. Vucetic and J. Evans, " Improved iterative parallel interference cancellation for coded CDMA systems," *Proc. IEEE ISIT'2001,* (Washington*, DC*, USA, Jun 24-29, 2001), pp. 34.

[20] E. malkamaki, H. Leib, "Evaluating the performance of convolutional codes over block fading channels," *IEEE Trans. Inf. Theory*, vol. 45, no. 2, pp. 1643-1646, Jul. 1999.

[21] J. Hagenauer, E. Offer, and L. Papke, "Iterative decoding of binary block and convolutional codes," *IEEE Trans. Inform. Theory*, vol. 42, pp 429–445, March 1996.

[22] T. Abe and G. Bauch, "Comparison of MIMO Receivers: From APP or MMSE? ," *Turbo Coding 2006,* Munich, April 3-7*,* 2006.

[23] S.Baero, J.Hagenauer, and M.Witzke, "Iterative Detection of MIMO transmission using a List-Sequential (LISS) Detector," *International Conference on Communications (ICC)*, Anchorage, USA, May 2003.

[24] R. Y. Shao, S.Lin and M. P. C. Fossorier, "Two simple stopping criteria for turbo decoding, " *IEEE Trans. Commun.,* vol. 47, no.8, pp.x, Aug 1999.

[25] V. Tarokh, N. Seshadri, A. R. Calderbank, "Space–time codes for high data rate wireless communication: performance criterion and code construction," *IEEE Trans. Inf. Theory*, vol. 44, no. 2, pp. 744-765, Mar 1998.

[26] G. Caire, G. Taricco, E. Biglieri, "Bit-interleaved coded modulation," *IEEE Trans. Inf. Theory.*, vol. 44, no. 3, pp. 927-946, May 1998.

[27] R. Milner and L. K. Rasmussen, "Weighted extrinsic feedback in the iterative multiuser decoding of coded CDMA," *Proc. AusCTW 2006.*

[28] G. Knagge, G. Woodward, S. R. Weller and B. Ninness, "A VLSI optimised parallel tree search for MIMO," *Proc. of 6th Aus. Commun. Theory Workshop*, pp. 215 - 220, Feb. 2005.

[29] J. Lee, S. Park, Y. Zhang, K. K. Parhi and S. C. Park, "Implementation issues of a list sphere decoder," in *Proc. of Int. Conference on Acoustics, Speech and Signal Processing (ICASSP)*, vol. 3, pp. III-996 - III-999, May 2006.

[30] O. Y. Takeshita, O. M. Collins, P. C. Massey and D. J. Costello, "A note on asymmetric turbo-codes," *IEEE Letters. Commun.,* vol. 3, no. 3, pp. 69-71, Mar 1999.

[31] Z. Chen, J. Yuan, B. Vucetic and Z. Zhou, "Performance of Alamouti scheme with transmit antenna selection," *15th IEEE Inter. Symp. Personal, Indoor and Mobile Radio Communications (PIMRC)*, vol. 2, pp.1135 - 1141, Sep 2004.

[32] A. Gueguen, "Comparison of suboptimal iterative space-time receivers," *57th IEEE Sem. Vehi. Tech. Conf. 2003 (VTC 2003)*, vol.2, pp. 842 - 846, Apr 2003.

[33] F. Brannstrom, L. K. Rasmussen and A. J. Grant, "Convergence analysis and optimal scheduling for multiple concatenated codes," *IEEE Trans. Info. Theory*, vol. 51, no. 9, Sep 2005.

[34] S. ten Brink, G. Kramer and A. Ashikhmin, "Design of low-density parity-check codes for modulation and detection," *IEEE Trans. Communi.*, vol. 52, no. 4, pp. 670-678, Apr 2004.

[35] T. Lin, L. K. Rasmussen, "Maximal ratio combining for iterative multi-user decoding," in *Australian Commun. Theory Workshop 2004*, Newcastle, Australia, pp. 42–46, Feb. 2004.

[36] J. Ning, M. Fu and G. Wade, "Turbo-coded multi-alphabet binary CPM for concatennated continuous phase modulation," in *Proc. of IEEE. GlOBECOM 2005*, vol. 3, pp. 1418-1422, Nov. 2005.

[37] J. Wang, N. S. Othman, J. Kliewer, L. L. Yang and L. Hanzo, "Turbo-detected unequal error protection irregular convolutional codes designed for the wideband advanced multirate speech codec," *Proc. of IEEE 62nd Vehi. Techn. Conference (VTC)*, vol. 2, pp: 927 - 931, Sep. 2005.

[38] S. ten Brink, "Code doping for triggering iterative decoding convergence," *Proc.of IEEE International Symposium on Information Theory(ISIT)*, pp. 235, June. 2001.

[39] T. Lin, L. K. Rasmussen, "Truncated maximal ratio combining for iterative multiuser decoding," in *Australian Commun. Theory Workshop 2005*, pp. 35 - 41, Feb. 2005.

[40] G. J. Goschini and M. J. Gans, "On limits of wireless communications in a fading environment when using multiple antennas," *Wireless Personal Comm.*, vol. 6, pp. 311-335, Mar. 1998.

[41] H. Junsheng and O. Y. Takeshita, "On the decoding structure for multiple turbo codes," *Proceedings. IEEE Intern. Symp. on Inform. Theory*, pp. 98, June 2001.

[42] D. Divsala and F. Pollara, "Multiple turbo codes," *Conference Record of IEEE Military Communications Conference* (*MILCOM*), vol. 1, pp. 279 - 285, 1995.

[43] D. Tse and P. Viswanath, *Fundamentals of Wireless Communication,* Cambridge, U.K, Cambridge Univ. Press 2005.

[44] S. Verdu and S. Shamai, "Spectral efficiency of CDMA with random spreading," *IEEE Trans. Inform. Theory*, vol. 45, no. 2, pp 622-640, March 1999.

[45] X. Yang, S. Li, L. Li, X. Tao and P. Zhang, "MMSE-SIC-turbo receiver for CDMA-MIMO systems," *Proceedings. IEEE International Symposium on Microwave, Antenna, Propagation and EMC Technologies for Wireless Communications 2005 (MAPE 2005),* vol. 2, pp. 1496-1500 Aug. 2005.

[46] W. Zhao and G. B. Giannakis, "Sphere decoding algorithms with improved radius search, " IEEE Trans. Commun., vol. 3, no. 7, pp. 1104-1109, July 2005.

[47] Q. Liu and L. Yang, "A novel method for initial radius selection of sphere decoding," *Proc. of IEEE 60th Vehi. Techn. Conference (VTC 2004)*, vol. 2, pp. 1280 - 1283, Sept. 2004.

[48] G. Ungerbock, "Channel coding with multilevel/phase signals," *IEEE Trans. Inf. Theory*, vol. 28, no.7, pp. 55-67, Jan 1982.

[49] S. Verdu, "*Multiuser Detection.*" Cambridge, U.K.: Cambridge Univ. Press, 1998.

[50] G. D. Golden, G. J. Foschini, R. A. Valenzuela, and P. W. Wolniansky, "Detection algorithm and initial laboratory results using the V-BLAST space-time communication architecture," *Electron. Lett.*, vol. 35, no. 1, pp. 14–15, 1999.

[51] A. Lozano and C. Papadias, "Layered space-time receivers for frequency selective wireless channels," *IEEE Trans. Commun.*, vol. 50, pp. 65–73, Jan. 2002.